DOTTORATO DI RICERCA IN SCIENZE CHIMICHE

CICLO XXIX

COORDINATORE Prof. PIERO BAGLIONI

Microwave pyrolysis of polymeric materials: lignocellulosic biomasses as case of study

Dottorando

Dott.Mattia Bartoli

Tutore

Dott.Marco Frediani

Co-tutore

Dott.Luca Rosi

DOTTORATO DI RICERCA IN SCIENZE CHIMICHE

CICLO XXIX

COORDINATORE Prof. PIERO BAGLIONI

Microwave pyrolysis of polymeric materials: lignocellulosic biomasses as case of study

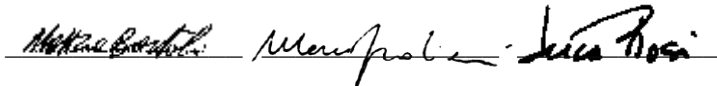Settore Scientifico Disciplinare CHIM/04

Dottorando	**Tutore**	**Co-tutore**
Dott. Mattia Bartoli	Dott.Marco Frediani	Dott.Luca Rosi

Coordinatore

Prof. Piero Baglioni

_____

Anni 2013/2016

"Et ait Deus: "Germinet terra herbam virentem et herbam facientem semen et lignum pomiferum faciens fructum iuxta genus suum, cuius semen in semetipso sit super terram". Et factum est ita."

Genesis 1:11

"Omnia in mensura et numero et pondere disposuisti."

Sapientiae 11:21

Index

1. ABSTRACT

This research project was focused on the use of microwaves (MWs) as an alternative energy source, microwave (MW), for pyrolytic treatments of waste polymeric materials. Particularly it was focused on processing waste biomasses using a multimode microwave oven in a batch process using different reaction conditions and correlating the products obtained with the biomass tested and the conditions adopted.

The liquid fraction, also known as bio-oil, has been obtained with very interesting yields (from 20 to 40 %) and showed very promising performances (*i.e*. low viscosity and limited water content). A large set of analysis was run to characterize the very complex nature of bio-oil: gas chromatographic analysis (GC-MS, GC-FID; spectroscopic analysis (UV-Vis, FT-IR ATR); NMR (^{1}H-NMR); rheological and proximate analysis.

Solids, also known as biochar, have been characterized by FT-IR ATR, ultimate and proximate analysis to assess its possible uses and proving to be suitable as a solid fuel for carbon sequestration processes. Furthermore the samples did not contain any extractable materials.

α-cellulose was studied in order to evaluate the behaviour of the main component of lignocellulosic biomasses during microwave assisted pyrolysis (MAP). With the same aim MAP of Kraft lignin at different pressure was tested to correlate the residual pressure on the yield of aromatics compounds generated from the most abundant aromatic containing polymer.

Finally MAP of common wastes coming from different lignocellulosic sources such as *Arundo donax, Oliva*

europea, Vitis vinifera, and different poplar clones, were tested under different pyrolysis conditions in order to evidence their behaviour during MAP experiments.

Various degradation mechanisms of cellulose and Kraft lignin were deeply investigated and some reaction pathways proposed. The interaction between microwave absorbers and feedstocks was also object of this study.

2. INTRODUCTION

2.1 Lignocellulosic biomasses

Lignocellulosic biomasses are commonly identified as a great number of different sources as algae, weeds and woody biomasses. Among them woody ones are the most available natural and renewable resources[1]. The global amount of lignocellulosic biomass is presently estimated to be 1.24×10^{15} Kg, among which 80% is attributed to woody ones. Wood is exploited as raw material for structural timber[2], sawn wood[3], furniture[4] and pulp[5] but its use for energy production in industrialized countries is presently limited to pellets[6].

Wood is generally defined as the inner tissue of stems, branches, and roots of perennial plants and it is classified like hardwood and softwood Hardwood means wood from dicot angiosperm trees while softwood means from gymnosperm trees. The main components of wood are cellulose, hemicellulose, and lignin but it contains also other inorganic and organic compounds as reported in **Figure 1**.

Figure 1: Scheme of main component of wood

```
                        ┌──────────┐
                        │   Wood   │
                        └────┬─────┘
              ┌──────────────┴──────────────┐
    ┌───────────────────┐       ┌───────────────────┐
    │   Low molecular   │       │   High molecular  │
    │  weight compounds │       │  weightcompounds  │
    └─────────┬─────────┘       └─────────┬─────────┘
       ┌──────┴──────┐             ┌───────┴───────┐
  ┌──────────┐ ┌──────────┐ ┌──────────────┐ ┌──────────┐
  │ Organics │ │Inorganics│ │Polysaccarhydes│ │  Lignin  │
  └──────────┘ └──────────┘ └──────┬───────┘ └──────────┘
                              ┌─────┴──────┐
                        ┌──────────┐ ┌──────────────┐
                        │Cellulose │ │Hemicellulose │
                        └──────────┘ └──────────────┘
```
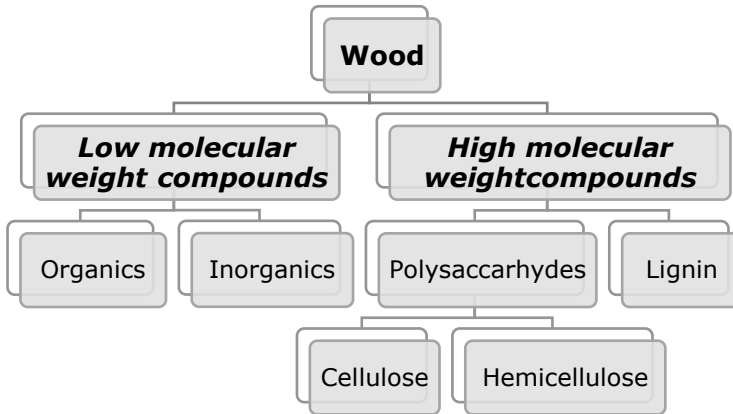
Amount of wood components is affected by several parameters like the composition of the growing soil [7], the climate [8], the harvest period [9] and the species [10].

2.1.1 Components

2.1.1.1 Cellulose

Cellulose is a fibrous, high-crystallinity, water-insoluble polymer, which is found in the protective cell walls of plants, particularly in stalks, stems, trunks and all woody portions of plant tissues[11]. Cellulose is the most important wood component (up to 40% of total weight in a common wood) having linear long chains of *D*-glucopyranose units linked by β-(1,4) glycosidic bonds as shown in **Figure 2**.
Figure 2: Basic structure of the cellulose
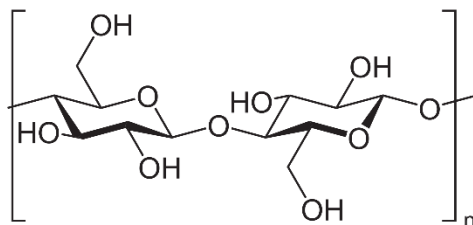
The average molecular weight of native cellulose is between 1.800 KDa and 2.500 KDa[12]. In industrial pulping, cellulose is degraded to average molecular weight among 180 KDa and 540 KDa[13].

Cellulose is one of the useful raw material for textile industry as cotton [14], it is industrially modified to produce viscose and rayon [15], biofuels [16] and paper [17]. Furthermore cellulose is currently used for a lot of fine applications like filler for polymers [18, 19] or drugs [20], stationary chiral phase for liquid chromatography [21], environmentally material for building insulation [22], fire retardant [23] or smokeless gunpowder [24].

2.1.1.2 Lignin

Lignin is a cross-linked macromolecule containing several aromatic units, which are linked together by at least ten different C−C and C−O bonds[25] and it costitute up to 30% of wood weight. Lignin final structure may derive in part from monomers and conjugates other than the three primary monolignols known as *p*-coumaryl, coniferyl, and sinapyl alcohols, **Figure 3**.

Figure 3: Example of a possible structure of lignin with the three basic units evidenced
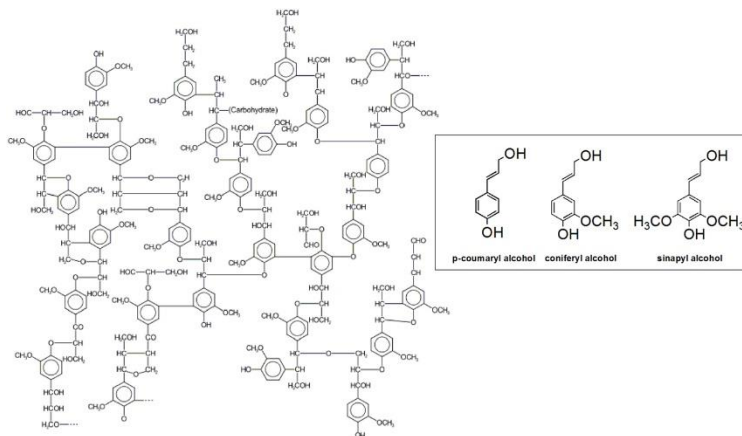
The plasticity of the combinatorial polymerization reactions allows monomers substitution and significant variations in final structure. The final irregular structure of lignin arises from the last step of its biosynthesis that is a random recombination of phenoxy radicals as reported by Felby et al.[26]. Commonly lignin is isolated as pure, sulphonate or Kraft derivatives from biomass feedstock as a residue [27] from pulp and mills industry or from bioethanol production[28]. For its many application Kraft lignin gained an addressable global market [29]. Indeed it is used as low energy solid fuels[30] as currently employed as dispersant in high performance conglomerate[31], for water treatment[32] and for chemicals productions[33].

2.1.1.3 Hemicellulose

Hemicellulose is formed by heterogeneous groups of polysaccharides along with cellulose in almost all plant cell wall in the amount of 10-15% of weight. Hemicellulose biosynthesis is mostly unknown and its composition is highly variable. It can be classified in six main different groups (Xyloglucans, Xylans, Mannans, Glucomannans, CESA-CSL and mixed-linked Glucans) [34] present in different amounts in all species around the world.

2.1.1.4 Inorganic and organics components

Many inorganic components are present (Ca, K, Si, Mg, Al, S, Fe, P, Cl, Na, Mn) as salts or oxide accordingly with Vassilev et al.[35, 36]. Calcium, potassium, magnesium, and phosphorus are the principal trace elements in temperate woods. In fact as reported by Pettersen et al. [37] the inorganic content is strictly correlate to the region of the harvest. Woods from tropical regions have a higher potassium and magnesium content and a lower calcium content those grown in the temperate forests. Obviously the inorganic content is a straight consequence of the soil compositions as reported by several authors[38, 39].

Organic extractives are one of the most interesting component of biomasses and their description is out of this study but for their great relevance two great compounds families have to be mentioned: alkaloids[40] and fatty acids[41].

2.2 Resources demand and consumption: from fossil fuels to biomasses

The primary energy demand in 2010 was 5% higher than the previous year [42]. In parallel, the greenhouse gas emissions recorded a new peak, with growth of 5.8% compared to 2009[43]. The increase in primary energy consumption between 2000 and 2009 is concentrated in a few countries, primarily India and China, and it was mainly driven by coal consumption but this trend has been decreased in the last years[44]. In Europe primary energy demand grew by 3% compared to 2009[45] and the most interesting trend consists of an increase from renewable sources[46]. Anyway oil continues to be the most widely used source in the world: in 2009, constituted 33% of primary demand[47], followed by coal (27%) and gas (21%)[48]. Renewable sources instead meet the 13% and nuclear 6%[45] of total demand. The coal accounted for almost 50% of the increase in global energy demand by source from 2000 to 2010, driven mainly by China's consumption (almost half of the global demand from this source). The global demand for natural gas reached 3,284 Gm^3 in 2010, an increase of 7.4% compared to 2009, one of the highest growth rates recorded in the last 40 years. At the same time chemicals demand rise year by year and in this optic the use of renewable resource have been approached like a promising way to supply, at least partially, the demand of chemicals[49]. There are many examples as the study concerning replacement of synthons for poly(ethylentereftalate) with those produced from renewable resources[50] or producing diesel addictive [51] and green solvent for industrial purposes [52]. While there are many mature and developing technologies for converting biomass to liquid and gas fuels, one of the more straight-forward means of exploiting biomass energy production

through the combustion of solids such as in the application of conventional thermal power generation. Nevertheless release of CO_2 during combustion is an unneglectable environmental issue impossible to be avoided. Anyway in the case of using biomasses the general balance results as zero. Another important task for chemicals manufacturing is the high content of oxygen in raw chemicals from biomass sources with respect to oil derivatives.

2.3 Lignocellulosic biomasses conversion to fuel and chemicals thermal treatments

Thermal treatments of biomass without total or with only partial combustion have the potential to offer a major contribution to meet the increasing demands of energy and chemicals from renewable sources avoiding the production of CO_2. This may be achieved through different three pathways: gassification, liquefaction and pyrolysis.

2.3.1 Gasification

Gasification is the conversion of biomass into a gaseous fuel by heating in a gasification medium such as air[53], oxygen or steam[54] generally at temperatures >800 °C with or without a catalyst[55]. Products from gasification are a mixture of carbon monoxide, carbon dioxide, methane, hydrogen and water vapour. The gas produced can be standardised in its quality and it is easier and more versatile to use than the original biomass. As an examples it can be used as fuel for gas engines and gas turbines, or used as a chemical feedstock to produce liquid fuels[56].

2.3.2 Liquefaction

Liquefaction is a thermal depolymerization process used to convert wet biomass into crude-like oil under moderate temperature and high pressure[57] using acqueous solvent[58], non-acqueous solvent[59, 60] or sub-critical/critical media[61]. This process can be performed with[62] or without a catalyst[60] that is usefully for the improvement of properties of products[63]. Products from biomass liquefaction show interesting energy content for fuel application as reported by several authors[64, 65].

2.3.3 Pyrolysis

Pyrolysis is a high temperature treatment which breaks polymeric macromolecules giving compounds having a lower molecular weight in free-oxygen atmosphere[66]. A pyrolytic treatment leads to three classes of products: a gas (volatile), a liquid, also known as bio-oil, and a bio-char. Several technologies were developed to convert efficiently any sort of polymeric structure into useful products; it is achieved by different heating technology[67], apparatus design[68-71], and sometimes also a catalysts was employed[33, 72, 73].

Among all available technologies this work was focused on the use of an alternative energy source, the microwave (MW), to supply the energy required to induce the cracking reaction (microwave assisted pyrolysis, MAP).

2.4. Microwave assisted pyrolysis

2.4.1 Microwave and materials

MW heating shows a sound and worthwhile application in several fields (food industry, chemical synthesis, material science) due to the benefits of this heating technology[74-76]. MW propagation through the air or materials depends on the dielectric and the magnetic properties of the medium. The electromagnetic permittivity (ε) expressed by a complex number :

$$\varepsilon = \varepsilon' - i\varepsilon''$$

The real component of the permittivity, ε', is commonly referred as the dielectric constant. This value vary significantly with the frequency and temperature[77]. The imaginary component of permittivity, ε'', is the dielectric loss factor ($\tan\delta$). A material showing a low $\tan\delta$ ($<10^{-3}$) is almost no heated when MW pass through the material. Some materials having this property are quarz or polyolefins. On the contrary materials heated using MW are those having dielectrics[78] or conductive properties. A dielectric material contains permanent or induced dipoles and when placed between two electrodes acts as a capacitor. In this situation dipoles try to be oriented with the electric field. The electric field change very frequently causing reorientation of dipoles and this movement cause a friction and consequently the material is heated. A conductive material is crossed by the electric field the charge movement cause a heating due to the joule effect. For this reason materials absorbing MW are heated. These behaviours can be observed in metals as well as in carbon-based materials having a graphitic texture[79].

2.4.2 MAP: a promising tool for waste polymers and biomass valorisation

In the last 10 years MAP gained a remarkable interest for processing waste/contaminate plastic materials in order to obtain fuels or raw materials[80-88]. MAP of biomasses was studied by several authors to obtain high quality bio-oils thanks to a fast heating at moderate temperature (500-700K) followed by a rapid quenching of the intermediate volatile products [89-91]. Moreover MAP can be performed without finely milling the feedstock because MW allows the volumetric heating of sample [92], furthermore the presence of water inside the material may enhance the heating rate and mitigate the temperature reached during pyrolysis avoiding advanced cracking degradation. Even if biomass can absorb MW the addition of a MW absorbers, better if homogeneously blended, improve significantly the quality/quantity of the products formed [93].

MAP of biomass was deeply studied and the main mechanisms can be rationalized in few different steps. The first is the release of moisture from the feedstock, increasing the surface area and improving the pore structure, which favours a quick release of volatiles and minimized char-catalysed secondary cracking. After these primary degradation started other reactions such as formation of levoglucosan from cellulose[94] or formation of multisubstituted aromatic rings from lignin[95] take place. The last step is the occurrence of secondary reactions among the intermediates present with formation of furans, small organic molecules (*i.e* acetic acid, hydroxypropanone), and char. Finally MW power may be easily controlled and the reaction behavior may be tuned to achieve mild pyrolysis conditions as reported by Undri et al.[89].

2.4.3 Thermal heating induced pyrolysis and MAP: briefly overview on differences

Actually the most usefully pyrolytic process for the obtaining of bio-oils is the fast pyrolysis approach. [67]. The conditions required for fast pyrolysis process namely, dry feedstock needed (less than 10%), small particles (less than 3 mm), short residence times (0.5–2s), moderate temperatures (673–773 K), rapid quenching at the end of the process and gave the typical yields of bio-oil, char and gaseous products of 60–70%,12–15% and 13–25%,respectively. Fast pyrolysis approach was used to process a spread of materials such as algae biomasses[96] with low bio-oils yield (around 24%), rice straw, sugarcane bagasse and coconut shell[97] with general yields of 50-60 wt% of bio-oil. Nevertheless in each case the water content into bio-oils was around 50 wt%. MAP approach generally involved lower yield of bio-oil around 30-40 wt% [98-100] and spread values of water content (from 20 to 30 wt%).

As in the case of the yields also the composition of bio-oils is very different. In fast pyrolysis processes the composition is strongly correlated to residence time and for this reason it may vary very much for different types of reactors such as fluidized catalytic cracking [101] simple fluidized-bed reactor[102], auger reactor[103], fixed-bed reactor[104], bubbling fluidized-bed reactor[105]. Contrary to this variety of reactors MAP approached generally involved the use of batch monomode or multimode oven[106]. This prevents to fix the temperature of the process and at the same time allows to spread the variety of reactions during the temperature increase of the process. So in

the case of fast pyrolysis the process can be orientated to the production of different classes of compounds such as phenols[107] or anhydrosugars [108] fixing a proper temperature of the reactor and residence time of feedstock. In the case of MAP this is also possible but it require the use of additive as in the case of levoglucosenone production[109], the application of in-flow condenser systems or for reduced pressure in order to change of the residence time of the products inside the oven. But the spread types of reactors for fats pyrolysis processes have the same problem: the high cost for installation and maintenance up to 200000 $ [110, 111]. MAP industrial plants are cheaper with and average cost of 20000-40000 $[112] and they can be used with little modification both for biomasses and plastic materials[86, 87].

3.MATERIALS, INSTRUMENTS AND METHODS

3.1 Materials

3.1.1 Biomass sources

α-cellulose powder was purchased from Sigma Aldrich dried until constant weight to remove moisture and stored in nitrogen atmosphere at 269 K.

Lignin was supplied by BioChemTex-Mossi Ghisolfi Group and it was dried up to constant weight to remove moisture and stored in nitrogen atmosphere at 269 K.

Rhizomes, stems and leaves of *Arundo donax* were collected during September 2014 from a single ecotype growing in a nursery plantation nearby Sesto Fiorentino, Florence, Italy (N 43°48', E 11° 11', altitude 70 m) [113]. Rhizomes and stems were cutted at a dimension of 30 x 30 x 8 mm while leaves at 30 x 30 x 1 mm.

Fresh residues form single pass pruning of olive trees were collected on December 2009-January -2010 at the Santa Paolina experimental farm of Trees and Timber Institute, National Research Council, located in Follonica, central Italy (42°55' 58" N, 10°45' 51" E, 17 m a.s.l.). Pruning residues were collected from 14-year-old olive trees (*O. europaea* , mixed cultivars belonging to Tuscany germoplasm) cultivated at single-trunk free canopy at a spacing of 5 x 7 m as reported by Spinelli et al.[114].

On August 2015, woody stems of current-year shoots of *Vitis vinifera* (cv. cabernet) were collected from 10 years old plants growing in a farm nearby S. Vincenzo (central Italy). Shoots were 40-80 cm long and they were cut into pieces of 2-3 cm.

Stump-root samples of *two hybrid poplars (P. deltoides x P. nigra*), named clone I and clone II were collected on March 2013 from four years old plants growing in a short rotation coppice poplar plantation (rotation 2

years) at the Santa Paolina experimental farm of Trees and Timber Institute-National Research Council, located in Follonica, central Italy (42°55' 58" N, 10°45' 51" E, 17 m a.s.l.). Poplar stump-roots were ground in a rotor mill and the chips were freeze dried for 96 h and then used for chemical analysis. Mature leaves of ten years old plants of *Populus alba*, named clone III, growing in the garden of CNR in Sesto Fiorentino (Florence) (latitude 43° 50' 4" N, 11° 11' 71" E, 55 m a.s.l.)e were collected on August 2014. After drying (72 h at 338 K) in a ventilated oven they were stored in closed Erlenmeyer flask in nitrogen atmosphere far from light sources.

3.1.2 Chemicals

The carbon powder, employed as MW absorber was the solid from MAP of tires, metal wires depleted (C: 89.01 %, H: 0.83%, N: 0.48%, S: 2.0%). A more detailed characterization of the carbon powder was previously reported [88, 115]. Iron (purity 99.9%), SiC (400 mesh), SiO_2 (400 mesh), Al_2O_3 and DMSO-d_6 (Aldrich 99.8%) were supplied by Sigma Aldrich and used without any purification.

Analytical standard for GC-MS and acetonitrile employed (99.99%, GC grade) were purchased from Sigma Aldrich and used as received.

3.2 Instruments and methods

Ultra Centrifugal mill ZM 200 (Retsch, Haan, Germany) equipped with a 12-tooth rotor and ring sieves or 0.75 and 0.25 mm trapezoid holes, respectively was used for characterization of non structural carbohydrates, starch and lignin.

High-performance liquid chromatography equipped with a pre-column Guard Pak Insert Sugar Pak II (Waters) followed by a SHODEX SUGAR Series SC 1011 8 × 300 mm column (Showa Denko, Germany) was used to evaluate the sugar content of the

samples. The mobile phase was water, Milli Q grade, at 0.5 ml min^{-1}and compounds were quantified by means of a calibration curve using the internal standard method. One sample from each bio-oil was prepared dissolving each sample (10 mg) in MilliQ water (1 mL) obtaining a concentration of 10.00 mg/mL.

A Beckman Coulter DU 800 UV/Vis Spectrophotometer employed at working at a wave length of 280 nm was used to evaluate the lignin percentage.

Kinematic viscosity was detected according to the ASTM method D 2854-00 using an Ostwald viscosimeter thermostated at 298.14 K with a Julabo model ME-18 V. Cyclohexane, chlorobenzene and 1,4-dimethylbenzene were used as standards [116].

Density was determined with a pycnometer thermostated at 298.14 K.

CHN analysis were performed using a Perkin-Elmer CHN/O analyzer model 2400 Series II.

Values of theoretical effective heat of combustion (EHC) were calculated according with Dorez et al. [117].

FT-IR analysis were performed with a Shimadzu model IRAffinity-1, equipped with a Golden Gate single reflection diamond ATR accessory supplied by Specac for liquids analysis and a sapphire cell (length 10 cm) for gas analysis.

^{1}H-NMR spectra were recorded with a NMR Varian Mercury 400 using dimethylsulfoxide-d$_6$ (DMSO-d$_6$) as solvent. Residual hydrogens of the solvent were employed as internal standard and spectra were referenced to tetramethylsilane (TMS). The resonances of protons were attributed according to the ranges reported by Özbay et al.[118] and classical NMR data base [119], that is: δ 10.0-9.0 (aldehyde); 9.0-6.5 (aromatic, furan, and C=CH-OCC); 6.5-5.0 (phenolic OH or C=CH); 5.0-3.3 (CH$_2$-O-C; or CH$_2$-OOC; or Ar-CH$_2$-Ar); 3.3-2.0 (CH$_3$, CH$_2$, and CH linked to an

aromatic ring); 2.0-1.6 (CH, CH_2 of alkyl groups; CH_2 and CH in β position to an aromatic ring); 1.6-1.0 (CH_2, CH_3 of alkyl groups, CH_3 in β–position and CH_2 and CH in γ-position to an aromatic ring or ethereal oxygen); 1.0-0.5 (CH_3 of alkyl groups or CH in γ-position or further of an alkyl chain linked to an aromatic ring).

The water content was evaluated through ^{1}H-NMR spectroscopy using the standard addition method. Three spectra were recorded on the same sample: pure solvent; after the addition of a weighed sample of bio-oil, and after the addition of a known amount of Milli Q water. Areas in each set of three spectra were referenced to the area of the residual hydrogen of the solvent used as internal standard.

Gas chromatographic analysis were performed using a Shimadzu GC–MS QP5050A equipped with a capillary column Petrocol[TM] DH 24160-U, (100 m length, 0.25 mm diameter, 0.5 µm stationary phase) using a 1:30 split ratio operating at 298 K for 15 min, then heated at 2.5 K/min up to 523 K and kept at this temperature for 15 min. A quadrupole mass (MS) detector, with a 70 eV electron ionization ions generator, operating in the range 40–450 m/z was used. Other noteworthy peaks were not detected at higher temperature. Total ion chromatography (TIC) was obtained with a signal/noise ratio of five. Compounds were tentatively identified using the NIST mass spectral library and composition was reported as concentration of single compounds using response factors calculated as reported in the following chapter and using diphenyl as internal standard..

3.2.1 GC-MS quantitative method

Characterization of bio-oils is a difficult task because they are composed by a very large number of compounds. For this purpose a quantitative GC–MS

method was employed to identify the compounds present together with the evaluation of their concentrations. Relative response factors (RRF) of some standard compounds were experimentally determined, while the RRF of the other compounds were calculated according to an upgrading of the method proposed by Undri et al.[120] for GC-FID/MS as reported by Bartoli et.[121] for GC-MS.

3.2.1.1 Sample preparation

One sample from each bio-oil was prepared for GC-MS analysis dissolving 50 mg of bio-oil in acetonitrile (1 mL) obtaining a concentration of 50.00 mg/mL. As internal standard were employed diphenyl (0.5 mg/mL). Solutions of analytical standards were prepared according to the same procedure, at a concentration of 1.0 mg/mL in AcN.

3.2.1.2 RRF prediction

The relative response factor (RRF), with respect to diphenyl, for analytical standards was calculated using **Eq.1**; the results are reported in **Table 1** in the **RRF$_{found}$** column, where the value are reported as molar RRF

$$RRF_i = \frac{MW_i \cdot A_i \cdot C_S}{MW_S \cdot A_S \cdot C_i} \qquad \textbf{Eq. 1}$$

and subscript "i" refers to analytical standard and "S" to the internal standard (diphenyl); A is chromatographic area; MW, molecular weight, and C concentration in mg/mL.

The equation proposed to predict the RRF (called **RRF$_{calc}$**) is reported in **Eq.2**.

$$RRF_{calc\ i} = \frac{rt_S \cdot MW_i \cdot (\sum_k (P_k \cdot n_{kS}^{Z_k}) + Q)}{rt_i \cdot MW_S \cdot (\sum_k (P_k \cdot n_{ki}^{Z_k}) + Q)} \qquad \textbf{Eq. 2}$$

Where subscript "i" refers to an analyte, "S" to an internal standard compound (diphenyl), and "k" to the

type of atom or group present into each compound (Table 1); rt refers to the chromatographic retention time; MW to molecular weight; P_k, and Z_k, are numerical parameters refined for each atom and groups, n is the number of atoms or groups into reference or standard compounds and Q a numerical constant (**Table 1**). The numerical parameters P_k and Z_k and constant Q, used in **Eq.2** were calculated and optimized using the plugin "solver" of MS Excel. This iterative procedure linearized the relation between the RRFs experimentally evaluated with **Eq. 3**, reported in **Figure 1** (**RRF$_{found}$**) for 34 reference compounds, and the **RRF$_{calc}$** obtained with **Eq.2**.

Figure 4: Plott of **RRF$_{calc}$** and **RRF$_{found}$** and **Eq.3**
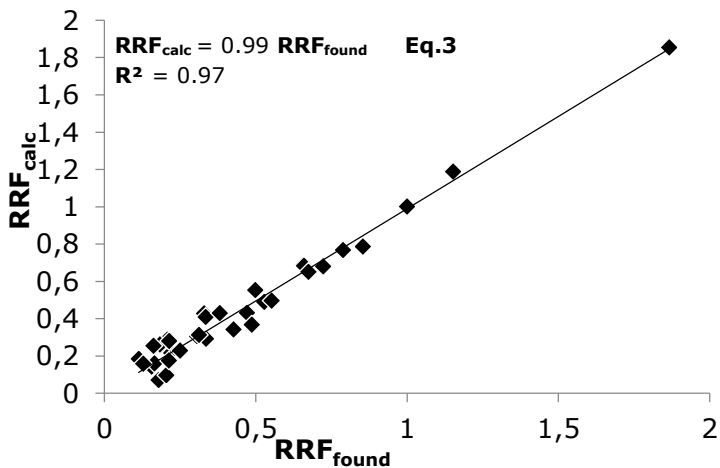
Table 1: List of standard employed with **RRF$_{calc}$** and **RRF$_{found}$**

	Standard compounds	RRF $_{found}$	RRF $_{calc}$
1	3-Penten-2-one	0.11	0.18
2	Furfural	0.13	0.16
3	Pyridine	0.16	0.14
4	Toluene	0.16	0.25
5	3-Methyl-2-butanone	0.17	0.16
6	Acetic acid	0.18	0.07
7	2,4-Pentandiol	0.18	0.26
8	3,3-Dimethyl-2-butanol	0.19	0.26
9	Butyraldehyde	0.20	0.10
10	Valerolactone	0.21	0.29
11	2-Pentanone	0.21	0.17
12	Anilin	0.21	0.28
13	p-Benzoquinon	0.22	0.22
14	Cyclopentanol	0.25	0.23
15	Salicylaldehyde	0.31	0.30
16	Cyclohexanone	0.31	0.31
17	1-Hydroxy-1-methylcyclohexane	0.33	0.43
18	Vanillin	0.33	0.41
19	Phenol	0.34	0.29
20	Sesamol	0.38	0.43
21	Guaiacol	0.43	0.34
22	Acetophenone	0.47	0.43
23	p-Xylene	0.49	0.37
24	Cinnamaldehyde	0.50	0.55
25	1,3,5-Trimethylbenzene	0.53	0.49
26	7-Methyloctadiene	0.55	0.49
27	(-) Carvone	0.66	0.69
28	Benzilidenaceton	0.66	0.68
29	4-Phenyl-2-butanone	0.67	0.65
30	4-Phenyl-2-butanol	0.72	0.68
31	Menthol	0.79	0.77
32	Endo (-) borneol	0.85	0.79
33	2.6-Ditertbutyl-4-methylphenol	1.15	1.19
34	Phenantrene	1.82	1.85

As an example the RRF of a specific compound, vanillin for instance, using diphenyl as the internal standard (**Table 2**) (where vanillin: MW: 152.15; 8 carbon atoms, 8 hydrogen atoms, 3 oxygen atoms, 1 ring, 3 double bonds, 1 carbonyl group, 1 hydroxyl group, 1

ether group; diphenyl: MW:154,21; 12 carbon atoms, 10 hydrogen atoms, 0 oxygen atoms, 2 ring, 6 double bonds, 0 hydroxyl group, 0 ether group), **Eq. 2** could be expressed as reported in **Eq. 4**:

$$\mathbf{RRF_{calc\,i}}$$
$$= \frac{rt_S \cdot 152.15}{rt_i \cdot 124.14}$$
$$\cdot \frac{\left[(P_C\,8^{Z_C}) + (P_H\,8^{Z_H}) + (P_O\,3^{Z_O}) + (P_{ring}\,1^{Z_{ring}}) + (P_{C=C}\,3^{Z_{C=C}}) + (P_{C=O}\,1^{Z_{C=O}}) + (P_{OH}\,1^{Z_{OH}}) + (P_{COC}\,1^{Z_{COC}}) + Q\right]}{\left[(P_C\,7^{Z_C}) + (P_H\,7^{Z_H}) + (P_O\,2^{Z_O}) + (P_{ring}\,1^{Z_{ring}}) + (P_{C=C}\,3^{Z_{C=C}}) + (P_{OH}\,1^{Z_{OH}}) + (P_{COC}\,1^{Z_{COC}}) + Q\right]}$$

Eq.4

The use of RRFs has provided a more accurate way to obtain useful information from the analysis of bio-oils, in comparison with the composition calculated using only the area of the chromatographic peaks. This last method, in fact, did not take into account undetected compounds (non-volatile compounds in GC conditions or non detectable products, such as water).

3.3 Process schemes

Pyrolysis were carried out in a MW oven working at 2.45 GHz, designed and supplied by Bi.Elle s.r.l. (Italy). Two set-ups were used as shown in **Figure 5**.

Figure 5: Set-ups used during MAP experiments
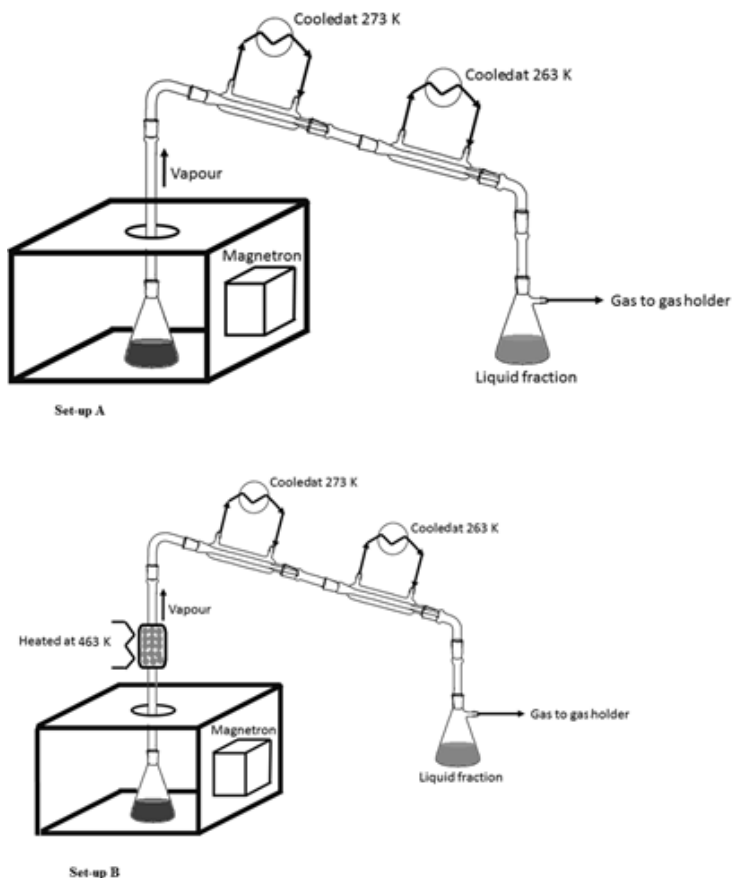
The first one was equipped with an oven with four external MW generators, having an electric power absorption of 8 KW, able of supply up to 6 KW of microwave power inside the oven. It was equipped with a wide angle measuring infrared thermometer, which provides information on the overall temperature inside the oven but not the temperature on the sample

surface. Samples were placed in a 1000 mL borosilicate Erlenmeyer flask inside the oven and connected with two condensing systems cooled at 298 K and 263 K, respectively. Liquids were collected in a flask and gas in a gas holder. This equipment was called set up A. The second equipment, called set up B, used the same MW oven but a fractionating column was placed between the oven and the condensing system. The column had a length of 0.2 m, internal diameter of 30.0 mm, it was filled with glass spheres having a diameter of 4.0 mm.

In MAP experiments samples (100 g) were mechanically mixed with the MW absorber prior the pyrolysis. The Erlenmeyer flask was introduced in the oven then the MW (3KW) was supplied to induce the pyrolysis process. Both set-ups were used at different pressure in experiments with Kraft lignin. Pyrolysis was stopped when gas evolution was not further evidenced. At the end of the experiments when iron was removed from bio-char using a magnet, then bio-char was weighted and characterized. Bio-chars containing carbon, SiC or graphite as MW absorber were also characterized as recovered. Bio-chars containing SiO_2 or Al_2O_3 as MW absorber were washed several times with water and dried into a vacuum oven at 50°C for 24 h, then residues were weighted and bio-char quantified and characterized.

4. RESULTS AND DISCUSSION
4.1 MAP of α-cellulose
4.1.1 Pyrolysis results

MAP of α-cellulose was performed with different MW absorbers, to evaluate the relationship between different MAP conditions, and the amount and composition of bio-char, bio-oil and gas (**Table 2**).

Table 2: Experimental conditions and mass balance of MAP of α-cellulose

Set-up	Time [min]	Absorber		T [K][a]	Products (%)		
		Type	tan δ		Bio-char	Bio-oil	Gas
ID1 A	20	Carbon	0.57-0.80 [122]	723	15.7	32.6	51.7
ID2 A	33	Fe	2.7 [123]	702	27.2	37.0	35.8
ID3 B	20	Carbon	0.57-0.80 [122]	745	16.2	30.0	53.8
ID4 B	37	Fe	2.70 [123]	681	23.6	37.6	38.8
ID5 A	40	SiC	5.15 [124]	659	58.3	29.9	11.8
ID6 A	33	SiO_2	0.40 [124]	481	62.9	35.1	2.0
ID7 A	32	Al_2O_3	0.86 [125]	455	64.1	32.9	3.0
ID8 A	18	Graphite	0.57-0.80 [122]	532	26.7	28.5	44.7

    a) temperature was determined according to Undri *et al.[126]*

Different absorbers convert MW radiation into heat with different efficiency and this allow to heat the material more quickly or slowly. This behavior is mainly attributed to tan δ (**Table 2**) but a strict correlation between results and dissipation factor is hardly obtained because this parameter change with the material and the temperature of the experiment in a different way. Furthermore in the course of pyrolysis the bio-char formed absorb MW and the global

dissipation factor will be further changed. The influence of the MW absorber on the fate of the pyrolysis, was carried out and yield of char, bio-oil or gas from MAP of α-cellulose was reported. Carbon as MW absorber caused a large gasification of cellulose reaching a yield up to 53.8%. On the contrary using iron the formation of gas was reduced while the bio-char was increased up to 27.3% (**ID2**). However the better MW absorbers for the production of bio-char from cellulose were SiO_2 and Al_2O_3, that is the absorbers having a low loss factor, because they gave a bio-char yield of 62.9% (**ID6**) and 64.1% (**ID7**), respectively, with a very low amount of gas (2.0% and 3.0%, respectively).

Substituting carbon with iron as MW absorber, that is using an absorber with a higher loss factor, an increase of the solid from 15.7 to 27.2% and the liquid fraction from 32.6 to 37.0% were obtained at the expense of the gaseous fraction (see **ID1** and **ID2**).

Surprisingly the use of SiC (**ID5**), that is the absorber having the highest dissipation factor, involved a very long reaction time with respect to **ID1** and **ID3** where carbon or iron were employed. In this experiment (**ID5**) abundant formation of a solid and a low gas formation was observed. The use of graphite (**ID8**) instead of carbon (**ID1**) as MW absorber involved the production of a larger amount of solid and lower production of liquid (using the same set up) even if graphite and carbon must have the same dissipation factor. Probably the different rheological properties of these two solids or traces of impurity present in carbon gave a different behaviour. In experiments **ID6**-**ID8** a temperature lower than the starting temperature reported for thermal degradation of cellulose [127] was observed. The presence of hot spots [74, 115] in the bulk of the mixture between cellulose and MW

absorber may be the cause of the large thermal degradation of α-cellulose as shown in **ID5**-**ID7**.

Some experiments were carried out with two different set-ups, where in the first the oven was directly connected with the condensing system (set up A) while in the second a fractionating system was inserted between the oven and the condensing system (set-up B). In this last arrangement high boiling materials were not distilled but remained in the oven for a long time causing a decrease of the liquid fraction and an increase of gaseous and solid fractions (see **ID1** and **ID3**) when carbon was the MW absorber. Different results were obtained using iron as MW absorber (see **ID2** and **ID4**) because the yield of bio-char was reduced and those of bio-oil and gas were improved. This different behaviour may be attributed to the formation of compounds having a low molecular weight that were easily distilled when iron was the MW absorber while these compounds were not formed using carbon as MW absorber.

4.1.2. Characterization of products

4.1.2.1 Bio-chars

Ultimate analysis showed a very low hydrogen amount in all samples (**Table 2**) that is an almost complete pyrolysis and, as a consequence, a very low values of the H/C and O/C ratio [128, 129]. These data suggest the use of this bio-char in carbon sequestration processes [130]. An amount of hydrogen of 1 % was attributed to the batch process employed where a small part of the bio-oil remained in the oven due to the absence of nitrogen as a gas of transport in all experiments [34].

Table 3: Ultimate analysis of char from MAP of α-cellulose

	Ultimate Analysis[a] (%)			O/C	H/C	EHC$_{calc}$
	C	*H*	*O*[b]	*molar ratio*	*molar ratio*	**[MJ/Kg]**
ID1	84.7	1.4	13.9	0.1	0.02	29.6
ID2	79.8	1.4	18.8	0.2	0.02	27.9
ID3	88.5	0.6	10.9	0.1	>0.01	30.9
ID4	79.0	0.2	20.8	0.2	>0.01	27.6
ID5	78.3	0.6	21.1	0.2	0.01	27.4
ID6	74.1	1.8	24.1	0.3	0.02	25.9
ID7	74.3	1.2	24.5	0.3	0.01	26.0
ID8	83.5	1.6	14.9	0.2	0.02	29.2

a) Calculated taking in account the presence of the MW absorber
b) calculated as difference

All bio-chars are suitable to be used as solid fuels in consideration of their EHC$_{calc}$ values (**Table 2**) after an elutriation process in order to remove MW absorbents.

4.1.2.2 Bio-oils

4.1.2.2.1 Physico-chemical properties and ultimate analysis

Brown liquids were collected in all experiments with exception of **ID5** and **ID8** where clearly orange liquids were obtained. Physico-chemical properties and ultimate analysis of bio-oil from MAP of α-cellulose are reported in **Table 3**

Bio-oils did not show any phase separation at room temperature, however their density were very close to 1 g/mL with exception of **ID6** (1.41g/mL) suggesting

the presence of large amount of water. Viscosities of bio-oils were in the range of 1.43-2.34 cP, lower than those reported in several papers, sometimes up to two orders of magnitude [131, 132].

Low values of EHC_{calc} were attributed to high concentration of oxygenated compounds (see ultimate analysis and the following paragraphes on GC-MS analysis) and water present in bio-oils.

Table 4. Rheological properties and ultimate analysis of bio-oil from MAP of α-cellulose.

	Density [g/mL]	Viscosity [cP]	Ultimate Analysis (%)			O/C	EHC_{calc} [MJ/Kg]
			C	H	O^a		
ID1	1.09	2.34	19.6	8.4	72.0	3.7	0.4
ID2	1.09	2.03	19.8	8.9	72.1	3.6	0.4
ID3	1.09	2.16	13.5	2.5	84.0	6.2	0.3
ID4	1.07	1.89	11.4	2.7	85.9	7.5	0.3
ID5	1.05	1.43	14.3	12.7	73.0	5.1	0.4
ID6	1.41	2.13	12.1	8.4	79.5	6.6	0.3
ID7	1.18	1.59	11.3	8.4	80.3	7.1	0.3
ID8	1.07	2.14	20.6	9.2	70.2	3.4	0.4

a) Calculated as difference

4.1.2.2.2 ^{1}H-NMR

In **Figure 6** are showed the ^{1}H-NMR of liquid fractions while normalized integrals, after subtracting water resonance, are reported in **Table 4**.

^{1}H-NMR of all bio-oils showed a large abundance of alkyl groups directly linked to oxygen or in α position to C-O-C while signals of lower intensities were present in the other regions of the spectra. Resonances of mobile protons of carboxylic acids were not detected and this absence may be attributable to acid-base equilibria among acids and hydroxylic functions with formation of protonated species or hydrogen/deuterium exchange between solvent and acids.

Surprisingly the resonances in the region between 4.5-3.3 ppm, that is due to compounds containing CH_2-O-C; CH_2-OOC; ring-join methylene, and Ar-CH_2-Ar moieties, showed high intensities when iron was the MW absorber (**ID5**) and set up B was employed. On the contrary these resonances showed a low intensities when silica, alumina or graphite were used as MW absorber (**ID6**-**ID8**).

Figure 6: ^{1}H-NMR of liquid fraction, water resonance depleted
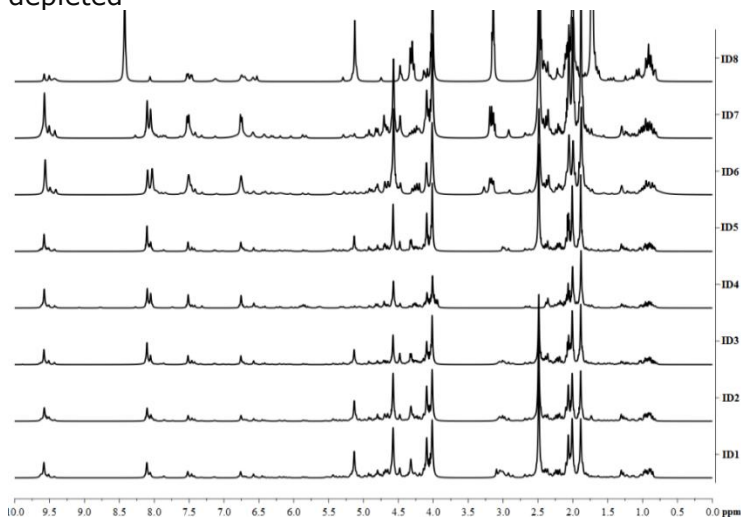
Table 5: Composition (area %) of bio-oils from MAP of *cellulose* obtained from ^{1}H-NMR data

δ (ppm)	Aldehydic protons	Aromatic, furan, and C=CH-OCC	Phenolic "OH" and C=CH olefin	CH_2-O-C; CH_2-OOC; ring-join methylene, and Ar-CH_2-Ar	CH_3, CH_2, and CH linked to aromatic ring and in α-position of carboxylic groups or etheric moiety	CH, CH_2 of alkyl groups; CH_2 and CH in β-position to an aromatic ring	CH_3 in β-position and CH_2 and CH in-γ position to an aromatic ring or ethereal moiety	CH_3 of alkyl groups or further of an alkyl chain linked to an aromatic ring
	10.0-9.0	9.0-6.5	6.5-5.0	4.5-3.3	3.3-2.0	2.0-1.6	1.6-1.0	1.0-0.5
ID1	2.3	5.0	5.1	34.2	38.9	8.9	2.8	2.7
ID2	2.3	8.7	3.4	42.1	29.3	8.9	2.3	2.8
ID3	2.8	5.4	4.7	35.3	37.9	8.0	3.0	3.0
ID4	2.8	7.9	5.1	33.3	34.1	10.4	3.1	3.4
ID5	0.4	0.8	1.4	85.7	8.8	1.5	0.9	0.5
ID6	5.2	13.4	2.5	16.9	36.2	17.9	3.7	4.2
ID7	4.9	15.2	4.2	15.4	33.7	16.8	3.7	6.2
ID8	1.3	9.3	4.1	13.7	36.5	25.8	3.3	5.9

Water content of bio-oils were evaluated through ^{1}H- NMR using an internal standard method as reported in the experimental section and results are shown in **Figure 7.**

Figure 7: Water amount in bio-oils from MAP of α–cellulose through ^{1}H-NMR analysis
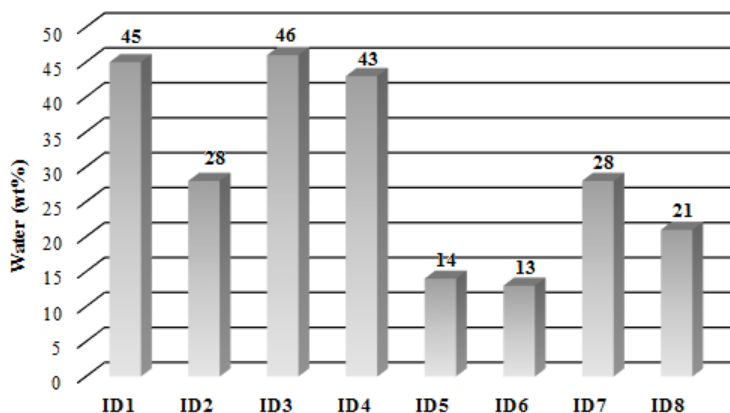
Carbon as a MW absorber (**ID1** and **ID3)**, gave the highest amount of water (45-46 %) among all tests, independent from the set up employed while iron as MW absorber (**ID2**), gave a bio-oil containing 28% of water. However increasing the reaction time of MAP by the use of set up B, the amount of water was increased up to 43% (**ID4**). These results are in agreement with those reported by Undri et al. [89] in the pyrolysis of wood pellets using a MW oven. Pyrolysis using SiC or SiO_2 as MW absorber (**ID5** and **ID6**) required a long reaction time but leading to obtain a bio-oil with a very low water amount (respectively 14% and 13%). Also the use of Al_2O_3 (**ID7**) or graphite (**ID8**) as MW absorber gave a bio-oil with a water content higher than that present in bio-oil **ID5** and **ID6** but lower than 30% (respectively 28% and 21%) confirming the strong influence of the MW absorber on the water formation.

4.1.2.2.3 FT-IR ATR

Bio-oils were also characterized through FT-IR, showing absorptions in the region of 1800-1700 cm^{-1}

($\nu_{C=O}$) due to the presence of carbonyl and carboxylic compounds while absorptions at 1650-1600 cm^{-1} ($\nu_{C=C}$) suggested the presence of C=C bonds. Furthermore bands in the region 1316-1050 cm^{-1} (ν_{C-OH}) showed the presence of hydroxylated compounds. Stretching of C-H bonds were also present, but with a low intensity, in the region of 3200-2750 cm^{-1} (ν_{C-H}) with the exception of **ID5** where these bands had an higher absorbance indicating the presence of large amounts of hydrocarbon moieties, in agreement with the results observed through ^{1}H-NMR analysis (**Figure 8**).

Figure 8: FT-IR spectra of bio-oils **ID1** and **ID5** from MAP of α−cellulose
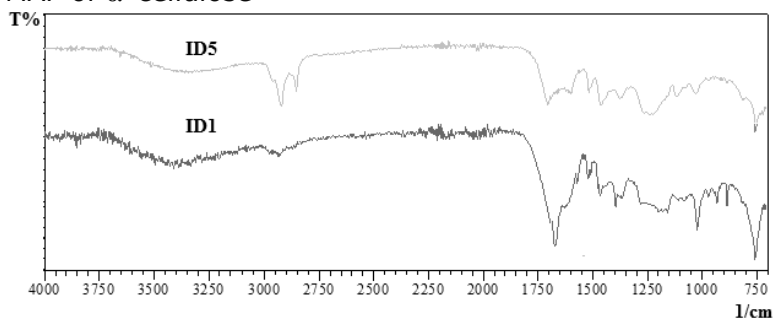
4.1.2.2.4 Quantitative GC-MS

All compounds identified in MAP of α-cellulose with their experimentally found or calculated RRFs, are reported in **Table 6.** The identification of the compounds present was very useful for the suggestion of the mechanism of pyrolysis. The TICs of the GC-MS analysis of **ID1**-**ID8** are reported in **Figure 9** where the peak of diphenyl, employed as internal standard, is marked by a star.

Table 6: Compounds identified in bio-oil from MAP of α−cellulose

COMPOUNDS	RRF	Concentration [mg/mL]							
		ID1	ID2	ID3	ID4	ID5	ID6	ID7	ID8
Acetaldehyde	0.04	12.0	15.6	14.1	10.8	9.9	11.5	6.8	50.3
Diethyl ether	0.08	0.0	0.0	0.0	0.0	6.3	0.0	0.0	0.0
Vinyl acetate	0.06	0.0	10.7	0.0	12.7	0.0	23.8	2.9	22.6
Formic acid	0.05	27.1	58.1	41.3	49.0	80.6	37.3	26.7	67.6
Allyl alcohol	0.07	0.0	0.0	1.6	1.0	0.0	0.0	0.0	4.1
2,3-Butanedione	0.08	10.3	18.9	12.6	12.9	15.5	15.6	10.2	0.0
2-Butanone	0.10	4.2	8.8	4.9	4.9	4.1	3.5	1.5	4.1
Acetic acid	0.07	47.4	69.9	3.4	51.8	89.2	120.6	101.2	43.1
2,3-Dihydrofuran	0.11	1.4	2.6	2.3	1.8	0.0	0.0	0.0	1.3
2-Butenal	0.12	0.0	0.0	0.0	0.0	1.7	0.0	0.0	0.0
1-Hydroxy-2-propanone	0.09	31.5	5.7	32.4	23.6	49.7	68.1	49.8	36.9
Allyl butanoate	0.14	0.0	0.0	0.0	0.0	0.3	0.0	0.4	0.0
Methyl acetate	0.10	2.9	24.6	0.0	0.0	0.0	0.0	0.0	0.0
Benzene	0.16	0.0	0.0	0.0	0.4	0.0	0.0	0.0	0.0
3-Methyl-3-buten-2-one	0.14	1.0	3.4	1.3	1.9	5.4	3.1	1.0	2.3
2,3-Pentanedione	0.14	0.8	2.3	1.1	1.2	2.6	3.0	1.5	4.8
1,3-Dioxol-2-one	0.09	1.7	4.4	2.0	2.6	0.0	4.9	0.0	0.0

2,5-Dimethylfuran	0.18	0.0	0.4	0.0	0.3	2.4	0.0	0.0	0.0
3-Hydroxy-2-butanone	0.13	0.0	0.0	0.0	0.0	0.0	0.3	0.0	0.0
Propanoic acid	0.12	1.4	0.8	2.5	1.4	0.0	6.7	18.7	2.9
Acrylic acid	0.10	1.3	1.3	1.4	1.2	2.2	2.4	2.1	1.0
3-Penten-2-one	0.18	0.8	1.2	1.4	0.9	0.6	0.6	0.2	1.5
1-Penten-3-one	0.18	0.9	0.0	0.0	0.0	0.0	0.0	0.0	0.4
2-Methylfuran	0.16	0.0	0.7	0.3	0.4	0.6	0.3	0.3	0.0
Methyl acrylate	0.13	0.3	0.8	0.7	0.8	1.4	0.0	0.0	0.1
2-Pentenal	0.21	0.0	0.0	0.0	0.0	0.1	0.0	0.0	0.0
5-Hexen-2-one	0.22	0.0	0.0	1.5	0.0	0.0	0.0	0.0	0.0
Ethyl pyruvate	0.15	0.4	1.3	0.0	2.7	0.0	12.3	1.8	1.9
3-Butenyl propyl ether	0.27	0.0	0.0	0.0	0.0	1.2	0.0	0.0	0.0
1-Hydroxy-2-butanone	0.15	3.8	2.5	2.8	1.4	3.1	7.1	3.3	1.8
Methyl pyruvate	0.13	8.4	9.4	7.3	8.1	10.9	3.1	2.2	0.0
3-Methylbutanoic acid	0.21	0.0	0.0	0.0	0.0	0.0	0.0	2.8	0.9
Toluene	0.25	0.0	0.0	0.0	0.2	0.0	0.0	0.0	0.4
Cyclopentanone	0.21	0.3	0.7	0.7	0.5	0.5	0.5	5.7	0.8
γ–Butyrolactone	0.19	0.0	0.0	0.0	0.0	0.0	0.0	0.0	4.7
Ethylene oxide	0.15	0.0	0.0	0.0	0.0	0.0	0.0	0.0	1.3
Allyl formate	0.13	0.0	0.0	0.0	2.5	0.0	0.0	0.0	0.0
Tetramethyloxirane	0.27	0.0	0.0	0.0	0.0	0.1	0.0	0.0	0.0

Butanoic acid	0.18	0.0	0.0	2.0	0.7	0.2	3.4	0.0	0.0
2,4-Dimethylfuran	0.23	0.7	0.0	0.0	0.0	0.0	0.0	0.0	0.0
Furfural	0.16	20.3	1.8	23.9	0.8	83.1	3.1	0.0	48.3
Maleic anyhydryde	0.13	0.0	0.0	0.0	0.0	0.0	6.7	0.7	0.3
Crotonic acid	0.16	0.0	0.0	0.4	0.0	0.0	0.0	0.0	0.0
2-Cyclopenten-1-one	0.21	2.9	2.7	3.3	0.0	0.1	0.0	2.4	0.0
Methyl-2-furoate	0.17	0.0	24.2	0.9	0.0	0.0	39.3	40.5	0.5
2-Ethyl-5-methylfuran	0.28	0.0	0.0	0.0	15.8	0.0	0.0	0.0	0.0
Allyl acetate	0.20	0.0	0.0	1.1	0.0	0.2	2.4	1.1	1.2
2-Oxopropyl acetate	0.19	0.0	0.0	0.0	0.0	0.0	11.7	1.8	3.7
1,2-Ethanediol diacetate	0.21	0.0	0.0	0.0	0.0	0.0	0.0	3.7	0.0
3-Methyl-2-pentanone	0.29	0.0	1.2	0.1	0.0	0.0	0.0	0.0	0.0
2-Methyl-1-pentanol	0.31	0.7	0.0	0.0	0.0	0.0	0.0	0.0	0.0
2-Ethylbutanal	0.21	0.0	0.0	0.0	1.0	1.7	1.3	1.0	0.0
3-Hexanone	0.28	0.0	0.0	0.0	0.0	0.1	0.0	0.0	0.0
Tetrahydro 2-methylfuran	0.25	0.4	0.0	0.4	0.3	0.0	0.0	0.0	0.0
2-Methyl-3-hexanone	0.36	0.0	0.0	0.0	0.0	0.2	0.0	0.0	0.0
Acetoxyacetone	0.19	2.8	3.3	3.9	2.4	4.8	0.0	0.0	0.0
3-Furanmethanol	0.18	0.8	1.3	0.0	0.8	2.6	0.0	0.0	1.7
2-Furanmethanol	0.25	2.3	2.1	0.9	1.8	1.6	1.1	2.9	1.3
5-Methyl-2(5H)-furanone	0.20	0.0	1.7	0.0	0.0	0.0	0.0	0.0	1.4

2-Furanmethanol acetate	0.23	1.1	0.0	0.0	1.4	2.4	2.2	0.0	0.0
γ–Valerolactone	0.97	0.0	0.0	0.0	0.0	0.0	1.0	0.4	0.0
1-Methylcyclohexane	0.35	0.0	0.3	0.2	0.0	0.0	0.0	0.0	0.0
4-Cyclopentene-1,3-dione	0.19	0.4	0.5	0.5	0.4	0.4	0.9	1.3	0.0
4-Methylcyclohexanol	0.35	0.0	0.0	0.1	0.0	0.0	0.0	0.0	0.0
2-Ethyl-1,3-dioxolane	0.23	0.9	0.0	0.0	0.0	0.0	0.0	0.0	0.0
1,3-Dioxolane	0.16	0.0	0.4	0.5	0.4	0.0	0.0	0.0	0.0
1,4-Butanediol	0.21	0.0	0.0	0.0	0.0	0.7	0.0	0.0	0.0
2(5H)-Furanone	0.18	5.5	4.2	4.8	4.6	4.2	11.0	0.0	0.0
3-Methyl-2-butenoic acid	0.22	0.0	0.0	0.2	0.0	0.0	0.0	0.0	0.0
2,3-Dimethyl-cyclohexanol	0.42	0.0	0.0	0.1	0.0	0.0	0.0	0.0	0.0
Methyl 2-butenoate	0.23	0.0	0.5	0.3	0.4	0.2	0.0	0.0	0.0
Glycidyl methacrylate	0.27	0.0	0.0	0.0	0.0	0.4	0.0	0.2	0.0
3-Methyl-2-cyclopenten-1-one	0.29	0.9	0.0	0.0	0.0	0.0	0.7	0.0	0.0
2-Methyl-2-Cyclopenten-1-one	0.29	0.0	1.3	1.2	1.0	0.6	0.0	0.4	0.0
2-Acetylfuran	0.23	1.7	1.0	1.7	1.1	2.2	1.8	0.0	0.0
3-Methyl-2,5-furandione	0.19	0.9	0.0	0.0	0.0	0.4	0.8	0.6	0.0
2,5-Hexanedione	0.28	0.6	0.5	0.6	0.3	0.3	1.7	0.0	0.0
4-Penten-2-one	0.23	0.0	0.0	0.0	0.0	0.0	0.0	0.0	1.2
3-Methylcyclopentanone	0.32	5.3	3.0	3.9	3.3	2.9	7.0	0.0	0.3
Acetic anhydride	0.19	6.5	0.0	0.0	0.0	0.4	10.4	2.5	7.1

3-Methyl-3-penten-2-one	0.32	0.0	0.5	0.0	0.0	0.0	0.6	0.0	0.0
5-Methyl-2(3H)-furanone	0.23	0.4	0.0	1.5	0.7	1.0	1.7	6.6	5.0
4-Methyl-1-penten-3-one	0.32	0.0	0.0	0.0	0.0	0.0	0.0	0.0	0.4
5-Methyl-3-hexen-2-one	0.37	0.1	0.0	0.0	0.0	0.0	0.0	0.0	0.0
Dihydro-3-methylene-2,5-furandione	0.63	0.2	0.0	0.0	0.0	0.1	0.0	0.0	0.0
2-Methyl-1,3-dioxolane	0.22	0.0	0.7	0.0	0.0	0.0	1.1	0.0	0.0
Propylene carbonate	0.20	0.0	3.4	0.0	0.0	0.0	0.0	0.0	0.0
Vinyl propanoate	0.25	2.0	0.0	2.3	3.7	6.0	0.0	0.0	0.0
2-Oxobutyl acetate	0.26	1.3	2.4	1.7	2.2	5.5	10.8	9.3	0.0
Butylpropyl ether	0.43	0.0	0.0	0.0	0.0	0.0	5.8	0.0	0.0
2H-Pyran-2-one	0.21	0.0	0.0	0.2	0.0	0.0	0.0	0.0	0.5
5-Methyl-2-furancarboxaldehyde	0.24	10.7	12.5	10.4	11.3	15.7	16.5	19.0	15.5
Tetrahydro-3-furanmethanol	0.18	0.0	0.0	0.0	0.0	0.0	3.1	0.0	1.7
Tetrahydro-2-furanmethanol	0.28	0.0	0.0	0.0	0.0	0.0	0.0	1.4	0.6
Phenol	0.29	1.9	2.0	1.7	1.8	0.0	3.2	0.9	4.2
Furan-2-carboxylate	0.23	0.0	0.0	0.0	0.0	0.0	1.7	0.0	0.0
3,4-Dihydro-2-methoxy-2H-pyran	0.14	0.0	4.1	11.4	0.0	0.0	0.0	0.0	15.4
Benzofuran	0.47	0.0	0.0	0.0	0.0	0.0	0.0	0.0	0.3
3,4-Dihydroxy-3-cyclobutene-1,2-dione	0.14	14.9	0.0	0.0	10.2	0.0	0.0	0.0	0.0
1,2-Dimethyl-cyclohexene	0.50	0.3	0.0	0.0	0.0	0.0	0.0	0.0	0.0
Glycidol	0.19	0.0	0.0	0.2	0.0	0.0	0.0	0.0	0.0

4,5-Dimethyl-2-cyclohexen-1-one	0.44	0.2	0.0	0.2	0.0	0.1	0.0	0.0	0.0
3-Methylbutanal	0.32	0.0	0.0	0.5	0.0	0.0	0.0	0.0	0.0
2-(2-Furanyl)-1-propanone	0.32	0.0	0.0	0.0	0.0	0.4	0.0	1.3	0.5
4-Methyl-5H-furan-2-one	0.26	1.0	0.6	0.7	0.6	0.3	1.6	0.9	1.0
3-Methyl-1,2-cyclopentanedione	0.31	3.3	0.0	2.8	0.0	2.7	0.0	0.0	2.4
2-Hydroxy-3-methyl-2-cyclopenten-1-one	0.29	0.8	3.3	0.4	3.3	0.2	12.4	9.2	0.0
5-Methyl-3-hexanone	0.45	0.5	0.0	0.0	0.0	0.0	0.0	0.0	0.0
3-Pentanone	0.35	0.0	0.0	0.0	0.0	0.3	0.0	0.0	0.5
Guaicol	0.34	0.0	0.3	0.0	0.0	0.0	0.0	0.0	0.0
1-Acetyl-2-methyl-1-cyclopentene	0.46	0.0	0.0	0.0	0.2	0.0	0.0	0.2	0.0
2,3-Dimethyl-2-cyclopenten-1-one	0.40	0.9	0.7	0.6	0.6	0.4	0.0	0.0	0.5
2,3-Dimethyl-3-pentanol	0.48	0.0	0.0	0.0	0.0	0.0	0.0	0.0	0.3
2-Acetyl-5-methylfuran	0.33	0.0	0.0	0.0	0.0	0.3	0.0	0.5	0.0
5-Methyl-2(5H)-Furanone	0.27	0.0	0.0	0.0	0.0	0.5	0.0	0.0	0.0
Orcinol	0.33	1.8	0.0	0.0	0.0	0.0	0.0	0.0	0.0
o-Cresol	0.37	1.0	1.5	1.2	1.6	0.0	0.0	0.0	2.0
Indene	0.61	0.0	0.0	0.0	0.0	0.0	0.0	0.0	0.2
2,5-Dimethyl-4-hydroxy-3(2H)-furanone	0.27	3.9	4.3	2.9	3.7	3.5	6.0	11.3	0.0

3-Ethyl-2-hydroxy-2-cyclopenten-1-one	0.36	0.6	0.1	0.3	0.3	0.0	3.2	0.6	0.0
1-(2-Furanyl)-ethanone	0.34	0.0	0.0	0.0	0.0	0.0	0.0	3.1	1.8
3-Methyl-ciclohexanone	0.45	0.4	0.0	0.3	0.0	0.0	0.4	0.0	0.0
3-Methylpyrocathecol	0.33	0.2	0.0	0.0	0.0	0.0	0.0	0.0	0.0
m-Cresol	0.38	0.0	2.0	1.2	1.4	0.0	0.0	0.0	0.0
4,5-Dimethyl-2-Cyclohexen-1-one	0.42	0.0	0.0	0.0	0.0	0.2	0.0	0.0	0.0
p-Cresol	0.37	0.0	0.0	0.0	0.0	0.0	0.0	0.0	2.6
Pentanal	0.35	0.0	0.0	0.0	0.0	0.7	4.9	0.8	0.0
Menthyl acetate	0.71	0.0	0.0	0.0	0.0	0.1	0.3	0.2	0.0
5-Hexen-1-ol	0.41	0.0	0.6	0.3	0.5	0.0	0.0	0.0	0.0
2-Ethylcyclohexanone	0.46	0.0	0.0	0.0	0.0	0.0	0.7	9.2	0.0
Maltol	0.26	3.1	1.8	1.2	1.9	2.2	11.2	0.0	0.0
2,3-Dihydro-3,5-dihydroxy-6-methyl-4H-pyran-4-one	0.26	3.1	1.7	1.1	1.6	0.6	1.0	1.6	0.0
4-Methyl-1,3-Dioxane	0.33	0.0	0.0	0.0	0.0	0.9	0.0	0.8	0.0
2-Methylpentanal	0.44	0.0	0.0	0.3	0.0	0.0	0.0	0.0	0.0
Pyrocathecol	0.32	0.0	0.0	0.0	0.0	0.0	5.8	1.7	0.0
4-(5-Methyl-2-furanyl)-2-butanone	0.54	0.0	0.0	0.0	0.0	0.1	0.2	0.3	0.0
Ethylene glycol acetate monomethyl ether	0.26	0.0	0.0	1.1	0.0	0.0	0.0	0.0	0.0

Dimethyl 3-hydroxy-2-methylglutarate	0.39	0.0	0.0	0.0	0.0	0.0	0.3	0.0	0.0
3,5-Dihydroxy-2-methyl-4H-pyran-4-one	0.25	4.7	2.1	2.9	2.3	1.9	0.0	0.0	0.0
Ethyl crotonate	0.39	0.0	0.0	0.0	0.0	0.2	0.0	0.0	0.0
Dihydro-2H-pyran-2,6(3H)-dione	0.27	0.0	0.0	0.0	0.0	0.0	0.0	0.0	0.4
Ethyl methacrylate	0.39	4.4	2.8	1.5	1.8	0.0	0.0	8.0	5.8
Hydroxymethylfurfural	0.28	12.9	12.4	4.3	7.0	5.8	25.7	13.0	13.2
4-Methylpyrocatechol	0.41	0.0	0.0	0.0	0.0	0.0	0.9	0.0	0.0
Ethyl cyclopropanecarboxylate	0.40	0.0	0.0	0.0	0.0	1.8	0.0	0.0	0.0
Triacetin	0.42	0.0	0.0	0.0	0.0	0.1	0.0	0.0	0.0
1,3-Cyclohexanediol	0.41	1.5	0.4	0.4	0.0	0.0	0.0	0.3	0.0
4-Methoxy-ciclohexanone	0.46	0.0	0.0	1.4	0.0	0.0	0.0	0.0	0.0
2-Butene-1,4-diol	0.28	0.0	0.0	0.0	0.0	0.3	0.0	0.0	0.0
Methyl 3-hydroxybutanate	0.34	0.0	0.0	0.4	0.0	0.0	0.0	0.0	0.0
1-(2,5-Dihydroxyphenyl)ethanone	0.41	0.0	0.0	0.0	0.0	0.0	1.1	0.0	0.0
5-Acetoxymethyl-2-furaldehyde	0.39	0.0	0.0	0.0	0.0	0.1	0.6	0.6	0.0
2,6-Dimethyl-4H-Pyran-4-one	0.26	0.0	0.0	0.0	0.0	0.0	0.5	0.0	0.0
tert-Butyl 3-Oxobutanoate	0.52	0.0	0.0	0.0	0.0	0.3	0.0	0.0	0.0
2,2'-Bis-1,3-dioxolane	0.43	0.0	0.0	0.3	0.0	0.0	0.0	0.0	0.0

3-Methyl-2-hexanone	0.62	0.0	0.0	0.0	0.0	0.1	0.0	0.0	1.6
Syringol	0.42	0.0	0.0	0.0	0.0	0.0	0.9	0.0	0.0
Tetrahydro-2-furanmethanol acetate	0.47	0.0	0.0	0.2	0.0	0.0	0.0	0.0	0.0
5,5-Dimethyl-2(5H)-furanone	0.42	0.0	0.0	0.0	0.0	0.0	0.6	0.4	0.0
1,2,4-Trimethoxybenzene	0.55	0.0	0.0	0.0	0.0	0.0	0.3	0.0	0.0
Hexanoic acid	0.49	0.0	0.0	0.0	0.0	0.0	0.0	0.0	20.6
Levoglucosan	0.43	88.4	30.7	42.9	17.3	0.0	5.5	0.8	133.9
Levulinic acid	0.37	2.8	1.4	1.2	0.8	0.0	4.5	0.8	5.5
Galactitol	0.36	0.0	0.8	0.9	0.0	0.0	0.0	0.0	0.0
Ethyl 2-methyl-3-oxo-butanoate	0.53	0.0	0.4	0.4	0.0	0.0	0.0	0.0	0.0
Sorbitol	0.36	3.9	0.0	2.0	0.0	0.0	0.0	0.0	0.0
sec-Butyl Propanoate	0.64	0.4	0.0	0.0	0.0	0.0	0.0	0.0	0.0
3,4,4-Trimethyl-2-cyclopenten-1-one	0.84	0.3	0.0	0.0	0.0	0.0	0.0	0.0	0.0
sec-Propyl propanoate	0.64	0.0	0.0	0.2	0.0	0.0	0.0	0.0	0.0
3,4,4-Trimethyl-2-cyclopenten-1-one	0.84	0.0	0.0	0.1	0.0	0.0	0.0	0.0	0.0
Total assignment %	57.6	47.1	46.5	45.8	49.9	46.0	47.2	57.6	

a) Total assignment was calculated with formula :100*(summa of weight of assignment compounds)/(weight of 1 mL bio-oil-water content

Figure 9: GC-MS chromatograph of MAP of α-cellulose, diphenyl as internal standard is evidenced with a star (*)
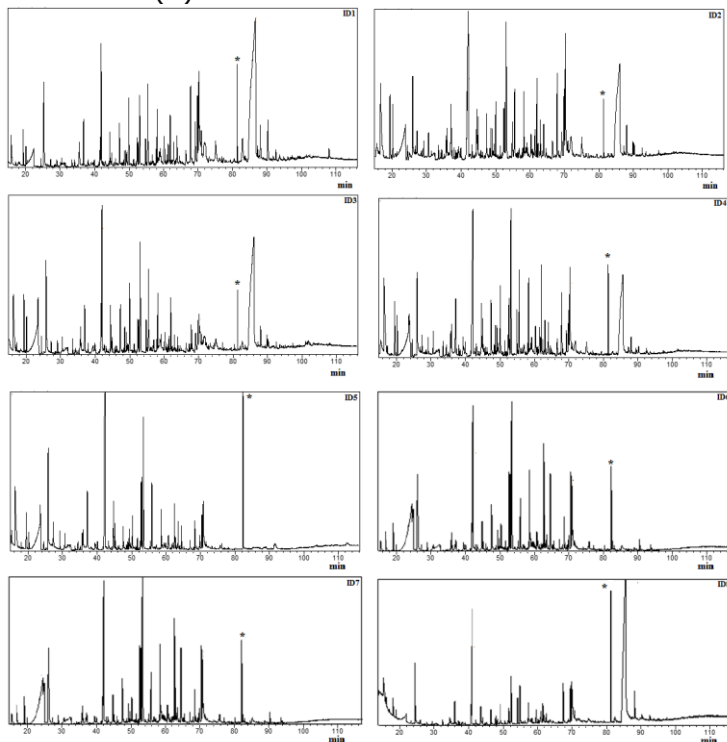
Several authors [133-135] reported levoglucosan as the main compound formed in the pyrolysis of cellulose. It is not thermally stable and decomposes with formation of furanosidic compounds as reported by Kanugia et al. [136] and decomposition increases in the presence of traces of alkali, as catalyst, as reported by Lay et al. [137]. In **Figure 10** are shown the amounts of levoglucosan in the bio-oils formed in the MAP of α–cellulose. Relevant amount of levoglucosan was present in all samples with exception

of **ID4-ID7** but the main factors causing the different amount are hardly rationalized.

**Figure 10:** Levoglucosan content in bio-oils from MAP of α-cellulose
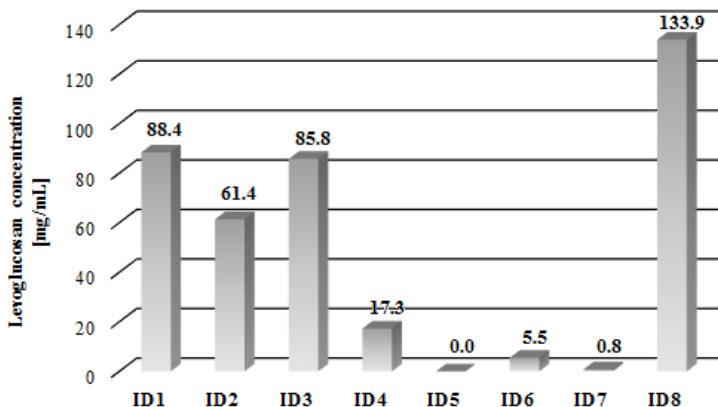
The thermal degradation of cellulose takes place through different mechanisms [138] with high production of levoglucosan however its formation is strongly affected by the MW absorber using MAP. In fact it decreased when carbon (**ID1**) was substituted with iron (**ID2)** as MW absorber using set up A. However different set ups did not affect the formation of levoglucosan if carbon was employed as MW absorber (**ID1** and **ID3**) while iron as MW absorber and set up B caused a drastic decrease of levoglucosan as shown in **ID4**. Surprisingly the use of other MW absorbers such as SiC, SiO_2 and Al_2O_3 (**ID5, ID6** and **ID7**) involved a drastic decrease of levoglucosan concentration. This behaviour was probably due to a catalytic activity of these MW absorbers in the degradation of levoglucosan. Surprisingly graphite as MW absorber (**ID8**) let to obtain the higher amount of levoglucosan (133.9 mg/mL) among all pyrolysis tested. The different concentrations of levoglucosan in **ID1** and **ID8** may

be attributed to residual traces of metal in the carbon used as MW absorber (**ID1)** according with the analysis reported by Undri et al. [115]. It is in fact reported by Richards et al., by Williams et al. [139, 140] that iron may catalyze the partial decomposition of levoglucosan and more in general metal traces can promote sugar degradation [141]. The results obtained in **ID4** were in agreement with these suggestions.

Furans derivatives, acetic acid, acetaldehyde, 1-hydroxy-2-propanone and formic acid were other important products identified in all bio-oils in agreement with the results reported by Collard et al. [127] and Shen et al. [142]. These last authors reported the formation of these small molecules through fragmentation of carbonyl and carboxyl containing compounds. Surprisingly some aromatic compounds were identified in several bio-oils (**ID1-ID4** and **ID6-ID8)** even if their concentration was in the range 2.6-12.2 mg/ml as reported in **Figure 11**.

Figure 11: Content of aromatic compounds in bio-oils from MAP of α-cellulose.
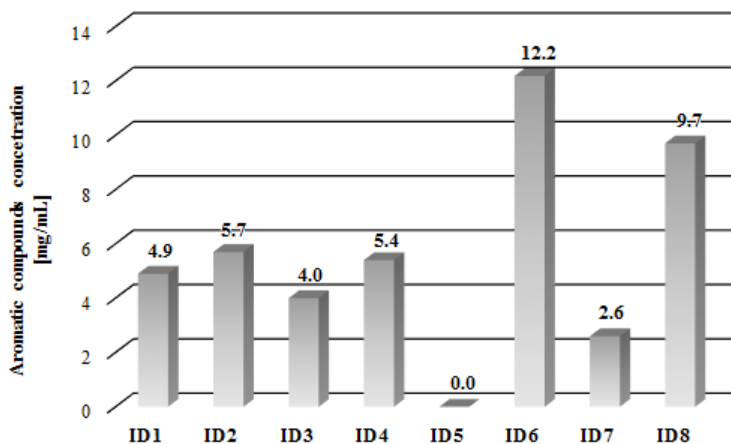
The formation of aromatic compounds from cellulose during MAP was in agreement with results of Al Shra'ah et al. [143] even if in this paper any hypothesis on chemical pathways was reported, while a mechanism of these formations was proposed in **Figure 12**.

Figure 12: Proposed pathways for the formation of aromatic derivatives
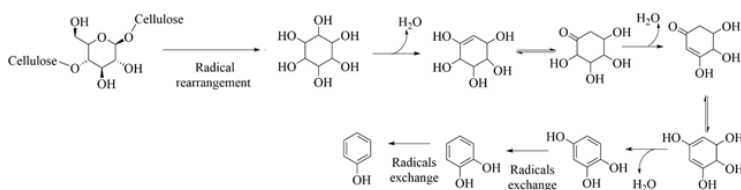
Aromatic moieties may be formed by radical rearrangement of glucose units into cyclic polyhydroxyalkanes. These intermediates through dehydration, tautomeric equilibria and hydrogenolysis may give phenolic derivatives. Different stereoisomers of cyclic polyhydroxyalcohol intermediates were detected through HPLC analysis and these data support the reliability of the pathways proposed for the compounds identified through GC-MS analysis.

4.1.3 Gas fraction

The gas formed through MAP pyrolysis were collected and characterized by FT-IR analysis. These spectra showed strong bands due to the presence of CO_2 and CO with absorptions at 2300 cm^{-1} (ν_{OCO}) and 2150-2000 cm^{-1} (ν_{CO}). Other bands in the range 3750-3500 cm^{-1} and 1875-1750 cm^{-1} were attributed to the presence of water vapor (ν_{OH}) while very small absorptions were attributable to hydrocarbons. As an example the IR spectrum of the gas collected in the experiment **ID1** is reported in **Figure 13.**

Figure 13: IR spectrum of gas fraction of **ID1** from pyrolysis of α–cellulose.
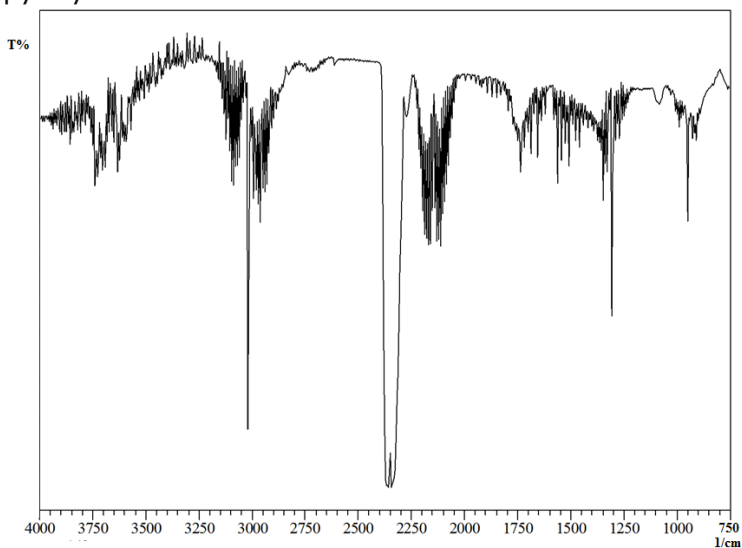
4.2 MAP of Kraft lignin
4.2.1 Pyrolysis results
MAP of Kraft lignin was carried in a multimode microwave oven with a power of 3 KW using carbon as MW absorber and different residual pressure, **Table 7**.
**Table 7:** Experimental conditions and mass balance of MAP of Kraft lignin

	Set- ups	Lignin/Absorber	T [min]	T [K]	Pressure [bar]	Yields [wt%]		
						Bio-char	Bio-oil	Gas
ID9	A	1.98	20	723	1.0	36.8	43.6	19.5
ID10	B	2.00	16	681	1.0	47.6	26.4	26.1
ID11	A	2.00	13	638	0.13	45.0	27.5	27.6
ID12	B	2.00	19	721	0.13	41.4	25.5	33.1
ID13	A	1.99	9	720	0.013	33.2	37.7	29.1
ID14	B	2.00	15	618	0.013	58.4	27.1	14.5

ID9 was carried out at atmospheric pressure (1 bar) for a preliminary estimation on MAP yields and compounds. In this experiment using set-up A a bio-oil yield of 43.6 % and a bio-char yield of 36.8% were reached. Another experiment (**ID10**) was carried out at the same pressure but with the fractionating system. As expected, in this case, a lower bio-oil yield was observed (26.4%) and an increased bio-char (47.6%) and gas (26.1%) production in agreement with Undri et al.[88]. Working with a residual pressure of 0.013 bar, using set-up A or B (**ID11** and **ID12**) a

very close bio-oils yields that is almost the same than **ID10** was obtained (yield   respectively 27.5% and 25.5%). These results were probably due to thermal degradation reactions as shown in **Figure 14**.

Figure 14: Hypothesized chemical pathways for gas phase degradation of high molecular weight lignin fragments
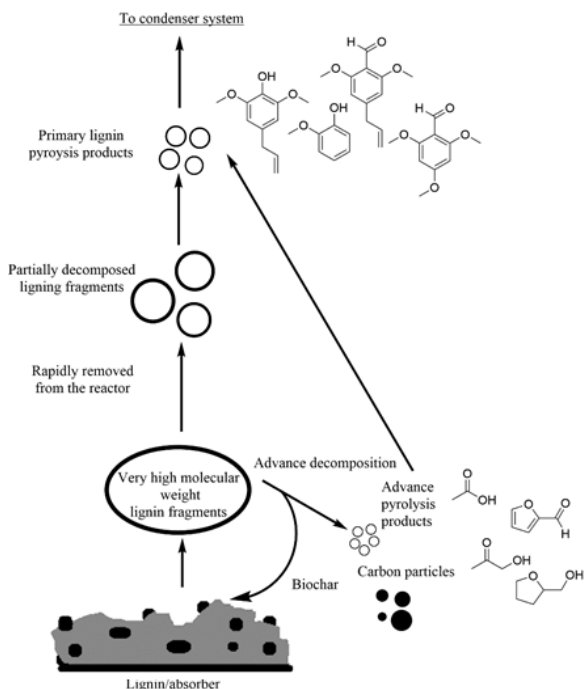
Very high molecular weight lignin fragments can be dragged up from bulk by the gas streaming and reduced pressure applied to the system. In the gas phase these compounds may be involved in further degradation reactions [95, 144]   and produce light products with other carbon particles[81]. Moreover further carbon particles can be formed by cracking reaction [127]. Lignin fragments having high molecular

weight were not removed fast enough and rapidly reacted to single ring aromatic compounds. For this reason in **ID11**-**ID12** production of bio-char was increased (45-47%). On the contrary working at very low residual pressure (**ID13**) an increased yield in bio-oil was observed. This result might be due to a reduced residence time and pressure adopted (0.013 bar). In this case condition may allow the rapid evolution of high molecular weight lignin fragments to products having lower molecular weight with a decrease of other pyrolytic products. This hypothesis was supported by the very short reaction time (9 min), high bio-oil yield (up to 37.7%) and reduced bio-char formation (down to 33.2%). The presence of a fractionating system in (**ID14**) confirm this hypothesis because a very high bio-char yield was obtained (58.4 %).

4.2.2 Bio-oils

4.2.2.1 Physico-chemical properties

All bio-oils collected were deep dark brown liquid at room temperature. In **Figure 15** physico-chemical data of bio-oils are shown.

Figure 15: Trends of viscosity and density values of bio-oils
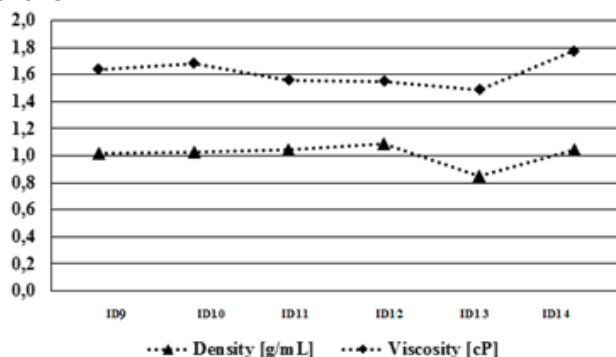
As expected all density and viscosity values were strong influenced by water content. They were close to 1 mg/mL with exception of **ID14** that was significantly lower (0.85 g/mL) in agreement with low content of water and higher content of organic compounds. Viscosity values were lower than those reported for bio-oils obtained through pyrolysis from different lignocellulosic materials[145].

4.2.2.2 ^{1}H-NMR analysis

As previously reported NMR technique was employed for characterization of bio-oils to evaluate the amount of water present. As an example in **Figure 16** is shown the ^{1}H-NMR spectrum of **ID13**.

Figure 16: ^{1}H-NMR spectrum of **ID13**, water signal is depleted
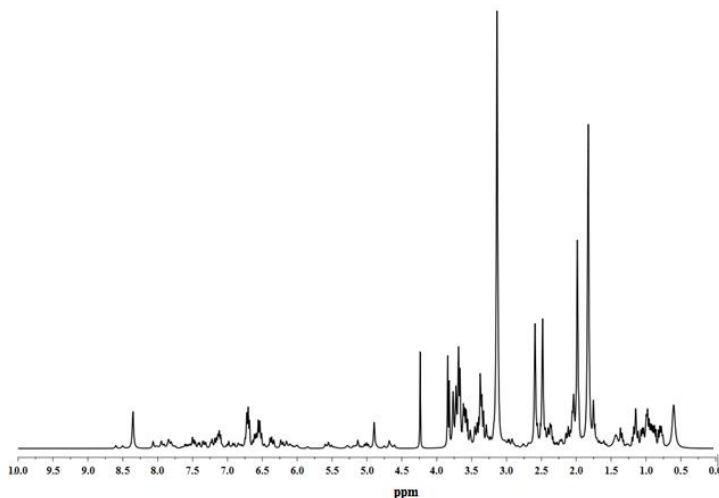
A high percentage of substituted aromatic compounds were present in comparison with data previous reported [90]. In particularly a great amount of aromatic compounds with one or more alkyl substituents were present. Moreover ^{1}H-NMR analysis showed the presence of ethers derivatives (Ar-O-R, R-O-R) particularly in **ID12** (up to 33.08%), unsaturated compounds and a few aldehyde derivatives in all samples. Signals of mobile protons of carboxylic compounds were hardly detected but signals of protons in α position to carboxylic groups were abundant (region 2.5-2.3 ppm) particularly in **ID9** as shown in **Table 9**.

Table 9: Composition (area %) of bio-oils from MAP of Kraft lignin obtained from ^{1}H-NMR data

δ (ppm)	Aldehydic protons	Aromatic, furan, and C=CH-OCC	Phenolic "OH" and C=CH olefin	CH$_2$-O-C; CH$_2$-OOC; ring-join methylene, and Ar-CH$_2$-Ar	CH$_3$, CH$_2$, and CH linked to aromatic ring and in α–position of carboxylic groups or etheric moiety	CH, CH$_2$ of alkyl groups; CH$_2$ and CH in β–position to an aromatic ring	CH$_3$ in β–position and CH$_2$ and CH in γ position to an aromatic ring or ethereal moiety	CH$_3$ of alkyl groups or further of an alkyl chain linked to an aromatic ring
	10.0-9.0	**9.0-6.5**	**6.5-5.0**	**4.5-3.3**	**3.3-2.0**	**2.0-1.6**	**1.6-1.0**	**1.0-0.5**
ID9	0.1	5.6	2.9	7.6	60.8	16.4	2.9	3.8
ID10	0.1	6.0	1.8	14.0	51.8	20.6	2.9	3.0
ID11	0.2	7.6	2.0	19.1	44.3	20.6	3.8	2.7
ID12	0.3	3.7	1.5	33.1	26.1	29.6	2.7	3.1
ID13	0.1	11.8	3.7	19.1	32.8	18.8	6.1	7.8
ID14	0.1	6.7	2.6	26.2	34.8	23.7	2.8	3.1

Water content of bio-oils was evaluated by using internal standard technique as reported and data are shown in **Figure 17.**

Figure 17: Water content (wt%) of bio-oils from MAP of Kraft lignin
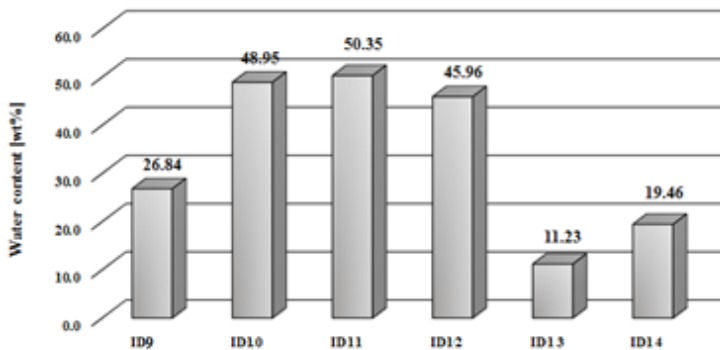
A water percentage of 26.8% was detected in **ID9** in agreement with the data reported in literature for pyrolysis of lignin[131, 146, 147]. A very high water contents were detected in **ID10-ID12** in agreement with experimental set ups and mechanism proposed in **Figure 14**. Very low water content were detected in **ID13** (11.2%), lower than similar bio-oils reported in literature [73, 148]. Also in **ID14** a low content of water was detected and it was attributable to residual pressure (0.013 bar) employed in this experiment.

4.2.2.3 FT IR-ATR analysis

Bio-oils were analysed through FT-IR ATR technique and spectra are shown in **Figure 18**.

Figure 18: FT-IR ATR spectra of all bio-oils
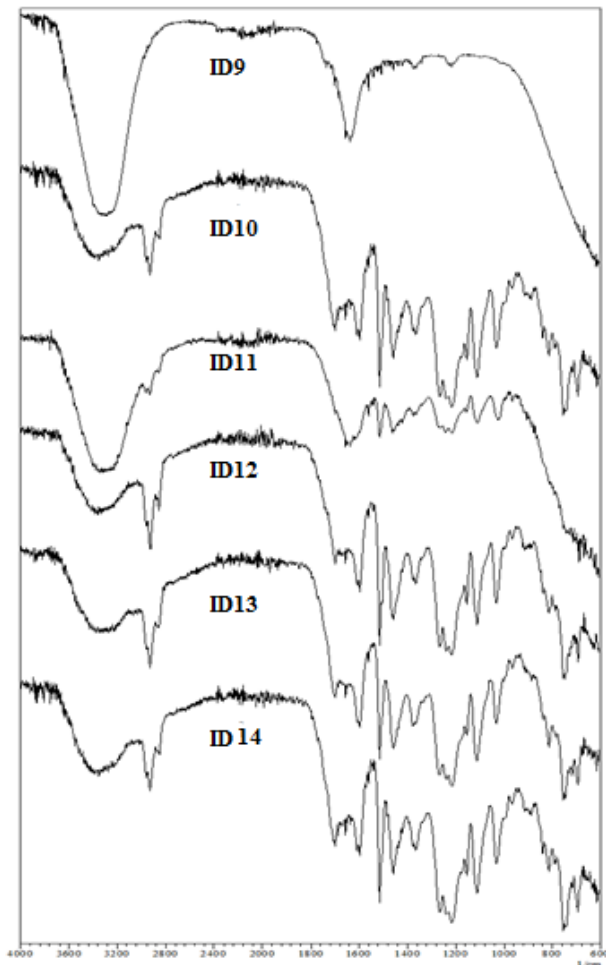
Broad bands in the range of 3750-3500 cm^{-1} showed the presence of water (ν_{OH}) and carboxylic acid (ν_{COO}). According with water contents and water percentage these bands were very strong in **ID9** (acetic acid concetration of 145.2 mg/mL) and **ID11** (water content of 50.4%). The presence of compounds with

an aliphatic chains were confirmed by bands in the range and 2950-2750 cm^{-1} (ν_{C-H}). Meanwhile bands in the range of 3250-3000 (stretching of CH of methylenic groups) cm^{-1} were not observed due to overlapping with the close bands of ν_{OH}. Presence of carbonyl moieties was evidenced by bands in the range of 1875-1750 cm^{-1} ($\nu_{C=O}$) while bands in the close range of 1660-1600 cm^{-1} ($\nu_{C=C}$) were particularly appreciable in **ID10**-**ID14** as well as bands in the range of 1300-1100 cm^{-1}(ν_{C-O} and δ_{O-H}). These bands confirm the presence of aromatic compounds detected in previous analysis.

4.2.2.4 Quantitative GC-MS analysis

Bio-oils were checked also by quantitative GC-MS analysis and a very large amount of compounds were identified (**Figure 19**).

Figure 19: GC-MS chromatograms of **ID9** and **ID14** are showed as case examples.
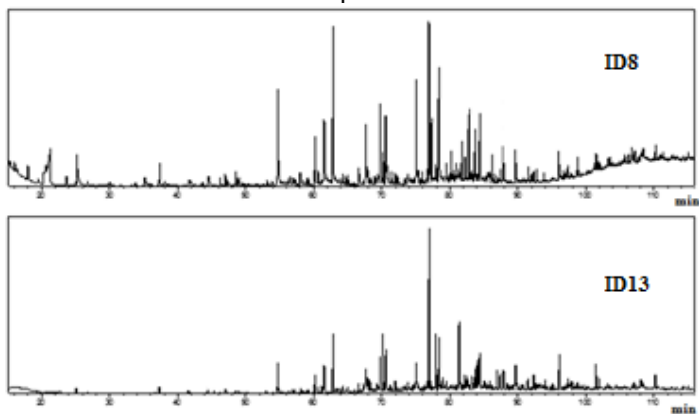
All compounds identified in MAP of Kraft lignin with their experimentally found or calculated RRFs, are reported in **Table 9**.

Table 9: Compounds identified in bio-oil from MAP of Kraft lignin

Compounds	RRF	Concetration [mg/mL]					
		ID1	ID2	ID3	ID4	ID5	ID6
Acetaldehyde	0.04	11.0	0.0	7.2	0.0	0.0	0.0
Formic acid	0.05	19.2	0.0	0.0	0.0	0.0	0.0
Methyl acetate	0.10	0.0	11.7	0.0	0.0	0.0	0.0
Vinyl acetate	0.13	0.0	0.0	2.7	0.0	0.0	0.0
2-Butanone	0.11	0.0	4.7	0.0	0.0	0.0	0.0
Acetic acid	0.18	145.2	39.7	57.6	46.5	0.0	95.5
1-Hydroxy-2-Propanone	0.09	9.3	13.6	105.3	86.5	0.0	136.8
Acetic acid anhydride	0.13	44.1	0.0	0.5	0.0	22.0	28.6
Benzene	0.16	0.0	2.8	0.0	0.0	0.0	0.0
3-Hydroxy-2-butanone	0.13	0.0	0.0	0.0	1.7	0.0	0.0
Propanoic acid	0.12	0.0	0.0	2.9	0.0	0.0	0.0
2-Propenoic acid	0.11	0.0	0.0	0.9	0.0	0.0	0.0
3-Penten-2-one	0.18	0.0	0.0	0.3	0.0	0.0	0.0
3-Propyl-cyclopentene	0.32	0.0	0.0	0.0	2.1	0.0	0.0
1-Hydroxy-2-butanone	0.15	0.0	0.0	3.9	2.4	0.0	0.0
4-Penten-2-one	0.20	0.0	0.0	0.0	1.4	0.0	0.0
Dihydro-2,5-Furandione	0.12	0.0	0.0	1.8	1.7	0.0	0.0
Toluene	0.16	24.1	21.4	1.3	3.3	21.0	4.2

4,4-dimethyl-2-Pentanone	0.28	0.0	0.0	0.6	0.0	0.0	0.0
Cyclopentanone	0.25	0.0	1.8	1.2	1.2	0.0	0.0
2-Methylfuran	0.20	0.0	8.0	0.0	0.0	10.6	0.0
2-Cyclopenten-1-one	0.22	9.4	0.0	8.5	10.6	0.0	14.1
Furfural	0.13	0.0	0.0	3.5	2.2	0.0	19.0
1-(acetyloxy)-2-Propanone	0.19	0.0	4.8	0.0	6.2	0.0	13.3
2-Furanmethanol	0.18	21.4	16.9	26.2	21.3	15.5	43.4
4-Cyclopentene-1,3-dione	0.19	0.0	0.0	0.0	0.0	0.0	3.4
Ethylbenzene	0.36	0.0	1.8	0.0	0.0	1.9	0.0
1,3-Dimethyl-benzene	0.38	5.2	1.9	0.0	0.0	0.0	0.0
2-Oxepanone	0.27	0.0	0.0	0.0	17.3	0.0	0.0
Butyrolactone	0.19	0.0	11.0	0.0	0.0	9.9	0.0
1,2-Dimethyl-Benzene	0.38	4.6	4.0	0.0	0.0	3.4	0.0
2(5H)-Furanone	0.18	0.0	0.0	20.0	0.0	0.0	45.6
Styrene	0.37	0.0	0.0	0.0	0.0	7.6	0.0
2-Methyl-2-cyclopenten-1-one	0.30	0.0	4.8	1.9	3.6	0.0	6.9
1-(2-furanyl)-1-Butanone	0.32	0.0	0.0	0.0	1.1	0.0	0.0
3-Methyl-2-cyclopenten-1-one	0.32	3.4	3.7	3.0	2.9	0.0	8.4
Isobutane	0.15	0.0	0.0	0.7	0.0	0.0	0.0
Propylene Carbonate	0.15	0.0	0.0	0.9	0.0	0.0	0.0
2,3-Pentanedione	0.14	0.0	0.0	0.8	0.0	0.0	0.0
Phenol	0.34	3.7	39.2	15.5	20.8	50.1	34.3

Compound							
Pentanal	0.35	0.0	0.0	49.9	9.1	0.0	61.0
Phthalic anhydride	0.37	0.0	0.0	0.0	0.0	7.5	0.0
Butanoic acid, anhydride	0.38	51.6	0.0	0.0	0.0	0.0	0.0
1,2-Cyclopentanediol, trans-	0.28	0.0	0.0	0.0	0.0	0.0	10.9
Caprolactone	0.24	0.0	0.0	3.5	0.0	0.0	0.0
Benzofuran	0.45	2.4	0.0	0.0	0.0	0.0	5.1
2-Methyl-cyclopentanone	0.28	0.0	0.0	10.1	20.6	0.0	0.0
1,2,3-Trimethyl-benzene	0.52	1.4	0.9	0.0	0.0	0.0	0.0
3-Methyl-1-hexanol	0.46	0.6	0.0	0.0	0.0	0.0	0.0
2-Hydroxy-3-methyl-2-cyclopenten-1-one	0.29	2.1	0.0	0.0	0.0	0.0	0.0
1-Methoxy-4-methyl-benzene	0.42	3.4	0.0	0.0	0.0	0.0	0.0
3-Methyl-1,2-cyclopentanedione	0.32	0.0	7.3	8.6	0.0	0.0	13.1
1-Methoxy-2-methyl-benzene	0.41	0.0	1.9	0.0	0.0	0.0	2.3
2,3-Dimethyl-2-cyclopenten-1-one	0.41	1.2	2.1	1.1	0.0	0.0	0.0
1-Ethyl-3-methyl-benzene	0.53	2.3	0.0	0.0	0.0	0.0	0.0
Dihydro-4-methyl-2(3H)-furanone	0.24	0.0	0.0	1.3	0.0	0.0	0.0
1-Ethyl-2-methyl-benzene	0.54	0.0	0.0	0.0	0.0	0.0	1.2
1-Methyl-3-(1-methylethyl)-benzene	0.60	0.0	0.0	0.0	0.0	0.0	1.9
Limonene	0.67	0.0	2.1	0.0	0.0	6.4	3.5
2-Methylphenol	0.38	18.4	17.8	4.7	0.0	17.9	10.2
Indene	0.57	4.5	2.0	0.0	0.0	4.7	3.0
2,5-Dimethyl-1-hexene	0.49	0.0	0.0	1.4	0.0	0.0	0.0

Compound							
Acetophenone	0.43	0.0	0.0	0.0	0.0	6.8	4.0
4-Methyl-phenol	0.38	41.3	40.7	0.0	17.5	52.6	79.1
2-Methoxy-phenol	0.43	45.3	1.6	25.0	39.5	68.5	2.3
Oxepane	0.27	0.0	0.0	2.0	0.0	0.0	0.0
3,4-Dimethyl-phenol	0.46	0.9	3.0	2.6	1.6	0.0	0.0
1,6-Hexanediol	0.36	0.0	0.0	0.8	0.0	0.0	0.0
3-Ethyl-2-hydroxy-2-cyclopenten-1-one	0.37	0.0	0.0	1.9	0.0	0.0	0.0
2,4-Dimethyl-phenol	0.48	4.0	9.9	0.0	0.0	0.0	0.0
2,3-Dimethyl-phenol	0.48	3.5	1.5	2.4	0.0	5.6	0.0
4-Ethyl-phenol	0.49	15.5	1.1	5.1	7.0	19.0	9.0
Benzoic acid	0.37	0.0	0.0	0.0	0.0	6.9	0.0
2-Pentanone, 5-hydroxy-	0.21	0.0	0.0	2.9	0.0	0.0	0.0
2,5-Dimethyl-phenol	0.49	3.1	15.9	0.0	0.0	0.0	0.0
1-Methyl-1H-indene	0.70	1.8	0.7	0.0	0.0	7.9	0.0
Dihydro-5-propyl-2(3H)-furanone	0.39	0.0	0.0	2.7	0.0	0.0	0.0
3-Methyl-1H-indene	0.75	0.9	0.0	0.0	0.0	5.9	0.0
(2-methylbutyl)-Benzene	0.80	0.0	0.3	0.0	0.0	0.0	0.0
2-Methoxy-5-methylphenol	0.44	2.0	1.8	0.0	0.0	0.0	0.0
4-Ethoxy-phenol	0.44	0.0	0.0	0.0	5.5	0.0	0.0
1,2-Benzenediol	0.33	0.0	14.9	16.9	0.0	0.0	11.1
2-Methoxy-4-methyl-phenol	0.45	23.2	24.0	16.8	17.0	33.0	27.0
Propargyl butanoate	0.40	0.0	0.0	0.7	0.0	0.0	0.0

Compound							
Naphthalene	0.71	6.8	1.4	1.1	2.6	37.8	6.6
2,3-Dihydro-4,7-dimethyl-1H-indene	0.87	0.0	0.0	0.0	0.0	3.5	0.0
2,3-Dihydro-benzofuran	0.57	16.4	6.3	0.5	0.0	0.0	0.0
3-Methyl-benzaldehyde	0.48	0.0	0.0	0.0	0.0	29.3	0.0
2-Methyl-benzaldehyde	0.48	0.0	0.0	0.0	13.0	0.0	24.4
2,3-Dihydro-benzo [b]thiophene	0.53	0.0	0.0	0.0	0.0	5.1	0.0
2,3-Dimethoxytoluene	0.53	1.9	1.9	1.7	1.7	0.0	3.3
3-Ethyl-5-methyl-phenol	0.58	0.0	2.4	0.0	0.0	0.0	0.0
2-(1-methylethyl)-Phenol	0.60	1.3	0.0	0.0	0.0	0.0	0.0
4-Methoxy-3-buten-2-one	0.18	0.0	0.0	2.7	0.0	0.0	0.0
1-Ethoxy-4-methyl-benzene	0.61	1.1	3.5	0.0	0.0	0.0	0.0
3-Methoxy-1,2-benzenediol	0.35	9.3	8.1	12.6	0.0	18.2	10.5
Hexahydro-3-methylene-2(3H)-benzofuranone	0.57	0.0	0.0	7.7	0.0	0.0	0.0
4-Ethyl-2-methoxy-phenol	0.56	23.3	25.2	0.0	8.2	11.9	8.9
Indane	0.82	0.0	1.2	0.0	0.0	0.0	0.0
4-Hydroxy-2-methylacetophenone	0.55	40.4	0.0	0.0	0.0	0.0	0.0
1-Methyl-naphthalene	0.86	0.0	1.1	0.0	0.0	27.8	2.7
2-Methyl-naphthalene	0.90	4.6	0.0	0.0	0.0	4.0	0.0
2,6-Dimethoxy-phenol	0.45	49.1	36.9	0.0	22.5	56.5	32.6
2-Methoxy-5-(1-propenyl)-phenol	0.68	0.0	2.0	0.0	0.0	5.3	2.0
Eugenol	0.63	8.0	0.0	0.0	0.0	0.0	0.0
2-Methoxy-4-propyl-phenol	0.66	0.0	2.3	0.0	0.0	0.0	0.0

Compound							
2,5-Dimethyl-2-(1-methylethenyl)-cyclohexanone	0.87	4.6	0.0	0.0	0.0	0.0	0.0
1,2,4-Trimethoxybenzene	0.55	0.0	0.0	0.0	3.6	17.3	8.2
1-Ethyl-naphthalene	1.04	0.0	0.0	0.0	0.0	5.1	0.0
2,6-Dimethyl-naphthalene	1.05	0.0	0.0	0.0	0.0	5.1	0.0
4-Methoxy-3-(methoxymethyl)-phenol	0.66	11.8	0.0	0.0	0.0	0.0	0.0
1,8-Dimethyl-naphthalene	1.06	0.0	0.0	0.0	0.0	10.8	0.0
1,6-Dimethyl-naphthalene	1.06	0.0	0.0	0.0	0.0	13.3	0.0
2-Methoxy-4-(1-propenyl)-phenol	0.68	13.1	0.0	0.0	6.5	37.8	0.0
1-(4-hydroxy-3-methoxyphenyl)-ethanone	0.50	0.0	0.8	0.0	0.0	0.0	0.0
3-Methyl-1,1'-biphenyl	1.16	0.0	0.0	0.0	0.0	12.5	0.0
Acenaphthene	1.48	0.0	0.0	0.0	0.0	3.1	0.0
1,2,3-Trimethoxy-5-methyl-benzene	0.67	7.4	0.0	0.0	0.0	0.0	0.0
1-(3,4-dimethoxyphenyl)-Ethanone	0.68	6.6	0.0	0.0	0.0	16.6	0.0
2,3,6-Trimethyl-naphthalene	1.22	0.0	0.0	0.0	0.0	8.1	0.0
2,6-Dimethoxy-4-(2-propenyl)-phenol	0.76	0.0	0.0	0.0	0.0	20.2	4.7
Diethyl Phthalate	0.87	0.0	0.0	38.9	0.0	0.0	4.8
Fluorene	1.61	0.0	0.0	0.0	0.0	5.4	0.0
1-Methyl-4-(phenylmethyl)-Benzene	1.35	0.0	0.0	0.0	0.0	2.9	0.0
3,4,5-Trimethoxy-Benzaldehyde	0.64	0.0	0.0	0.0	0.0	3.7	0.0
Anthracene	1.84	0.0	0.0	0.0	0.0	5.9	0.0
Total assignment %		98.8	83.0	95.4	69.6	99.9	95.8

a) Total assignment was calculated with formula:100*(summa of weight of all assignment compounds)/(weight of bio-oil-water content)

A great amount of aromatic compounds were detected in agreement with the formation of primary pyrolytic products from MAP of lignin as reported in **Figure 14**. However aromatic compounds (**Figure 20**) in bio-oils was significantly different by each other bio-oil previously reported

Figure 20: Aromatic percentage calculated on total assignment compounds.
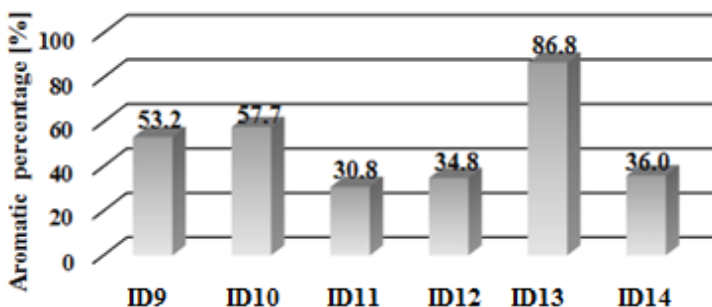

Different percentages of aromatic compounds were strongly connected with set up and residual pressure used in MAP experiments. Working with a residual pressure of 1 bar and the fractionating system (**ID9-ID10**) a little increased in aromatic compounds was detected (around 4%). A similar trend was observed working with residual pressure of 0.013 bar (**ID11-ID12**) but in this case, a large amount of non aromatic compounds was formed. These results were in agreement with the large production of carbon in these two experiments as reported in **Table 6**. In those experiments where a residual pressure of 0.013 bar and set-up A was used, a great percentage of aromatic compounds was detected (**ID 13**) indeed in (**ID 14**) a similar concentration to **ID12** was achieved. According to the pathway proposed in **Figure 14** the

fractionating system may promote a degradation of high molecular weight compounds with an increase of advanced pyrolysis products such as acetic acid (95.5 mg/mL) or 1-hydroxy-2-propanone (136.8 mg/ml) while these compounds were not present in **ID13**. Furthermore these compounds were largely present in experiments with room pressure (**ID9**-**ID12**), with a concentration of the acetic acid up to 145.2 mg/mL (**ID9**) and a concentration of the 2-hydroxy-2-propanone up to 105.3 mg/mL (**ID11**). A similar trend was observed for 2-cyclopenten-1-one, 2-methyl-2-cyclopenten-1-one, 2-methyl-2-cyclopenten-1-one that may be formed from degradative cyclization reaction of lignin aromatic side chains. A little percentage of multiple rings aromatic compounds such as naphtalene and its derivatives produced by radical rearrangement of single rings aromatic compounds was present among aromatic compounds. The main aromatic compounds present were phenol and its derivatives like guiacol, syringol, cresols and their alkylated and methoxylated derivatives. A low amount of aromatic compounds having a long alkyl chain (three or more carbon atom) such as eugenol, isoeugenol or 4-allylsyringol were also detected. These compounds were formed through decomposition process that involved these chains with a production of non aromatic compounds in agreement with Yang[131].

Particularly interesting is the presence of 2,3-bihydro-benzo [b]thiophene, 5.1 mg/mL in **ID5.** The presence of this compound was a proof that a part of the original sulphur content of Kraft lignin was retained into bio-oils as polycyclic organic compounds and they were not converted into light alkyl derivatives as showed in **Figure 21**

Figure 21: Radical degradation of sulphide functions on aromatic moiety of Kraft lignin
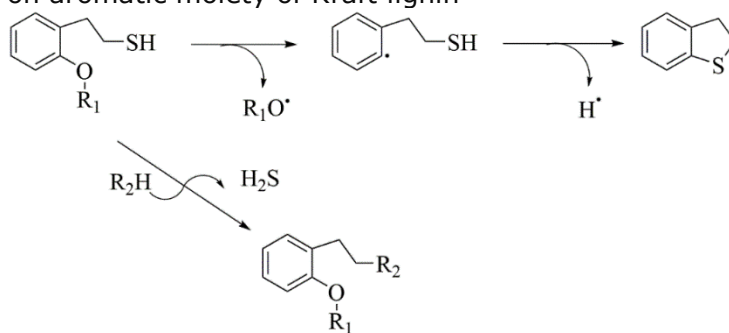
4.3 Arundo donax

Arundo donax (A. Donax) is a perennial rhizomatous cane, native to Eurasia (subtropical regions), ubiquitary in mediterranean basin [149] and considered invasive in many region of the world. *A. donax* has a fast growth rate and it may adapt to different soils and climatic conditions [150]. For these reasons it is commonly proposed as feedstock for bioethanol [151] and biofuels production [152]. From 19th century it has been introduced in southwest of North America where it was diffused rapidly [153]. The uncontrolled diffusion, due to the high vegetative propagation rate, had exposed numerous areas of the world to fire and landslide risk. For this reason this specie is considered a potential damage for a great number of ecosystems in the future. For this reasons a great attention was focused on methodologies to eradicate rhizomes from invaded areas but these procedures still remain time consuming and expensive [154]. Furthermore, a large amount of residues of *A. donax* have been produced every years from environmentally cleaning or biofuel industry and the most common way for their disposal is combustion. Other biological [155] and thermochemical [156-159] treatments are current available and they may be economical or environmental interesting to manage *A.donax* waste. Among thermochemical treatments MAP is a very attractive process in order to produce valuable products as bio-chars and bio-oils.

4.3.1 A. donax preliminary characterization

All *A. donax* organs were characterized in order to detect the amount of cellulose, lignin, proximate and ultimate analysis and results are shown in **Table 10**.

Table 10: Characterization of *A. donax* organs employed for MAP experiments

	Cellulose [wt%]	Lignin [wt%]	Proximate analysis [wt%]				Ultimate analysis [%]			
			Moisture	VOCs	Ash	Fixed Carbon	C	H	O	N
Leaves	35.1	26.2	3.4	83.8	3.1	9.7	49.2	11.2	37.3	2.3
Stems	36.8	27.3	2.9	80.3	2.6	14.2	48.7	12.3	36.8	2.2
Rhyzomes	40.6	23.9	3.8	78.8	5.9	11.5	47.5	10.4	40.2	1.9

The preliminary characterizations of different organs from *A.donax* showed different composition in agreement with results reported by Faix et al. [160]. Leaves and stems showed an amount of cellulose close to 35 % while rhyzomes had a high amount of cellulose (40.6%). Also the lignin content was almost the same in leaves and stems (26.2 and 27.3%, respectively) while rhyzomes showed a low amount of lignin (23.9%). On the contrary the proximate analysis showed the highest content of ash in rhyzomes (5.9%) meanwhile the stems had the lower content (2.6%). Each organs showed a very high VOCs content, very close to 80 %.

4.3.2 Pyrolysis results

MAP experiments on different organs of *A. donax* were carried out in a multimode MW batch reactor, using always carbon as a MW absorber. Experimental parameters and results concerning the amount of bio-oil, bio-char and gas are shown in **Table 11**.

Table 11: Experimental conditions and mass balance of MAP of *A.donax*

Sample		Set-up	r.t.[a] [min]	T [K][a]	Fractions (yield %)		
Code	Type				Bio-char	Bio-oil	Gas
ID15	Leaves	A	18	723	54.3	29.1	16.6
ID16	Stems	A	22	766	48.7	40.9	10.3
ID17	Rhyzomes	A	21	681	59.9	35.5	4.6
ID18	Leaves	B	31	638	60.9	22.1	17.0
ID19	Stems	B	32	702	43.8	38.9	17.2
ID20	Rhyzomes	B	40	707	62.9	28.7	8.4

a) r.t.: reaction time

The first three experiments (**ID15-ID17**) were carried out on different organs of *A. donax* (leaves, stems, and rhyzomes) using set-up A to check the influence of the type of organ in the same pyrolysis conditions. The reaction times of these experiments were close to 20 min indicating a fast pyrolysis process, but reaction temperatures and yields were very different. Leaves (**ID15**) and rhizomes (**ID17**) gave a large amount of bio-char (58.3% and 59.9%, respectively) while it was formed in low amount from stems (48.7%, **ID16**). Surprisingly a very few amount of gas was formed from pyrolysis of rhizomes (**ID17**, 4.6%) while a large amount was obtained from leaves (**ID15**, 16.6%). The largest amount of bio-oil was collected from pyrolysis of stems (**ID16**, 40.9%).

The different yields may be attributable to the different ash content, because it may catalyse in a very efficient way cracking reactions during biomass pyrolysis as reported by Yildiz et al. [141] using a classical heating. This influence was particularly evident in **ID3** where a large amount of bio-char (yield 59.9%) was formed. The use of set-up B caused an increase of the residence time of the materials inside the oven,

especially for high boiling compounds, and this parameter causes an increase of cracking and carbonization processes giving a lower bio-oils production (in the order of 2-7%) and a high yield of bio-char and/or gas as reported for **ID19**. However other factors may affect the products yields in these experiments such as the large variation in the maximum temperature measured during the 3 tests.. For example the highest char yields were obtained in tests where the maximum temperature was lower in agreement with results obtained in classical pyrolysis. Also the low temperature experienced by the sample during the test can affect gas release from rhizomes.

4.3.3. Characterization of products
4.3.3.1Bio-chars Bio-chars were collected at the end of each experiment and were not separated from the carbon used as MW absorber. The different set-ups affects the shape of the bio-char formed, pellets preserving their original form were obtained using set-up A (**ID16**) while disaggregated bio-char was formed using set-up B (**ID 19**) as shown in **Figure 22.**

Figure 22: Samples of bio-char recovered from MAP of *A.donax.*
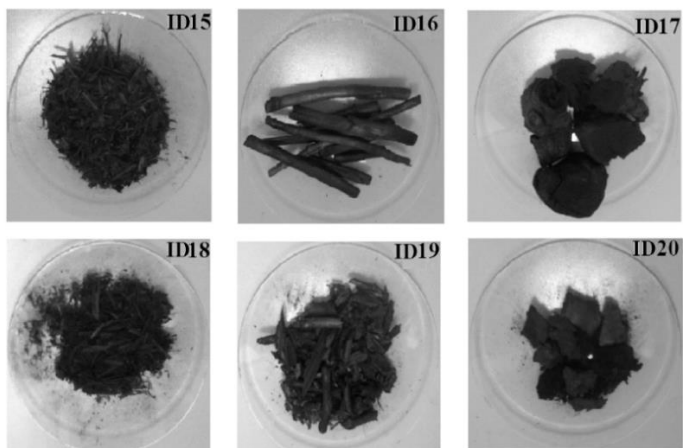
Biochars were analysed through proximate and ultimate analysis, taking into account the amount of carbon employed as MW absorber, in order to evaluate their main characteristics and data are shown in **Table 12.**

Table 12: Characterization of bio-chars recovered from MAP of *A.donax*.

	Proximate analysis [wt%]				Ultimate analysis [wt%]				EHC$_{calc}$ [MJ/Kg]
	Moisture	VOCs	Ash	Fixed Carbon	C	H	O	N	
ID15	2.3	25.3	18.1	54.3	70.4	1.9	26.8	0.9	24.8
ID16	3.3	23.6	10.7	62.4	69.4	1.3	28.3	1.0	24.5
ID17	2.7	20.3	11.1	65.9	85.5	2.1	11.3	1.1	30.2
ID18	2.4	16.4	10.4	70.8	77.4	1.0	20.8	0.8	27.3
ID19	3.9	17.8	10.2	68.1	79.4	1.2	18.5	0.9	28.0
ID 20	3.8	11.4	12.7	72.1	87.5	1.1	10.5	0.9	30.8

A very low amount of hydrogen was present in all samples confirming an advanced thermal degradation process, in agreement with the results reported by Domenach et al. [128, 129]. The O/C molar ratio of biochars was compatible with their use in the carbon sequestration process as reported by Spokas [130] The effective heat of combustion (EHC) of all bio-chars (**ID15-ID20**) was calculated and values obtained suggested the use of these bio-chars for energy production, even if some problems may be present when a high ash content (**ID15**) is present. All samples showed an amount of inorganics up to 18.1 % for **ID 1** and a remarkably high VOCs content (up to 25.3%). The large amount of VOCs may be partially attributed to the batch process where undistilled organic compounds remained in the oven at the end of the process. This VOCs residue was that found in the biochar. The low temperature reached in the pyrolysis may be another cause of the high yield of bio-char as well as of the high VOCs content of bio-char.

All samples were also analysed through FT-IR ATR whose spectra are reported in **Figure 23**.

Figure 23: FT-IR ATR analysis of bio-chars recovered from MAP of *A.donax*
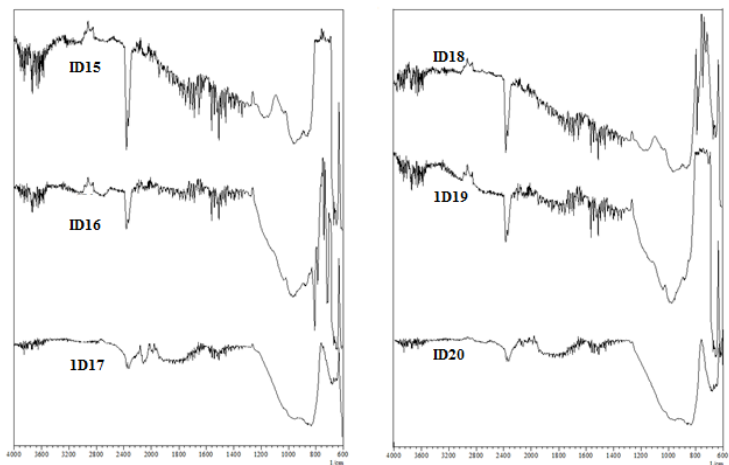
All samples showed the typical intense absorptions of bio-char in agreement with the results reported by Chia et al. [161] and very strong bands in the range of 1200-1000 cm^{-1} attributable to the ν_{C-O} typical of quinoid structures.

4.3.3.2 Bio-oils

4.3.3.2.1 Rheological properties and ultimate analysis

All bio-oils were dark brown liquids, and they were analysed in order to evaluate the main rheological properties and ultimate composition, as reported in **Table 13**.

Table 13: Rheological properties and ultimate analysis of bio-oils from MAP of *A.donax*

| | Viscosity [cP] | Density [g/L] | Ultimate Analysis (%) | | | | EHC$_{calc}$ [MJ/mol] |
			C	H	O^a	N	
ID15	1.52	1.06	23.5	6.4	69.8	0.3	8.2
ID16	1.79	1.05	25.2	7.1	67.1	0.6	8.9
ID17	1.90	1.03	26.1	5.1	68.4	0.4	9.2
ID18	2.11	1.13	20.4	8.7	70.4	0.5	7.2
ID19	1.63	1.04	23.1	8.6	66.0	0.3	8.3
ID20	1.77	1.03	23.2	7.9	68.3	0.6	8.2

a) calculated by difference

Bio-oils did not show any phase separation at room temperature but after storage at -4°C and heating again to room temperature, a partial separation was noticed. All bio-oils showed density in a close range around 1 mg/mL and the greater value of 1.13 mg/mL was shown by **ID 18**, the sample obtained from pyrolysis of leaves. All samples were fluid at room temperature on the contrary to other samples reported in the literature [148]. Viscosities were in the range among 2.11 (**ID18**) and 1.52 cP (**ID15**) and surprising the high value was shown by the sample from pyrolysis of leaves using the set-up B (**ID18**). EHC_{calc} showed low values for all samples and this behaviour was attributed to the presence of water and the high concentration of oxygenated compounds.

4.3.3.2.2 ^{1}H-NMR

NMR was used to perform a preliminary estimation of organic composition and water content through ^{1}H-NMR experiments, as shown in **Figure 25** .

**Figure 25:** ^{1}H-NMR spectra of bio-oils from MAP of *A.donax*, water signal was depleted.
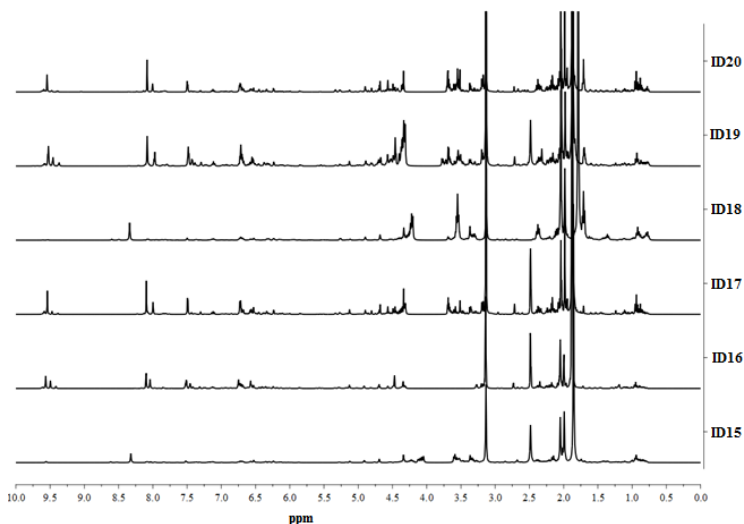
As reported in **Table 14** the ^{1}H-NMR data showed a significantly amount of substituted aromatic compounds (ether, unsatured hydrocarbons and aldehydes) as shown by the area of integrals in the range 4.5-1.6 ppm. Mobile protons of carboxylic acids were not detected due to their exchange with the hydrogen of the solvent, but resonances of protons in α position to carboxylic groups were abundant (region 2.5-2.3 ppm). Bio-oils contained a negligible amount of compounds having an alkyl moiety in agreement with the composition of biomass employed for these experiments

Table 14: Composition (area %) of bio-oils from MAP of *A.donax* obtained from ^{1}H-NMR data

δ (ppm)	Aldehydic protons	Aromatic, furan, and C=CH-OCC	Phenolic "OH" and C=CH olefin	CH_2-O-C; CH_2-OOC; ring-join methylene, and Ar–CH_2-Ar	CH_3, CH_2, and CH linked to aromatic ring and in α–position of carboxylic groups or etheric moiety	CH, CH_2 of alkyl groups; CH_2 and CH in β–position to an aromatic ring	CH_3 in β–position and CH_2 and CH in-γ position to an aromatic ring or ethereal moiety	CH_3 of alkyl groups or further of an alkyl chain linked to an aromatic ring
	10.0-9.0	9.0-6.5	6.5-5.0	4.5-3.3	3.3-2.0	2.0-1.6	1.6-1.0	1.0-0.5
ID15	0.2	1.9	4.9	13.0	32.9	39.9	2.9	4.3
ID16	2.6	11.6	3.8	3.6	30.5	42.9	2.7	2.4
ID17	1.4	6.8	2.3	7.8	27.1	50.1	1.7	2.7
ID18	0.1	1.2	4.0	16.7	24.6	45.5	3.0	4.9
ID19	1.9	9.0	2.7	15.6	26.4	39.8	2.0	2.6
ID20	1.3	5.6	2.0	9.1	24.3	52.5	1.9	3.4

Water content of bio-oils was evaluated by ^{1}H-NMR using internal standard technique as reported in experimental and data are reported in **Figure 26**.

Figure 26: Water content in bio-oils from MAP of *A.donax*
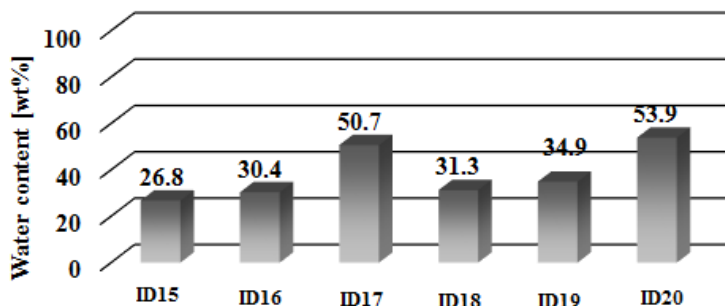

Water was present in different amount depending on different organs and set-ups. Rhizomes, due to the presence of a high cellulose content and other easy dehydratable compounds, gave a large water production (up to 50.7%) while leaves, in almost the same MAP conditions, gave bio-oils having a reduced amount of water (26.8%). Using set-up B (**ID18-ID20**) a higher production of water was observed, and it was attributed to a long reaction time causing a strong dehydration in agreement with the previous results reported by Bartoli et al. [90] using other biomasses.

4.3.3.2.3 FT-IR ATR

Bio-oils were analysed through FT-IR ATR analysis and spectra are reported in **Figure 27**.

Figure 27: FT-IR spectra of bio-oils collected from MAP of *A.donax*.
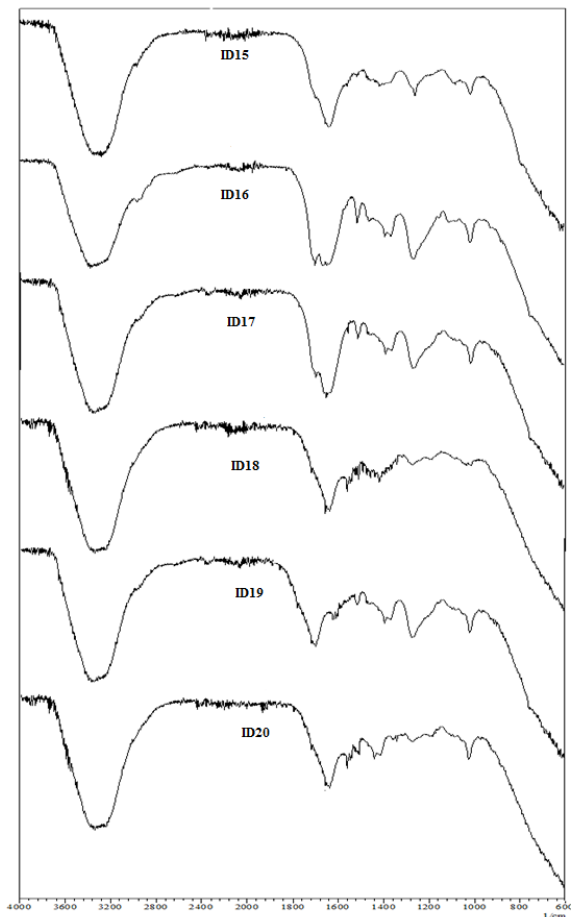
The presence of a large amount of water was confirmed in all bio-oils (bands in the range of 3600-3200 cm^{-1} ν_{OH}). Furthermore all spectra showed the presence of highly oxygenated compounds (bands in the range of 1380-1100 cm^{-1}, ν_{C-O}) in agreement with

GC-MS and ^{1}H-NMR analysis. In all spectra strong absorptions of free carboxylic acid and ester groups were present in the range of 1800-1680 cm^{-1} ($\nu_{C=O}$) while other bands in the range of 3600-3400 cm^{-1} were superimposed with typical water bands (ν_{OH}). Further absorptions attributable to aromatics were shown as medium intensity absorption in the range of 1680-1580 cm^{-1} ($\nu_{C=C}$)

4.3.3.2.4 Quantitative GC-MS

The sixty most abudant compounds identified in MAP of *A.donax* with their experimentally found or calculated RRFs, are reported in **Table 15.** Their identification was very useful for the suggestion of the mechanism of pyrolysis. The TICs of the GC-MS analysis of **ID15**-**ID20** are reported in **Figure 28** where the peak of diphenyl, employed as internal standard, is marked by a star.

Figure 28: GC-MS chromatograms of bio-oils from MAP experiments **ID15-ID20**. Diphenyl as internal standard is marked with a star (*).
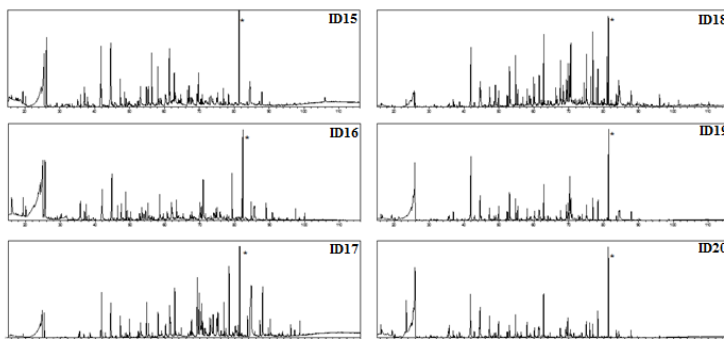
Table 15: Compounds identified in bio-oils from MAP of *A.donax*

Compounds	RRF	Concentration [mg/mL]					
		ID15	ID16	ID17	ID18	ID19	ID20
Acetic acid	0.18	107.0	64.2	22.9	66.7	0.5	78.0
1-Hydroxy-2-propanone	0.09	13.2	12.8	1.4	0.3	5.7	34.0
2-Cyclopenten-1-one	0.22	10.3	2.1	0.0	1.8	0.1	0.0
Furfural	0.13	12.7	20.0	3.8	3.4	6.9	18.3
2-Methylcyclopentanone	0.28	0.4	9.5	0.0	0.0	7.1	0.0
1,2-Ethanediol monoacetate	0.11	0.1	0.0	12.0	0.0	0.0	0.0
2-Oxopropyl acetate	0.19	9.1	4.5	1.9	2.8	9.2	7.7
2-Furanmethanol	0.25	20.4	9.5	4.6	7.0	0.6	14.5
g-caprolactone	0.29	0.0	0.0	0.0	0.0	0.0	16.0
2(5H)-Furanone	0.18	8.7	4.3	0.0	0.0	0.0	0.0
Cyclopropyl carbinol	0.11	9.1	0.0	0.2	0.0	0.0	2.3
1-(2-furanyl)-Ethanone	0.34	4.6	3.7	1.5	2.6	1.5	4.6
Cyclohexanone	0.31	0.0	0.0	0.0	0.0	0.0	11.9
3-Methyl-1,2-cyclopentanedione	0.31	0.5	5.3	0.0	5.8	1.5	8.3
5-Methyl-2-furancarboxaldehyde	0.24	1.3	11.2	2.4	0.0	2.1	7.6
Phenol	0.34	14.4	10.1	6.0	3.7	8.4	13.2
3,4-Dihydro-2-methoxy-2H-pyran	0.3	9.3	6.9	0.0	0.0	0.2	4.7
2-Methyl-4-pentenal	0.33	18.1	0.0	0.0	0.0	0.0	0.0

2,3-Dimethyl-2-cyclopenten-1-one	0.41	2.5	4.4	2.0	2.8	2.8	4.7
o-Cresol	0.38	0.8	6.7	2.9	3.6	6.8	2.8
1-(2-Methyl-1-cyclopenten-1-yl)-ethanone	0.48	0.4	0.0	0.0	0.0	12.9	0.6
p-Cresol	0.38	7.3	9.8	7.2	4.8	1.0	12.8
Pentanal	0.35	0.0	3.8	6.6	4.4	0.0	0.0
Guaicol	0.43	28.1	18.5	9.6	5.9	3.2	0.3
Mequinol	0.48	0.0	0.0	0.0	0.0	6.7	33.4
Maltol	0.27	0.0	2.0	0.9	0.0	10.8	0.5
3-Ethyl-2-Hydroxy-2-Cyclopenten-1-one	0.37	5.1	2.1	2.0	0.0	1.3	4.6
4-Methylpiperidine	0.42	13.3	0.0	0.0	0.0	0.0	0.0
Naphthalene	0.72	0.0	0.0	0.0	0.0	13.7	9.3
4-Ethylphenol	0.49	1.0	5.8	3.7	0.0	0.1	7.4
Heptanal	0.51	3.3	0.0	3.1	0.0	5.8	2.3
o-Tolualdehyde	0.47	0.0	0.0	0.0	0.0	11.5	0.0
Pyrocatechol	0.32	10.3	11.5	12.9	5.6	0.9	7.0
Ethyl methacrylate	0.39	18.6	0.0	0.0	5.7	0.0	0.0
5-Methyl-2-(1-methylethyl)-cyclohexanol	0.74	0.0	0.0	22.5	0.0	0.0	0.0
3-(1-Methylethyl)-cyclohexene	0.7	0.0	0.0	0.0	0.0	13.1	0.0
Homoguaiacol	0.45	0.0	16.2	0.0	0.0	3.6	14.0
5-(Hydroxymethyl)-2-Furancarboxaldehyde	0.27	0.0	29.5	5.5	0.0	11.7	0.0
5-Ethyl m-Cresol	0.57	0.0	0.0	0.0	0.0	22.5	0.0

2,3-Dihydrobenzofuran	0.57	4.7	21.6	10.6	1.9	2.8	9.7
3-(1-Methylethyl)-phenol	0.58	0.0	0.0	0.0	0.0	21.4	0.0
1,4-Dihydro-d-mannitol	0.29	0.0	0.0	0.0	12.7	0.0	0.0
1,3-Cyclohexanediol	0.42	0.0	10.8	4.1	0.0	0.0	0.0
Resorcinol	0.33	14.8	0.0	0.0	0.0	0.1	0.0
3-Methoxypyrocatechol	0.35	1.8	3.7	4.6	2.7	0.7	3.7
p-Ethylguaiacol	0.55	2.7	12.9	7.7	3.6	2.3	18.6
Homopyrocatechol	0.41	0.0	7.1	5.9	3.1	2.3	2.0
4-Hydroxy-2-methylacetophenone	0.55	11.4	0.0	7.9	0.0	3.3	10.6
3-Acetylanisole	0.55	0.0	14.8	0.0	0.0	2.3	0.0
3-Allyl-6-methoxyphenol	0.62	0.0	0.0	0.0	0.0	22.0	0.0
Syringol	0.45	0.0	10.7	13.9	9.6	11.4	20.2
2-Methyl-1-butyl acetate	0.56	5.3	0.0	7.9	0.0	0.0	0.0
2-methoxy-4-propyl-Phenol	0.53	0.0	1.1	0.0	0.0	8.8	1.4
1,3-Dimethylnaphthalene	1.02	0.0	0.0	0.0	0.0	18.7	0.0
Methyl vanillyl ether	0.56	0.0	0.0	0.0	0.0	18.6	5.8
Levoglucosan	0.43	43.9	27.7	47.6	15.2	0.1	0.0
1,2,3-Trimethoxy-5-methyl-benzene	0.68	0.0	0.0	0.0	10.2	0.0	12.5
4,4a,5,6,7,8-Hexahydro-4a-methyl-2(3H)-naphthalenone	1.02	9.7	0.0	8.9	0.0	0.0	0.0
Anthracene	1.84	0.0	0.0	0.0	0.0	26.2	0.0
Levulinic acid	0.38	11.0	7.7	16.8	0.0	0.5	0.0

| Acetophenone | 0.47 | 0.0 | 0.4 | 1.9 | 2.2 | 6.7 | 1.0 |
| Total assignment %[a] | | 65.9 | 62.2 | 70.8 | 31.6 | 53.4 | 66.5 |

a) Total assignment was calculated with formula : 100*(summa of weight of assigned compounds)/(1 mL bio-oil)

GC-MS analysis let to identify a large amount of the compounds present (from 31.6 to 70.8 %) with the exception of **ID18** where only 29.1 % of compounds were identified and quantified through GC-MS. These analysis showed the presence of compounds formed through degradation of lignin and cellulose in agreement with results reported by Isak et al. [162]. Aromatic compounds were also present in large amount as shown in **Figure 28**.

Figure 28: Total amount of aromatic compounds identified through GC-MS analysis
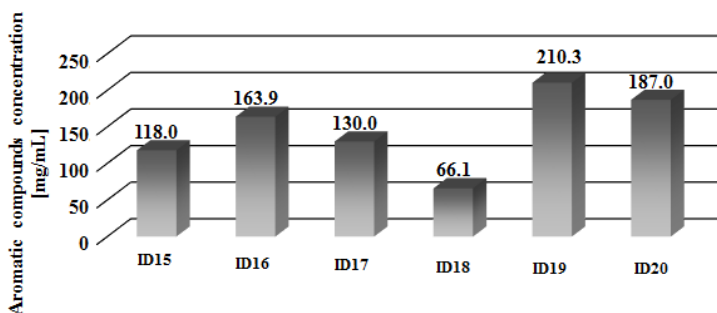
Generally a higher concentration of aromatic compounds were detected when stems were employed (**ID16** and **ID19**) and their formation was increased up to 210.3 mg/mL when set-up B was used (**ID19**).

Among these samples, compounds from primary degradation of lignin such as syringol and methoxyeugenol were detected in appreciable amounts, respectively up to 20.2 mg/mL in **ID16** and 7.0 mg/mL in **ID18** when rhizomes was used as feedstock. A very interesting compound, levoglucosan, was formed from primary degradation of cellulose, and its concentration was affected by all process parameters [133, 137]. It was detected in experiments **ID15- ID17** when set-up A was employed and its formation was in agreement with the cellulose content. It was produced in a concentration higher than 40 mg/mL when leaves or rhizomes were employed but this concentration was reduced to 27.7 mg/mL using stems (**ID16**). The use of set-up B, causing a long reaction time, involved a drastically decrease of levoglucosan in all cases, but this decrease was different among samples with a complete absence of levoglucosane in **ID20**. The progress of the pyrolysis process may be rationalized through a comparison among the data on acetic acid and levoglucosan concentrations in bio-oils. Acetic acid is usually one of the most abundant product formed through an advanced thermal degradation during pyrolysis of a biomasses [163]. A slight increase of acetic acid was shown in the bio-oil formed when the set-up B was employed together with a decrease of levoglucosan formation confirming that the set-up B cause a strong degradation of the biomass employed. The data reported in **Table 15** show the high concentration of furan derivatives when set-up A was used while their concentration decreased using set-up B, due to a strong degradation to simpler structures such as hydroxyacetone or light organic carbonyl and carboxylic compounds. The relevant presence of furanosidic compounds support the presence of only one-phase in the bio-oil because these compounds

show a high affinity with water and may act as a ligand among water and all other organic compounds present.

4.3.3.3Gas

All gaseous fractions were collected and analysed through FT-IR spectroscopy and spectra are reported in **Figure 29**.

Figure 29: FT-IR analysis of total gaseous fractions collected during MAP of *A.donax*.

Thin bands in the range of 3750-3500 cm^{-1} suggested the presence of water vapour (ν_{OH}) while the presence of CO_2 and CO were confirmed by the strong bands at 2400 cm^{-1} (ν_{OCO}), and

2150-2000 cm^{-1}(v_{CO}), respectively. The presence of light hydrocarbons such as methane, ethane, ethylene were evidenced by bands in the range of 3250-3000($v_{CH=C}$) cm^{-1} and 2950-2750 cm^{-1} (v_{CH}). Presence of light carbonyl compounds (such as formaldehyde or acetaldehyde) was evidenced by bands in the range of 1875-1750 cm^{-1} ($v_{C=O}$). The ratio between typical bands of CO_2 at 2400 cm^{-1} (v_{OCO}) and carbonyl compounds at 1875-1750 cm^{-1} ($v_{C=O}$) was practically the same in all spectra and this behaviour was in agreement with the close range of the maximum temperature reached in all experiments.

4.4 Oliva europea

The main issue in waste management of *Oliva europea* (*O.europea*) industry involved the mill residues as reported by several authors [164, 165] and Olive-mill wastewater [166]. The *O.europea* cuts from harvest waste stream are generally burned without any treatment [167]. To avoid combustion and for a full valorisation of this waste stream the use of MAP was studied.

4.4.1   O.europea   preliminary   characterization
O.europea representative samples were characterized in order to detect the amount of cellulose, lignin, proximate and ultimate analysis and results are shown in **Table 16**.

Table 16: Characterization of *O.europea* employed for MAP experiments

Cellulose [wt%]	Lignin [wt%]	Proximate analysis [wt%]				Ultimate analysis [%]			
		Moisture	VOCs	Ash	Fixed Carbon	C	H	O	N
40.2	28.1	1.3	78.7	1.0	19.0	43.1	5.9	49.8	1.2

Olive cuts showed an interesting cellulose content of 40.2 wt% and a lignin content of 28.1%. Proximate analysis showed a very low ash content (1.0%) and a high value of VOCs (78.7%). These values are consistent with the data of ultimate analysis that

showed a high content of carbon and oxygen according to high presence of cellulose.

4.4.2 Pyrolysis results

MAP experiments on *O.europea* were carried out in a multimode MW batch reactor using the set-up A and different absorbers. Experimental parameters and results concerning the amount of bio-oil, bio-char and gas are shown in **Table 17**.

Table 17: Experimental conditions and mass balance of MAP of O.europea

	Time [min]	Absorber	T [K]	Products (wt%)		
				Bio-char	Bio-oil	Gas
ID21	15	Carbon	723	26.5	40.3	33.1
ID22	18	Fe	702	29.5	40.6	29.9
ID23	21	SiC	705	60.3	27.9	11.8
ID24	27	SiO	446	61.2	28.5	10.4
ID25	36	Al_2O_3	450	56.1	25.5	18.4
ID26	17	NaOH	568	2.1	56.2	41.7
ID27	16	Carbon/ Al_2O_3	688	24.3	41.7	34.0

The first experiment was carried out with using carbon and iron as MW absorbers respectively. Yields of different fractions are very close with a bio-oils production around 40 wt% with larger gasification in **ID21** (33.1wt%) and a larger bio-char production in **ID22** (29.5wt%). Very different yields values were observed when silicone based

MW absorber, as SiC(**ID23**) or SiO_2(**ID24**), were used. In both experiments a great amount of bio-char were produced (up to 60 wt%) and a low amount, around 10 wt%, were obtained. A similar behaviour was observed when a different metal oxide, Al_2O_3 (**ID25**), was used. In this case gas production increased to 18.4 with a corresponding decreased of the other fractions. Moreover in **ID24** and **ID25** the maximum temperature reached were very low (446 and 450 K respectively) in comparison with **ID23**. The use of NaOH in **ID26** involved a decrease of bio-char production (24.3wt%) and an increase of gas fraction (up to 34wt%) according with advanced cracking processes as previously described from Guo et al.[168]. In **ID27** the use of carbon with an addition of (ratio 2:1) Al_2O_3 were used as MW absorber. In this case the practically the same yields of **ID 21** were achieved but lower temperature were reached (688K).

4.4.3. Characterization of products
4.4.3.1 Bio-chars

Bio-chars were analysed through proximate and ultimate analysis, taking into account the amount of MW absorber employed, in order to evaluate their main characteristics and data are shown in **Table 18.**

Table 18: Characterization of bio-chars recovered from MAP of *O.europea.*

	Proximate analysis [wt%]				Ultimate Analysis [wt%]			EHC_{calc} [MJ/Kg]
	Moisture	VOCS	ASH	Fixed Carbon	C	H	O^a	
ID21	3.1	14.1	3.0	79.8	79.1	1.2	19.7	27.6
ID22	3.9	13.1	9.6	73.4	81.2	1.2	17.6	28.4
ID23	2.9	12.0	5.9	79.2	78.8	1.4	19.8	27.5
ID24	3.2	16.3	11.6	68.9	72.1	1.3	26.6	25.2
ID25	3.6	11.0	5.5	79.9	77.0	2.4	20.6	26.9
ID26	3.0	9.9	6.3	80.8	75.1	2.1	22.8	26.2
ID27	3.2	8.1	5.4	83.3	79.3	1.8	18.8	27.7

a) Calculated as difference

All bio-chars showed interesting properties that is a low ash content (among 3.0 and 11.6 %), high values of fixed carbon (close to 80 wt%) and combustion values around 25-28 MJ/Kg. All bio-chars collected showed C in the range of 75-82 %.

Undri et al.[115] reported the presence of hot spots in the bulk during MAP. The use of Al_2O_3 allowed to check this behaviour through XRPD analysis. In fact Al_2O_3 has many different phases that have known transition temperatures and different XRPD patterns [169]. In **ID25** and **ID27** α-phase was used and in figure 30

were reported the XRPD analysis of Al_2O_3 mixed with bio-char recovered after MAP experiments.

Figure 30: XRPD analysis of 1) starting $\alpha-Al_2O_3$, 2) Al_2O_3 recovered from **ID25**, 3) Al_2O_3 recovered from **ID27**
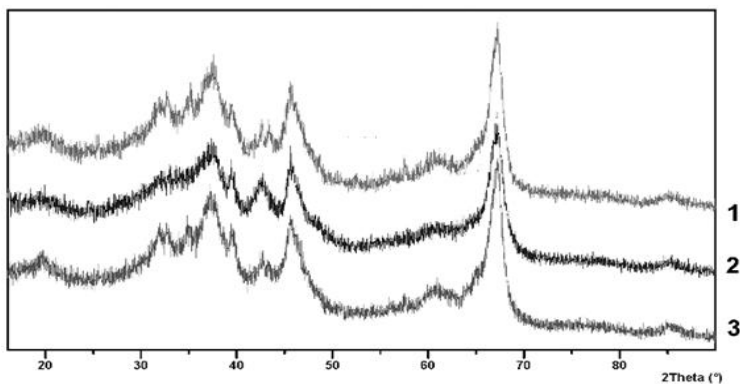
All XRPD traces showed the same peaks and these spectra are a strong suggestion that the same temperature was reached in tests **ID25** and **ID27** because the same Al_2O_3 specie were present.

4.4.3.2 Bio-oils

4.4.3.2.1 Rheological properties and ultimate analysis

All bio-oils were dark brown liquids, and they were analysed in order to evaluate the main rheological properties and ultimate composition, and results are reported in **Table 19**.

Table 19. Rheological properties and ultimate analysis of bio-oil from MAP of *O.europea*

	Density [g/mL]	Viscosity [cP]	Ultimate Analysis [%]			EHC_{calc} [MJ/Kg]
			C	**H**	**O[a]**	
ID21	1.1	1.91	22.4	6.8	70.8	7.8
ID22	1.0	1.72	24.0	6.1	69.9	8.4
ID23	0.9	1.60	25.9	5.0	69.1	9.0
ID24	1.0	1.53	23.4	7.4	69.2	8.2
ID25	1.0	1.40	23.1	7.6	69.3	8.1
ID26	1.1	2.10	23.2	8.5	68.3	8.1
ID27	1.0	1.54	23.8	8.3	67.9	7.8

a) Calculated as difference

Bio-oils did not show any phase separation at room. All bio-oils showed density in a close range around 1 mg/mL. All samples were fluid at room temperature differently to other samples reported in the literature Viscosities were in the range among 2.10 (**ID26**) and 1.40 cp (**I25**). EHC_{calc} showed low values for all samples, close to 8 MJ/Kg, and this behaviour was

attributed to the presence of water and the high concentration of oxygenated compounds.

4.4.3.2.2 ^{1}H-NMR

NMR was used to perform a preliminary estimation of the presence of organic compounds and water, as shown in **Figure 31** .

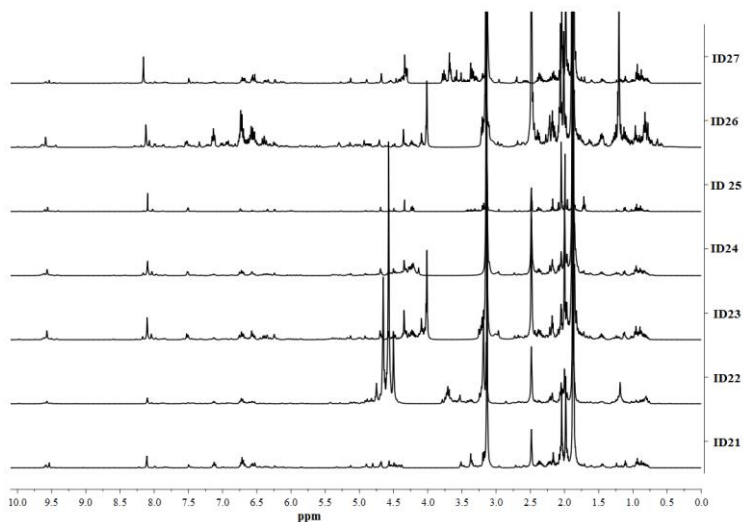**Figure 31:** ^{1}H-NMR spectra of bio-oils from MAP of *O. europea*, water signal was suppressed.

Table 20: Bio-oils from MAP of *O.europea,* composition (area %) obtained from ^{1}H-NMR data

δ (ppm)	Aldehydic protons	Aromatic, furan, and C=CH-OCC	Phenolic "OH" and C=CH olefin	CH_2-O-C; CH_2-OOC; ring-join methylene, and Ar-CH_2-Ar	CH_3, CH_2, and CH linked to aromatic ring and in α-position of carboxylic groups or etheric moiety	CH, CH_2 of alkyl groups; CH_2 and CH in β-position to an aromatic ring	CH_3 in β-position and CH_2 and CH in-γ position to an aromatic ring or ethereal moiety	CH_3 of alkyl groups or further of an alkyl chain linked to an aromatic ring
	10.0-9.0	9.0-6.5	6.5-5.0	4.5-3.3	3.3-2.0	2.0-1.6	1.6-1.0	1.0-0.5
ID21	0.1	0.3	4.6	2.0	11.0	34.9	44.2	2.9
ID22	0.8	10.6	3.9	4.5	38.3	24.4	11.2	6.2
ID23	1.0	3.6	1.5	3.4	42.4	43.5	1.8	2.8
ID24	0.9	4.5	1.9	7.2	34.8	45.3	2.4	3.0
ID25	0.7	4.4	2.6	9.2	37.4	40.8	2.3	2.6
ID26	0.9	5.7	2.3	14.8	38.8	26.7	7.1	3.8
ID27	0.9	6.1	2.2	3.9	38.4	41.8	3.4	3.4

As reported in **Table 20** the ^{1}H-NMR data showed a significant amount of substituted aromatic compounds (ether, unsatured hydrocarbons and aldehydes) as shown by the area of integrals in the range 4.5-1.6 ppm. Mobile protons of carboxylic acids were not detected due to their exchange with the hydrogen of

the solvent, but resonances of protons in α position to carboxylic groups were abundant (region 2.5-2.3 ppm). Bio-oils contained a negligible amount of compounds having an alkyl moieties in agreement with the composition of biomass employed for these experiments. Particularly interesting is the high value of the area percentage due to functionalized ether groups in **ID26** (14.3%) probably due to the presence of high amount of furan derivatives.

Water content of bio-oils was evaluated by ^{1}H-NMR using internal standard technique as reported in experimental and data are reported in **Figure 32**.

Figure 32: Water content in bio-oils from MAP of *O.europea*
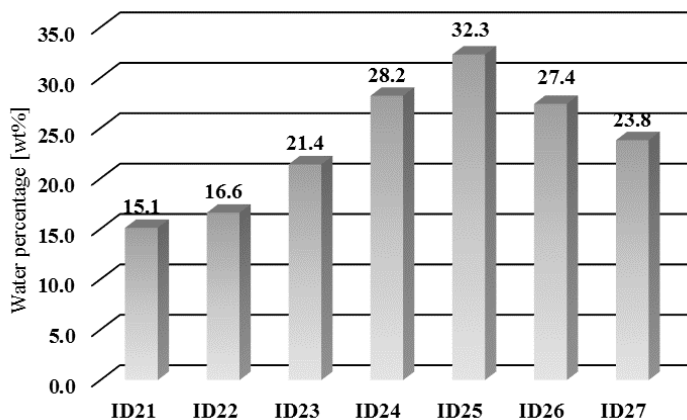
Water was present in different amounts depending on the MW absorber used. The use of carbon allowed to obtain a low percentage of water (15%). A similar result was reached with iron (17%). In this case the low amount of water was probably due to the formation of oxides species on the surface. Water

content increased with the use of SiC (21wt%) SiO_2 (28wy%) and reached a maximum with the use of Al_2O_3 in **ID25** (32%). The use of a mixture of carbon allows to obtain a bio-oil with a 24wt% water content, a value in between of **ID21** and **ID25** that explained the low combustion values of bio-oils previously reported.

4.4.3.2.3 FT-IR ATR

Bio-oils were analysed through FT-IR ATR analysis and spectra are reported in **Figure 33.**

Figure 33: FT-IR spectra of bio-oils collected from MAP of *O.europea.*
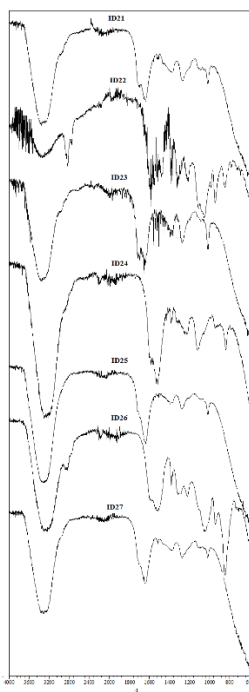
The presence of water amounts was confirmed in all bio-oils (bands in the range of 3600-3200 cm^{-1}, ν_{OH}). In all spectra strong absorptions of free carboxylic acid and ester groups were present in the range of 1800-1680 cm^{-1} ($\nu_{C=O}$) while other bands in the range of 3600-3400 cm^{-1} were superimposed with typical water bands (ν_{OH}). Further bands attributable to aromatics were shown as medium intensity absorption in the range of 1680-1580 cm^{-1} ($\nu_{C=C}$). In **ID22** and **ID26** the bands due to ν_{C-H} (2900-2750 cm^{-1}) can be recognised and this is a proof of the presence alkyl moieties linked to aromatic or furans.

4.4.3.2.4 Quantitative GC-MS

The fifty most abundant compounds identified in MAP of *O.europea* with their experimentally found or calculated RRFs, are reported in **Table 21.** The identification of the compounds present was very useful for the suggestion of the mechanism of pyrolysis. The TICs of the GC-MS analysis of **ID21**-**ID27** are reported in **Figure 34** where the peak of diphenyl, employed as internal standard, is marked by a star (*).

Figure 34: Chromatograms of GC-MS analysis of bio-oils from each MAP experiments. Diphenyl as internal standard is marked with a star (*).
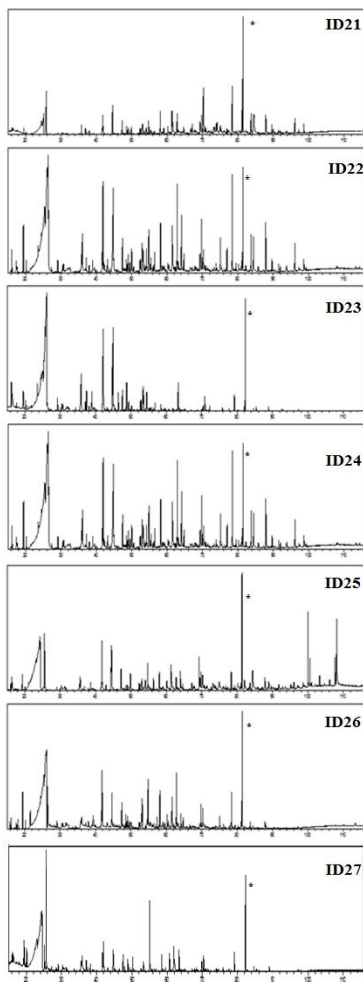
Table 21: Compounds identified in bio-oils from MAP of *O.euroepa*

Compounds	RRF	Concentration[mg/mL]						
		ID 21	ID 22	ID 23	ID 24	ID 25	ID 26	ID 27
Acetaldehyde	0.04	23.7	8.9	35.3	11.3	7.0	10.9	11.2
Methyl acetate	0.10	2.9	12.0	20.8	6.8	2.9	3.8	6.8
Formic acid	0.05	8.3	3.1	77.3	12.6	20.2	8.5	12.5
2,3-Butanedione	0.07	0.0	0.0	41.9	0.0	0.0	0.0	0.0
2-Butanone	0.11	2.1	4.0	0.0	3.2	0.0	3.0	3.2
Acetic acid	0.18	116.1	313.9	239.3	277.6	187.9	258.0	274.7
1-Hydroxy-2-Propanone	0.09	68.5	59.6	70.0	35.2	34.9	24.0	34.8
2,3-Pentanedione	0.14	1.5	0.7	5.9	2.5	0.9	1.6	2.5
Methyl hydroxyacetate	0.09	1.3	4.4	3.7	2.1	0.0	0.0	2.1
3-Hydroxy-2-butanone	0.13	1.4	2.4	5.7	1.5	10.9	0.0	1.5
Propanoic acid	0.12	0.0	21.4	0.0	9.1	0.0	1.1	9.0
2-Propenoic acid	0.11	1.1	0.0	1.0	0.4	1.6	5.7	0.4
Ethyl oxopropanoate	0.16	0.0	0.0	0.0	5.0	0.0	0.0	5.0
1-Hydroxy-2-butanone	0.15	6.4	17.5	40.9	8.2	3.6	3.9	8.1
Acetic acid anhydride	0.13	5.4	7.5	0.0	2.8	1.2	0.0	2.8
Methyl oxopropanoate	0.16	0.0	10.4	6.4	0.0	1.4	0.0	0.0
Toluene	0.16	5.2	0.0	9.5	0.0	0.0	0.0	0.0
Cyclopentanone	0.25	1.8	11.0	1.9	0.9	0.3	0.9	0.9

Compound								
2-Butene-1,4-diol	0.15	0.0	2.8	17.6	3.0	2.1	0.0	2.9
Furfural	0.13	22.6	17.2	79.0	27.4	11.9	16.8	27.1
2-Propenyl ester butanoate	0.14	0.0	4.8	0.0	1.7	2.1	0.0	1.7
Cyclohexanone	0.31	0.4	3.3	0.0	2.5	0.0	0.0	2.4
2-Oxopropyl acetate	0.19	13.5	0.0	0.0	0.0	5.8	4.7	0.0
2-Furanmethanol	0.18	28.0	17.6	68.7	17.2	10.8	0.0	17.0
1,2-Ethanediol, diacetate	0.21	0.0	0.8	0.0	11.7	0.0	0.0	11.6
5-Methyl-2(3H)-furanone	0.20	7.8	0.0	3.2	0.0	0.0	0.0	0.0
5-Methyl-2(3H)-furanone	0.21	24.9	6.1	3.3	7.3	3.4	7.0	7.2
Butyrolactone	0.19	0.0	0.0	16.8	7.4	4.8	6.9	7.4
2-Methyl-2-cyclopenten-1-one	0.30	5.9	1.7	0.0	1.1	0.5	1.2	1.1
Styrene	0.24	0.0	0.0	11.7	0.0	0.0	0.0	0.0
1-(2-furanyl)-Ethanone	0.24	7.7	1.5	5.5	2.1	0.9	1.7	2.1
2-Cyclohexen-1-one	0.31	4.0	5.9	0.0	3.1	1.1	2.1	3.1
Vynil propanoate	0.25	3.2	0.5	3.2	0.0	0.8	0.0	0.0
2-Oxobutyl acetate	0.27	3.5	2.1	3.2	2.0	0.8	1.1	2.0
Benzaldehyde	0.31	5.4	0.0	7.1	3.1	1.6	4.9	3.0
2-Furancarboxaldehyde, 5-methyl-	0.24	0.0	1.6	7.5	3.7	1.3	2.4	3.6
3-Ethyl-pyridine	0.35	4.2	0.5	1.6	1.0	0.5	0.0	1.0
2-Ethenyl-pyridine	0.22	10.0	0.0	8.7	0.0	0.0	0.0	0.0
4-Ethenyl-pyridine	0.23	0.0	1.5	0.0	3.7	1.4	0.0	3.6
Phenol	0.34	13.3	13.7	1.5	4.7	3.2	5.5	4.7

Compound								
3-Methyl-1,2-cyclopentanedione	0.30	23.9	0.0	1.9	0.0	0.0	0.0	0.0
Tetrahydro-2-Furanmethanol	0.18	0.0	0.0	3.8	3.9	0.0	0.0	3.8
2-Cyclopenten-1-one, 2-hydroxy-3-methyl-	0.29	0.0	11.8	0.0	5.8	2.3	5.3	5.8
Phenol, 2-methyl-	0.38	23.3	3.1	0.0	0.0	0.0	1.8	0.0
3-Ethyl-2-hydroxy-2-cyclopenten-1-one	0.37	10.9	2.6	0.8	4.3	0.6	1.9	4.3
Pentanal	0.35	11.7	6.8	0.6	6.3	2.9	0.0	6.3
Guaicol	0.43	12.4	6.2	6.4	6.2	1.3	4.7	6.2
Maltol	0.27	1.4	8.8	0.0	6.3	2.8	2.4	6.2
1,2-Benzenediol	0.32	13.3	5.8	0.0	0.0	5.2	1.3	0.0
1,4-Dimethoxy-benzene	0.44	9.9	0.0	1.1	3.5	0.0	1.9	3.4
1,4-anhydro-d-Mannitol	0.29	45.3	6.8	5.4	0.0	4.1	0.0	0.0
4-Methyl-1,2-benzenediol	0.41	4.4	1.6	0.0	0.0	0.9	0.0	0.0
4-Ethyl-2-methoxy-phenol	0.55	4.5	1.3	0.7	1.9	0.8	1.1	1.9
2,6-Dimethoxy-phenol	0.67	13.3	5.6	1.8	4.0	0.9	1.9	4.0
1,2,4-Trimethoxybenzene	0.67	5.9	2.2	0.3	1.3	0.3	0.3	1.3
Isoeugenol	0.65	8.7	0.0	0.6	1.3	0.0	0.0	1.3
Levoglucosan	0.40	0.0	3.9	0.0	0.0	4.7	0.0	0.0
1,2,3-Trimethoxy-5-methyl-benzene	0.67	9.4	2.1	0.5	0.0	0.0	0.7	0.0
Eugenol	0.75	7.7	1.4	1.0	0.0	0.3	1.4	0.0

Total assignment %	81.0	85.3	77.5	72.5	51.7	61.0	71.3

a) Total assignment was calculated with formula :
100*(summa of weight of assigned compounds)/(1 mL bio-oil)

GC-MS analysis let to identify a large amount of the compounds present (from 51.7 to 85.3 %). Aromatic compounds were also present in not large amount with exception of **ID21** as shown in **Figure 35**.

Figure 35: Total aromatic content detected by GC-MS
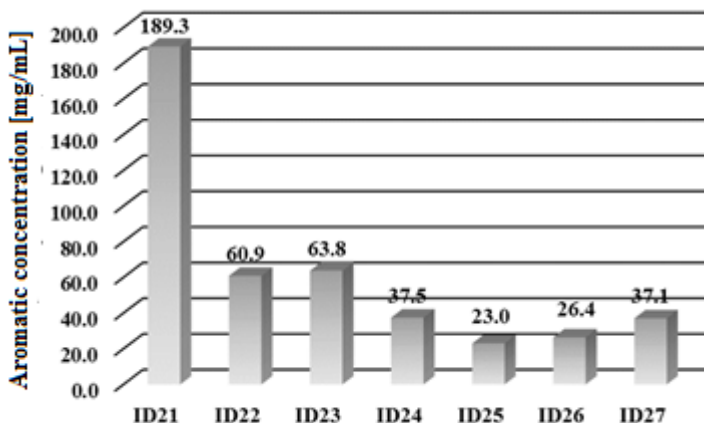
The behaviour observed in **ID21** is comparable with previously reported for *A.donax*. The aromatic content decrease to around 60 mg/mL in **ID22 ID23**. In the case of **ID22** the concentration of 60.9 mg/mL of aromatics was probably due to cracking reactions on the surface of iron particles, according with the concentration of advanced degradation product like

acetic acid that increased up to 313.9 mg/mL. Moreover in this case cracking processes induced a large production of bio-char (60.3wt%). A similar trend was observed in **ID24**-**ID26** with concetrations of acetic acid reached up to 200 mg/mL and a large amount of bio-char produced with high water content. Interestingly in **ID27** when the MW absorber was a mix of carbon and Al_2O_3, yields of fractions were similar to **ID21** but concentrations of acetic acid and aromatics were close to **ID25**. This is a strongly proof that low amounts of Al_2O_3 induced an efficient cracking process. An other relevant information was connected with the acetic acid produced in **ID26**. In this case NaOH, a strong base, acted only as MW absorber and cracking promoter while its use involved the massive production of acetic acid up to 258.0 mg/mL. The neglectable acid-base reactivity of NaOH was probably due to the different phase where acetic acid was produced. This represents a proof for the formation of acetic acid in gas-phase. Levoglucosan was very low in all experiments and it was due to its decomposition with formation of furfural and furans derivatives as reported by Bartol et al.[91].

All gaseous fractions were analysed through FT-IR and spectra collected were reported in **Figure 36**. **Figure 36:** FT-IR analysis of gaseous fractions collected during MAP of *O.europea*.
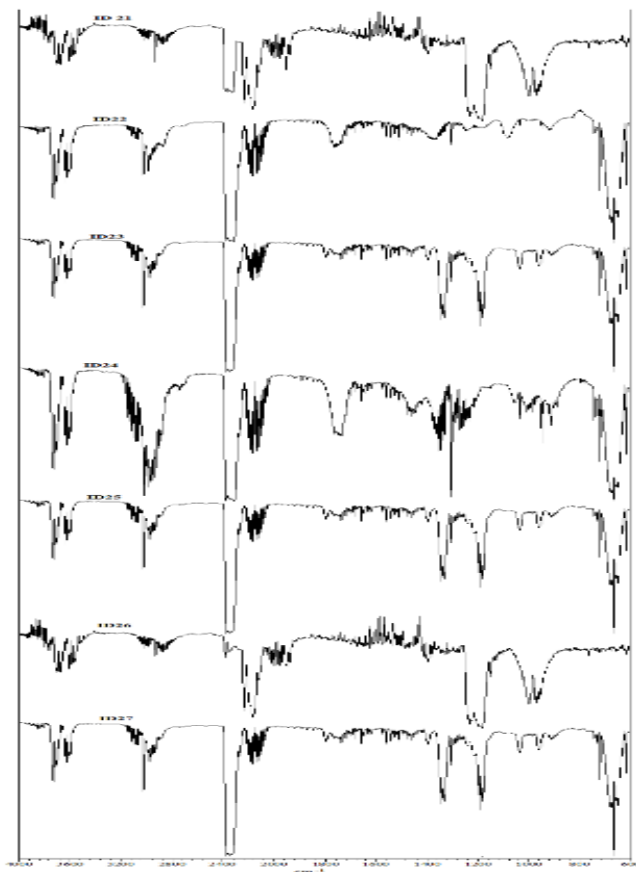
Thin bands in the range of 3750-3500 cm^{-1} were present evidencing the presence of water vapour (ν_{OH}) while the presence of CO_2 and CO were confirmed by the strong bands at 2400 cm^{-1} (ν_{OCO}), and 2150-2000 cm^{-1} (ν_{CO}), respectively. The presence of light hydrocarbons such as methane, ethane, ethylene were evidenced by bands in the range of 3250-3000 ($\nu_{CH=C}$) cm^{-1} and 2950-2750 cm^{-1} (ν_{CH}) particularly in **ID24**. Presence of light carbonyl compounds (such as formaldehyde or acetaldehyde) was evidenced by bands in the range of 1875-1750 cm^{-1} ($\nu_{C=O}$) in **ID22** and **ID24** while this absorption was neglectable in the other experiments. The ratio between typical bands of CO_2 at 2400 cm^{-1} (ν_{OCO}) and carbonyl compounds at 1875-1750 cm^{-1} ($\nu_{C=O}$) was very different in all spectra and it was in agreement with the strong influence of different absorbers on the maximum temperature reached in all experiments and consequently the progress of the pyrolytic degradation.

4.5 Vitis Vinifera

Vitis vinifera (*V.vinifera*) cultivations are one of the major business in the agrochemical industry[170]. The management of crops residues is a mandatory issue. There are many available technologies as mechanical recycling or composting [171] but combustion is the most used. MAP may be a sound approach to dispose this residue avoiding its combustion and recovering some usefull products..

4.5.1 V.vinifera preliminary characterization

Representative samples of *V.vinifera* were characterized in order to detect the amount of cellulose, lignin, and they proximate and ultimate analysis. Results are shown in **Table 21**

Table 21: Characterization of *V.vinifera* employed for MAP experiments

Cellulose [wt%]	Lignin [wt%]	Proximate analysis [wt%]				Ultimate analysis [%]		
		Moisture	VOCs	Ash	Fixed Carbon	C	H	O
41.1	23.2	2.0	75.4	4.4	18.2	45.5	5.6	47.8

V.vinifera showed an interesting cellulose content of 40.2 wt% and a lignin content of 28.1%. Proximate analysis showed a very low ash content (1.0%) and a high value of VOCs (78.7%). These values are consistent with the ultimate analysis that showed a high content of carbon and oxygen according to the high amount of cellulose.

4.5.2 Pyrolysis results

MAP experiments on samples of *V.vinifera* were carried out in a multimode MW batch reactor with different absorbers and set-ups. Experimental parameters and results concerning the amount of bio-oil, bio-char and gas are shown in **Table 22**.

Table 22: Experimental conditions and mass balance of MAP of *V.vinifera*

	Set-up	Time [min]	Absorber	T [K]	Products (%)		
					Bio-char	Bio-oil	Gas
ID28	A	16	Carbon	499	28.3	33.1	38.7
ID29	B	18	Carbon	644	33.0	32.3	34.7
ID30	A	14	Fe	751	30.7	34.9	34.3
ID31	B	20	Fe	723	36.9	30.4	32.7
ID32	A	22	SiC	475	71.4	15.3	13.3
ID33	B	25	SiC	506	31.1	23.3	45.7

In The use of set-up A and carbon as MW absorber (**ID29)** let to obtain a larg formation of gas (38.7%) and a good yield of bio-oil (33.1%) attributable to the low temperature of 499K reached in this experiment. Surprisingly a large gasification, up to 38.7%, was obtained, higher than that one reached with set-up B. Using Fe as MW absorber a higher temperature was reached using both set up A or B, (644K in **ID30** and

751 K in **ID31**) with comparable yields in the two experimentsr. In the use of SiC (**ID32** and **ID33**) the lower temperature was reached using set up A and B (475 K and 523 K, respectively). In this last experiment there was a very large production of bio-char, up to 71.4 wt%, and a low formation of bio-oils and gas . The use of set-up B, caused a higher reaction time and higher temperature was reached in agreement with the presence e of the fractionating system. The use of SiC as MW absorber and set-up B involved the largest gasification (up to 45.7%, **ID 33**).

4.5.3. Characterization of products

4.5.3.1 Bio-chars

Bio-chars were analysed through proximate and ultimate analysis, taking into account the amount of MW absorber present, in order to evaluate their main characteristics and results are shown. in **Table 23**.

Table 23: Ultimate and proximate analyse of char from MAP of *V.vinifera*

	Proximate analysis [wt%]				Ultimate Analysis [wt%]			EHC_{calc} [MJ/Kg]
	Moisture	*VOCs*	*ASH*	*Fixed Carbon*	*C*	*H*	*O^a*	
ID28	3.1	14.1	8.8	74.0	80.4	1.1	18.5	28.1
ID29	3.4	13.1	10.1	73.4	84.9	1.0	14.1	29.7
ID30	3.0	12.0	11.9	73.1	78.8	1.4	19.8	27.5
ID31	3.1	15.9	12.1	68.9	85.1	1.4	13.5	29.7
ID32	3.3	9.4	12.5	74.8	83.2	1.6	15.2	29.1

ID33	3.1	7.9	13.6	75.4	85.7	1.8	12.5	29.9

a) Calculated as difference

All bio-chars showed interesting properties among which a EHC around 28 MJ/Kg, connected with the high values of fixed carbon (close to 75 wt% with the exception of **ID30**) and C in the range of 78-85%. All samples had a relatively high ash content (between 8.8 and 13.6 %.

4.5.3.2 Bio-oils

4.5.3.2.1 Rheological properties and ultimate analysis

Dark-brown liquid having low density and viscosity were collected in all experiments, their rheological properties and ultimate analysis are reported in **Table 24**.

Table 24: Rheological properties and ultimate analysis of bio-oil from MAP of *V.vinifera*

	Density [g/mL]	Viscosity [cP]	Ultimate Analysis (%)			EHC_{calc} [MJ/Kg]
			C	*H*	*O*[a]	
ID28	1.14	2.33	21.4	7.8	70.8	7.5
ID29	1.05	2.01	24.3	5.3	70.4	8.5
ID30	1.12	1.96	23.2	6.8	70	8.1
ID31	1.04	1.88	22.9	7.9	69.2	8.0
ID32	1.16	1.93	23.1	7.3	69.6	8.1
ID33	1.01	1.74	23.1	6.4	70.3	8.1

a) Calculated as difference

Bio-oils did not show any phase separation at room temperature. All bio-oils showed density in a close range around 1 mg/mL. Viscosities were in the range among 2.33 (**ID28**) and 1.74 cp (**ID33**) generally higher than values of bio-oils obtained with the same experimental apparatuses. EHC_{calc} showed low values for all samples, close to 8 MJ/Kg, and this behaviour was attributed to the presence of water and the high concentration of oxygenated compounds.

4.5.3.2.2 ^{1}H-NMR

^{1}H-NMR was used to perform an estimation of organic composition of bio-oils and their water content and the collected spectra are shown in **Figure 37** .

Figure 37: ^{1}H-NMR spectra of bio-oils from MAP of *V.vinifera*, water signal was suppressed.
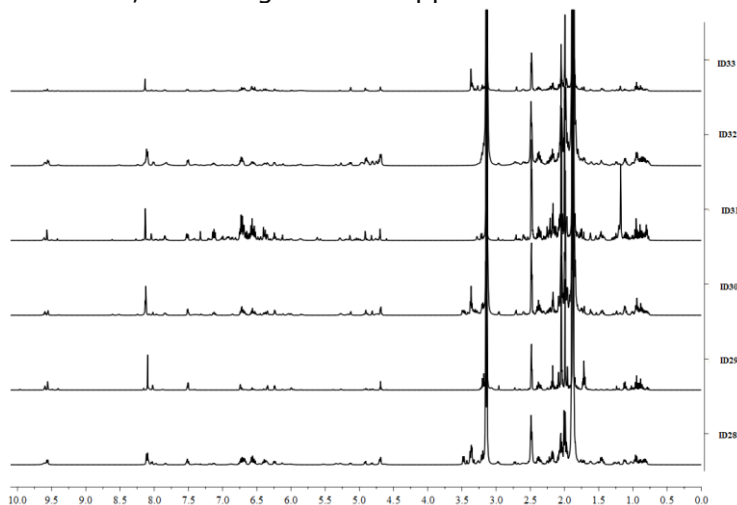
Table 25: Composition (area %) of bio-oils from MAP of *V.vinifera* obtained from ^{1}H-NMR data

δ (ppm)	Aldehydic protons	Aromatic, furan, and C=CH-OCC	Phenolic "OH" and C=CH olefin	CH_2-O-C; CH_2-OOC; ring-join methylene, and Ar-CH_2-Ar	CH_3, CH_2, and CH linked to aromatic ring and in α–position of carboxylic groups or etheric moiety	CH, CH_2 of alkyl groups; CH_2 and CH in β-position to an aromatic ring	CH_3 in β-position and CH_2 and CH in γ position to an aromatic ring or ethereal moiety	CH_3 of alkyl groups or further of an alkyl chain linked to an aromatic ring
	10.0-9.0	9.0-6.5	6.5-5.0	4.5-3.3	3.3-2.0	2.0-1.6	1.6-1.0	1.0-0.5
ID28	1.0	3.7	1.5	0.1	43.6	45.2	1.9	2.9
ID29	0.3	4.7	2.4	1.5	34.2	51.3	2.7	2.9
ID30	0.8	4.7	2.3	8.9	31.8	46.3	2.3	2.9
ID31	0.6	11.8	4.7	2.1	32.1	37.1	7.5	4.0
ID32	0.4	3.8	1.7	3.2	35.8	50.4	2.1	2.6
ID33	0.7	5.3	2.8	3.1	30.9	51.4	3.4	2.4

The ^{1}H-NMR data, as shown in **Table 25,** showed a significantly amount of substituted aromatic compounds (ether, unsatured hydrocarbons and aldehydes) as suggested by the area of integrals in the range 4.5-1.6 ppm. Mobile protons of carboxylic acids

were not detected due to their exchange with the hydrogen of the solvent, but resonances of protons in α position to carboxylic groups were abundant (region 2.5-2.3 ppm). Bio-oils contained a negligible amount of compounds having an alkyl moieties in agreement with the composition of biomass employed for these experiments.

Water content of bio-oils was evaluated by ^{1}H-NMR using internal standard technique as reported in experimental part and results are reported in **Figure 38**. Water content was in the range between 32.3% (**ID31**) to 45.6% (**ID33**), surprisingly it decreased with use of set-up B and carbon or Fe as MW absorber. These results were probably due to some water gas shift reactions between water and carbon, catalysed by iron, when present y or by a very rapid heat transfer from MW absorber to feedstock.

Figure 38: Water content in bio-oils from MAP of *V.vinifera*
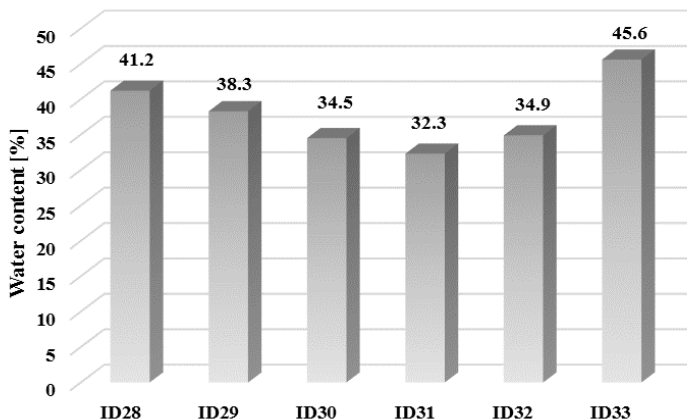
4.5.3.2.3 FT-IR ATR

Bio-oils were analysed through FT-IR ATR and spectra are reported in **Figure 39.**

Figure 39: FT-IR spectra of bio-oils collected from MAP of *V.vinifera.*
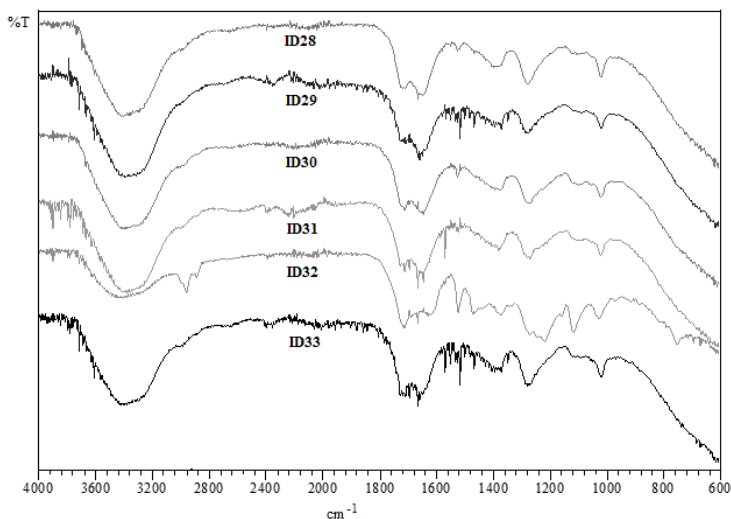
The presence of amount of water was confirmed in all bio-oils (bands in the range of 3600-3200 cm^{-1}, ν_{OH}). In all spectra strong absorptions of free carboxylic acid and ester groups were present in the range of 1800-1680 cm^{-1} ($\nu_{C=O}$) while other bands in the range of 3600-3400 cm^{-1} were superimposed with typical water bands (ν_{OH}). Further bands attributable to aromatics were shown as medium intensity absorptions in the range of 1680-1580 cm^{-1} ($\nu_{C=C}$). Bands due to ν_{C-H} (2900-2750 cm^{-1}) were detected (**ID32**) as a proof of the presence alkyl moieties linked to aromatics or furans.

4.5.3.2.4 Quantitative GC-MS

A very large number of compounds was present in bio-oils from MAP of *V.vinifera* and the sixty most abundant are reported in **Table 26**with their experimentally found or calculated RRFs. The identification of these compounds was very useful for the suggestion of a mechanism of pyrolysis. The TICs of the GC-MS analysis of **ID28**-**ID33** are reported in **Figure 40** where the peak of diphenyl, employed as internal standard, is marked by a star (*).

Figure 40: TIC of GC-MS analysis of bio-oils from MAP of V.vinifera. Diphenyl as internal standard is marked with a star (*).
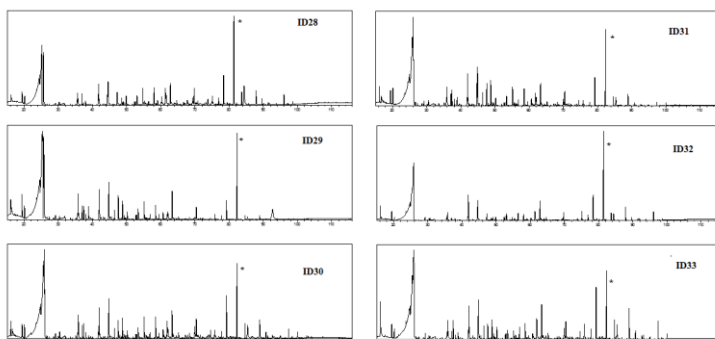
Table 26: Compounds identified in bio-oils from MAP of *V.vinifera*

Compounds	RRF	Concentrantion [mg/mL]					
		ID 28	ID 29	ID 30	ID 31	ID 32	ID 33
Acetaldehyde	0.04	0.6	1.1	1.8	2.5	2.7	0.7
Methyl acetate	0.1	0.5	1.8	1.7	1.9	4.7	2.4
Formic acid	0.05	2.8	2.9	3.7	2.1	2.9	1.1
2,3-Butanedione	0.07	2.0	3.2	3.6	2.9	3.4	1.9
2-Butanone	0.11	1.2	2.1	1.6	2.4	1.7	0.6
Acetic acid	0.18	75.6	143.7	138.5	121.6	172.5	97.5
1-Hydroxy-2-propanone	0.09	11.9	9.8	21.6	7.7	0.1	19.4
Benzene	0.16	0.2	0.4	0.2	0.5	0.3	0.0
3-Methyl-3-buten-2-one	0.15	0.4	0.5	0.5	0.6	0.7	0.3
2-Pentanone	0.21	1.2	0.7	0.3	0.6	0.5	0.2
2,3-Pentanedione	0.14	0.4	0.8	0.6	0.7	0.9	0.7
3-Hydroxy-2-butanone	0.13	0.2	0.5	0.3	0.3	0.4	0.1
Propanoic acid	0.12	0.5	0.8	0.5	0.8	0.6	0.4
2-Propenoic acid	0.11	0.0	0.0	0.0	1.7	0.0	0.0
Methyl butanoate	0.23	0.3	0.3	0.4	0.2	0.3	0.1
Isopropyl Alcohol	0.29	0.3	0.4	0.4	0.4	0.3	0.2
Pyrrole	0.15	0.0	1.1	0.0	1.1	0.0	0.0
2-Methyl-2-butanone	0.26	1.0	1.3	1.6	0.0	0.9	0.0
2-Methylpropanoic acid	0.16	2.1	3.8	0.0	3.2	4.1	2.7
Cyclopentanone	0.25	1.5	5.3	2.8	0.0	1.3	0.7

2-Methylbutanoic acid	0.23	0.7	0.0	0.7	0.6	0.0	0.4
Furfural	0.13	1.9	1.2	2.2	1.4	1.8	0.9
2-Butanone, 3-methyl-	0.08	0.0	1.2	0.0	0.8	0.0	0.0
1-Pentanol, 2-methyl-	0.31	0.1	1.7	0.5	0.3	2.8	0.0
1,2-Ethanediol, diacetate	0.11	0.1	0.0	0.0	1.9	0.0	0.0
Oxopropanoyl acetate	0.39	2.2	0.0	0.5	0.0	0.0	0.0
2-Furanmethanol	0.25	0.0	0.0	3.2	4.8	3.3	2.8
2(3H)-Furanone, 5-methyl-	0.2	3.1	7.9	6.0	6.0	7.7	4.1
Ethylbenzene	0.36	0.2	0.7	3.0	1.6	1.7	0.0
Butyrolactone	0.19	0.0	1.5	1.1	1.9	0.6	0.0
3,3-Dimethoxy-2-butanone	0.25	0.0	0.0	0.0	4.6	0.0	0.0
1-(2-furanyl)-Ethanone	0.24	0.0	3.7	2.8	3.9	3.6	0.0
2,5-Hexanedione	0.27	0.8	1.2	0.8	1.0	1.3	0.8
Cyclohexanone	0.31	0.5	0.8	0.4	0.6	0.0	0.0
3-Methylcyclopentanone	0.33	1.9	0.0	1.8	0.0	0.0	0.9
Oxobutyl acetate	0.28	0.4	0.6	0.6	0.5	0.7	0.6
5-Methyl-2-furancarboxaldehyde	0.24	0.4	0.8	0.8	0.7	1.0	0.9
4,6-Dimethyl-2H-Pyran-2-one	0.52	0.0	0.0	0.0	0.0	2.7	2.2
3-Methyl-2-cyclopenten-1-one	0.32	2.3	0.0	2.3	0.0	0.0	0.0
α-Methylstyrene	0.47	0.0	0.0	0.4	0.0	1.3	0.0
Benzofuran	0.45	0.7	0.0	0.0	0.0	0.0	1.8
4-Methyl-5H-furan-2-one	0.26	2.9	4.2	2.5	2.8	2.7	1.4
3-Ethyl-2-hydroxy-2-cyclopenten-1-one	0.37	1.4	2.0	3.6	1.6	0.2	0.4

Indene	0.57	1.2	1.8	0.0	1.0	3.3	1.0
5-(hydroxymethyl)-2-Furancarboxaldehyde	0.28	2.6	3.2	0.0	2.1	0.0	0.0
Maltol	0.27	3.1	4.5	3.9	3.4	5.6	3.9
2,6-Dimethylphenol	0.48	0.1	0.6	0.0	0.2	0.9	0.3
1,4-Dimethoxy-benzene	0.44	1.9	3.1	0.2	1.8	3.0	0.7
Pyrocatechol	0.32	2.9	3.5	0.0	2.5	3.5	1.7
3-Methyl-1,2-benzenediol	0.42	1.2	1.6	0.3	1.1	1.6	0.4
4-Ethyl-2-methoxy-phenol	0.55	0.0	2.1	0.0	0.7	0.0	0.0
4-Hydroxy-2-methylacetophenone	0.55	1.2	1.4	0.5	0.3	2.4	2.0
2,3-Hexanedione	0.27	1.0	1.0	0.5	0.5	1.6	1.1
Eugenol	0.63	4.3	5.7	2.3	3.5	7.8	5.6
3,4-Dimethoxyphenol	0.45	0.2	0.0	1.7	0.0	0.5	0.2
Levoglucosan	0.38	1.5	1.9	0.5	1.0	2.6	1.5
Apocynin	0.55	6.6	2.5	0.0	3.0	0.0	0.0
Levulinic acid	0.38	0.7	0.0	0.0	0.0	0.0	0.7
Acetophenone	0.66	0.4	3.0	0.4	0.4	0.0	0.0
Isoegugenol	0.64	0.0	0.9	0.0	0.0	1.1	0.0
Vanillin	0.34	1.8	3.4	5.2	0.4	6.7	3.8
Total assignment [wt%]		50.1	50.0	60.2	59.4	53.2	85.1

a) Total assignment was calculated with formula : 100*(summa of weight of assigned compounds)/(1 mL bio-oil)

118

GC-MS analysis let to identify almost 50% of compounds present with exception of **ID33** where 85.1% of compounds were identified. Aromatic compounds were present in amount between 19.5 and 39.5 mg/mL as shown in **Figure 41**.

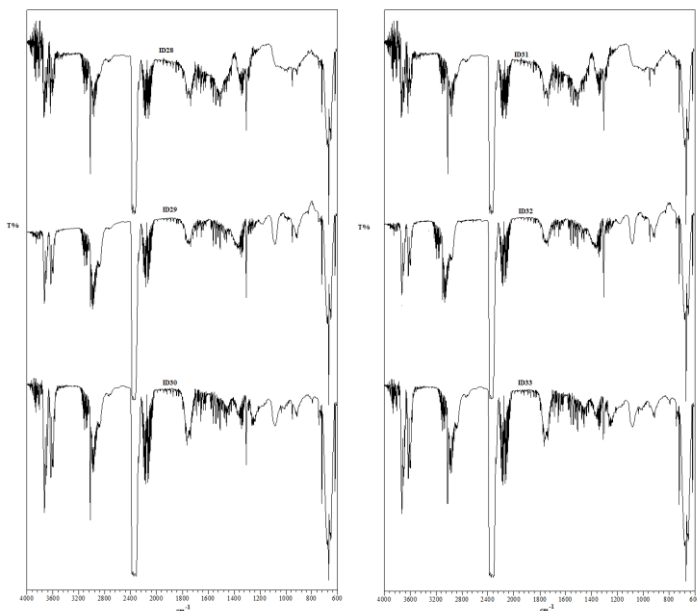**Figure 41:** Total aromatics content detected by GC-MS
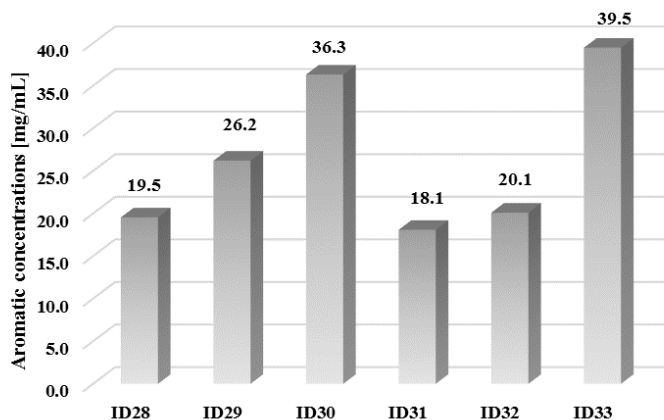
The aromatics were multisubstituited phenols as eugenol, isoegugenol or vanillin and they reached a maximum in **ID33** (39.5 mg/mL). The acetic acid was also identified in high concentration but generally lower that that one above reported sfor bio-oil from MAP of *O.europea* or *A.donax*. It reached a maximum of 130.5 mg/mL in **ID30** when Fe and set-up B were employed and a minimum of 75.5 mg/mL in **ID28** when carbon and set-up A.. Alsoe furans derivatives, such as furfural and 5-(hydroxymethyl)-2-furancarboxaldehyde, were detected in concentration, lower than 10 mg/mL.

4.5.3.3Gas

All gaseous fraction were analysed through FT-IR and spectra are shown in **Figure 42**.

Figure 42: FT-IR spectra of gaseous fractions collected from MAP of *V.vinifera*.

Thin bands in the range of 3750-3500 cm^{-1} suggested the presence of water vapour (ν_{OH}) while the presence of CO_2 and CO were confirmed by the strong bands at 2400 cm^{-1} (ν_{OCO}), and 2150-2000 cm^{-1} (ν_{CO}), respectively. The presence of light hydrocarbons such as methane, ethane, ethylene were evidenced by bands in the range of 3250-3000 ($\nu_{CH=C}$)cm^{-1} and 2950-2750 cm^{-1} (ν_{CH}) particularly in **ID24**. Presence of light carbonyl compounds (such as formaldehyde or acetaldehyde) was evidenced by bands in the range of 1875-1750 cm^{-1} ($\nu_{C=O}$) in spectra of **ID22**

and **ID24** while these absorptions were neglectable in the bio-oils from other experiments. The ratio between typical bands of CO_2 at 2400 cm^{-1} (ν_{OCO}) and carbonyl compounds at 1875-1750 cm^{-1} ($\nu_{C=O}$) was very close in all spectra.

4.6 Waste from Poplar SRC

Poplar short rotation coppice (SRC) plays an important role in biomass production because they are largely employed both in industry or used as solid fuel [172]. Recently there is a great interest in the below-ground biomass recovery (stump-root system) of poplar SRC because: a) it accounts for about 20% of the total plant dry weight [173] and the average poplar chips can yield 18 ton/ha of root biomass; b) it is easily accessible and harvested (sand-loamy soils); c) the root wood often has higher heating values than tops and branches, and they are a better fuel [174]. Furthermore, the removal of the stump-roots systems does not require the payment of a fee, and using efficient recovery systems, the delivered cost might range from 28 to 66 €/ton [175]. For these reasons valorisation of stump-roots systems from Poplar SRC was studied through MAP.

4.6.1 Poplar clones preliminary characterization

Poplar clones representative samples were characterized in order to detect the amount of cellulose, lignin, and they proximate and ultimate analysis and results are reported in **Table 27.**

Table 27: Characterization of poplar clones employed for MAP experiments

Clone	Starch [%]	NSC [%]	α-Cellulose [%]	Lignin [%]	Ultimate Analysis[wt%]				Proximate analysis[wt%]			
					C	H	N	O	Moisture	VOCs	Ash	Fixed carbon
I	1.5	1.5	43.1	29.1	44.1	5.0	1.2	50.9	7.8	73.3	4.0	14.9
II	3.6	2.9	42.2	28.0	45.7	4.6	1.1	49.6	6.4	78.9	2.6	12.1
III	8.1	4.7	22.3	23.2	39.9	6.4	0.9	52.8	5.8	83.3	5.8	5.1

Clone I showed a lower percentage of carbohydrates than clone II, while close amount of lignin, cellulose and ultimate composition were shown by all clones. Leaves composition was in agreement with previous works [176, 177].

4.6.2 Pyrolysis results

MAP of samples of different poplar clones were performed in the presence of different MW absorbers and setups. Experimental conditions and results are reported in **Table 28**.

Table 28: Experimental conditions and mass balance of MAP of poplar clones.

	Clone		Set-up	Time [min]	Absorber	T [K]	Products (%)		
	type	shape					Bio-char	Bio-oil	Gas
ID 34	I	Powder	A	20	Carbon	745	24.8	30.8	44.4
ID 35	I	Powder	A	25	Fe	745	28.7	20.9	50.4
ID 36	I	Powder	B	21	Carbon	745	20.6	27.7	51.7
ID 37	I	Powder	B	26	Fe	745	27.2	12.2	60.6
ID 38	I	Chips	A	21	Carbon	638	25.2	17.4	57.4
ID 39	II	Chips	A	16	Carbon	606	30.2	29.6	40.2
ID 40	I	Chips	A	21	Fe	702	36.4	32.0	31.5
ID 41	II	Chips	A	22	Fe	617	37.0	26.6	36.5
ID 42	III	Chips	A	30	Carbon	681	24.5	17.4	58.1

Experiments **ID34**-**ID37** were carried out on powder of stump-roots obtained from clone I to highlight the influence of different setup (A or B) as well as different MW absorber on materials having an homogeneous size. The highest yield of liquid was achieved for **ID34** by using carbon absorber and setup A. Use of iron or setup B caused a decreased of yield of liquid and this effect was particularly appreciable when both of them were employed (**ID37**).

Two couple of experiments **ID34** and **ID38** or **ID35** and **ID40** were carried out to check the influence of the size of the samples, powder (diameter < 1 mm) or chips (30 mm x 20 mm). A drastically decrease of

liquid yields was observed when the size of sample was increased (**ID34** and **ID38**, respectively**)**. It was probably caused by a decrease of the contact surface between the chips and MW absorber, in agreement with previous data [178]. On the contrary in the couple **ID35-ID40** an opposite trend was observed and bio-oil yield was increased up to 32.0%. Furthermore the use of iron (**ID40)** instead of carbon (**ID38**) as MW absorber caused a strong increase of bio-oil from poplar chips and the detected temperature was 702 K instead of 638 K. Clone II yielded an high amount of bio-oil in shorter time than clone I (experiments **ID39** and **ID38** respectively) but in this case the use of iron (**ID41**) as MW absorbed reduced the yields of bio-oils and increased the formation bio-char up to 37.0%.

Using also leaves of clone III MAP gave an amount of liquid yield very close (**ID42**) to those obtained with others samples.

A large amount of gas was formed in all experiments reaching up to 60.6 wt% of material pyrolyzed (experiment **ID37**).

4.6.3. Characterization of products

4.6.3.1 Bio-char

Ultimate analysis of bio-chars (**Table 30**) showed a very low percentage of hydrogen in all samples [128, 129] confirming a complete pyrolysis process. O/C molar ratio of all bio-char samples, with the exception of **ID35**, were compatible with their use in the carbon sequestration process [130]. **ID35** had high O/C molar ratio and this may be attributable to side reactions between carbon and water catalysed by iron in agreement with the results reported by Undri et al. [89]. EHC_{Calc} values of **ID1** and **ID3**-**ID9** showed that bio-chars can efficiently employed for energy storage. In agreement with these data EHC_{calc} value of **ID2** was

lower than others but it was high enough for a solid fuel.

Table 29: Characterization of bio-chars recovered from MAP of poplar clones

| | Ultimate Analysis | | | | Proximate analysis | | | | | |
| | [wt%] | | | | [wt%] | | | | EHC_{Calc} | [MJ/Kg] |
	C	H	O^a	N	Moisture	VOCs	Ash	Fixed carbon		
ID 34	83.8	0.6	15.4	0.3	2.3	2.3	28.1	67.3		29.3
ID 35	41.8	0.4	57.5	0.2	6.6	5.3	30.2	57.9		14.6
ID 36	82.0	0.7	17.2	0.1	5.5	2.9	37.6	54.0		28.7
ID 37	77.5	0.2	22.1	0.2	8.2	4.7	44.4	42.8		27.1
ID 38	76.2	0.7	22.6	0.5	3.0	3.5	37.7	55.8		26.8
ID 39	79.6	0.6	19.2	0.6	8.6	6.7	25.7	59.0		28.0
ID 40	80.5	0.3	19.1	0.1	4.8	5.6	39.8	57.7		28.1
ID 41	82.2	0.2	17.4	0.2	4.6	6.3	27.0	62.0		28.8
ID 42	76.3	0.6	21.6	1.4	3.1	3.8	46.2	46.9		27.1

a) calculated as difference

4.6.3.2 Bio-oils

4.6.3.2.1 Rheological properties and ultimate analysis

Dark-brown low density and viscosity liquids were collected in all experiments. Rheological properties and ultimate analysis of bio-oils are reported in **Table 31**.

Table 30: Rheological properties and ultimate analysis of bio-oil from MAP of poplar clones

	Density	Viscosity	Ultimate Analysis (%)				EHC
	[g/mL]	[cP]	C	H	N	O^a	[MJ/Kg]
ID 34	1.07	1.87	15.9	5.6	0.0	78.5	5.6
ID 35	1.06	4.56	15.6	9.7	1.3	73.5	5.5
ID 36	1.04	2.03	12.1	3.9	0.0	84.0	4.2
ID 37	1.04	1.48	11.1	10.7	0.6	77.6	3.9
ID 38	1.05	2.62	18.6	10.1	0.7	70.7	6.5
ID 39	1.07	1.68	16.2	9.6	1.4	72.9	5.7
ID 40	1.17	1.61	16.6	10.7	1.1	71.7	5.9
ID 41	1.23	1.82	12.6	11.7	0.9	74.9	4.4
ID 42	1.33	1.97	10.9	9.2	4.2	75.8	4.0

a) calculated as difference

All bio-oils collected in experiments **ID34**-**ID39** had density values close to water (1.04-1.07 g/mL), whereas **ID40-ID42** were quite higher (1.17-1.33 g/mL). Viscosity values of all experiments were in the range among 1.61 and 4.56 cP, lower than those reported in previous works by several authors when a classical heating [132, 179, 180] was employed however these data were in agreement with results reported by Undri et al. [89] using MAP processes. All bio-oils contained high percentage of oxygen and hydrogen. This result can be explained with large

presence of water and oxygenated chemicals formed from thermal degradation of cellulose and lignin, and this is the main reason for the low values of $EHC_{Theoretical}$.

4.6.3.2.2 ^{1}H-NMR NMR was used to perform a preliminary estimation of organic composition and water content through ^{1}H-NMR experiments, as shown in **Figure 43**.

Figure 43: ^{1}H-NMR spectra of bio-oils from MAP of poplar clones, water signal was depleted.
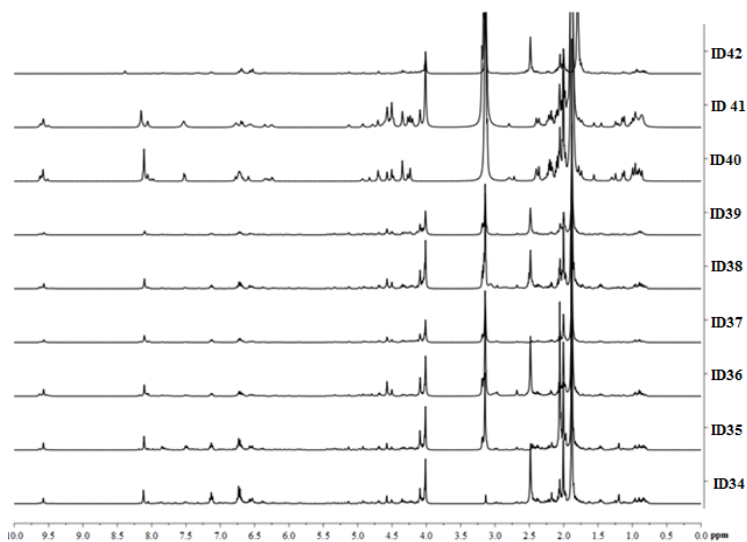
Compounds abundances from ^{1}H-NMR showed a high percentage of substituted aromatic compounds, ethers derivatives, unsatured compounds and aldehyde derivatives. Signals of mobile protons of carboxylic compounds were not detected but signals of protons in α position to carboxylic groups were abundant

(region 2.5-2.3 ppm) as reported in **Table 31**. Water content of bio-oils was evaluated by using internal standard technique as reported in experimental and data are reported in **Figure 44.**

Figure 44: Water content in bio-oils from MAP of poplar clones
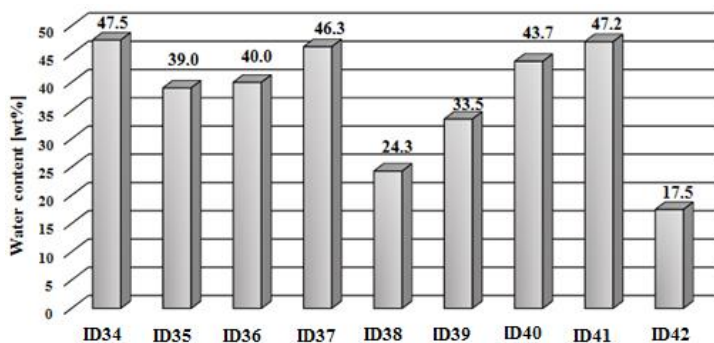
Water content of bio-oil was in good agreement with those in the literature for fast pyrolysis using a classical heating on samples of poplar [181]. A water percentage about 40% was observed in **ID34- ID37** and the water content was independent by setup (A or B) or MW absorber (carbon or iron) but it was likely related with the form of samples. Lower amount of water was found in bio-oils from chips (**ID38**, clone I) than **ID39**, (clone II). A higher water content was observed in **ID40** and **ID41** when bio-oils were obtained using chips and iron as MW absorber. Surprisingly a low amount of water (17.5 %) was found in sample **ID42**, obtained from leaves of clone III.

Table 31: Composition (area %) of bio-oils from MAP of poplar clones obtained from ^{1}H-NMR data

δ (ppm)	Aldehydic protons	Aromatic, furan, and C=CH-OCC	Phenolic "OH" and C=CH olefin	CH_2-O-C; CH_2-OOC; ring-join methylene, and Ar-CH_2-Ar	CH_3, CH_2, and CH linked to aromatic ring and in α–position of carboxylic groups or etheric moiety	CH, CH_2 of alkyl groups; CH_2 and CH in β–position to an aromatic ring	CH_3 in β-position and CH_2 and CH in-γ position to an aromatic ring or ethereal moiety	CH_3 of alkyl groups or further of an alkyl chain linked to an aromatic ring
	10.0-9.0	9.0-6.5	6.5-5.0	4.5-3.3	3.3-2.0	2.0-1.6	1.6-1.0	1.0-0.5
ID 34	1.1	11.1	3.5	9.8	36.1	31.8	3.5	3.2
ID 35	1.0	14.0	3.8	10.9	26.1	35.0	4.8	4.4
ID 36	1.7	6.4	2.4	16.0	36.6	32.3	1.9	2.6
ID 37	1.2	9.3	2.7	14.8	29.1	37.5	2.5	3.0
ID 38	1.2	6.4	2.9	12.5	36.5	34.3	3.0	3.3
ID 39	1.2	5.7	4.5	15.3	32.8	34.3	2.9	3.3
ID 40	0.2	0.9	0.2	73.3	13.2	10.9	0.5	0.6
ID 41	0.8	3.4	0.8	7.1	50.7	31.8	2.2	3.1
ID 42	0.0	8.6	3.4	11.7	44.6	24.0	3.3	4.4

4.6.3.2.3 FT-IR ATR

All bio-oils were characterized through FT-IR analysis as show in **Figure 45**.

Figure 45: FT-IR spectra of bio-oils collected from MAP of poplar clones
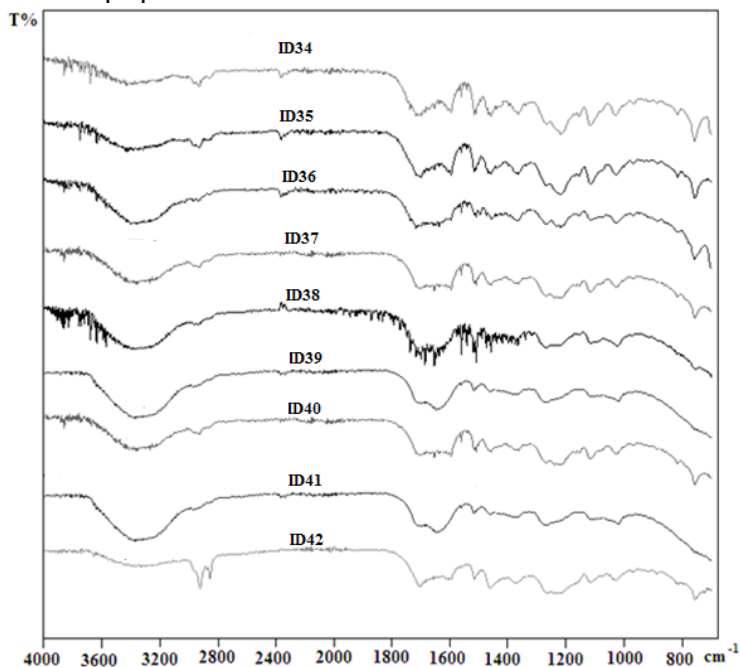
FT-IR spectra showed absorptions in agreement with the presence of highly oxygenated compounds (bands in the range of 1380-1100, ν_{C-OH}, GC-MS and ^{1}H-NMR analysis). In particular, a huge presence of water (band in the range of 3600-3400 cm^{-1}, and 1800-1680 cm^{-1}) can be detected in all the samples with exception of **ID42**. In the latter case, the intensity of water absorption was comparable with absorption of saturated CH stretching (band in the range 2900-2800 cm^{-1}). In all spectra strong absorptions of free carboxylic groups and ester groups (band in the range of 3600-3400 cm^{-1}, ν_{OH}, band in the range of 1800-1680 cm^{-1}, $\nu_{C=O}$) can be detected. Furthermore the presence of aromatic moiety was confirmed by absorption of $\nu_{C=C}$ in the range of 1680-1580 cm^{-1}.

4.6.3.2.4 Quantitative GC-MS

The sixty most abundant compounds identified in MAP of poplar clones with their experimentally found or calculated RRFs, are reported in **Table 32.** The identification of the compounds present was very useful for the suggestion of the mechanism of pyrolysis. The TICs of the GC-MS analysis of **ID34**-**ID42** are reported in **Figure 46** where the peak of diphenyl, employed as internal standard, is marked by a star (*).

Figure 46 :GC-MS chromatograph of MAP of poplar samples, internal standard diphenyl is marked with star (*)
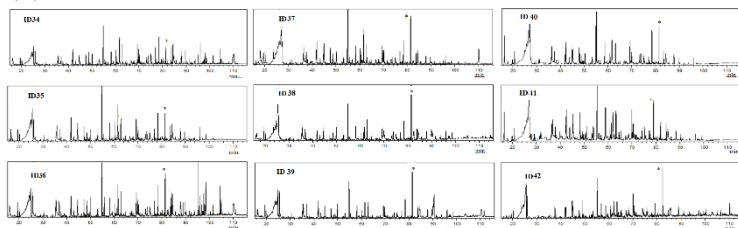
Table 33: Compounds identified in bio-oils from MAP of poplar clones

Compounds	RRF	Concentration [mg/m]								
		ID 34	ID 35	ID 36	ID 37	ID 38	ID 39	ID 40	ID 41	ID 42
Acetaldehyde	0.04	3.7	2.2	6.6	5.2	5.8	6.9	10..1	5.0	9.9
Formic acid	0.05	27.7	16.1	24.5	17.4	12.1	24.1	5.0	4.9	52.3
Methyl acetate	0.10	27.6	1.6	24.0	1.0	2.5	0.0	2.3	0.7	2.4

2,3-Butanedione	0.07	8.4	5.7	7.6	0.0	8.9	10.9	11.9	8.7	18.3
2-Butanone	0.11	3.6	2.1	3.0	2.8	3.8	3.4	4.5	1.8	0.0
Acetic acid	0.18	245.1	203.9	207.0	182.0	264.1	217.5	129.4	181.6	534.3
1-Hydroxy-2-propanone	0.09	2.0	27.7	2.1	2.4	2.5	41.2	23.0	19.2	4.5
Benzene	0.16	1.1	0.5	1.3	0.0	1.1	0.3	0.0	0.0	2.4
2,3-Pentanedione	0.14	0.8	0.5	0.6	0.6	0.8	0.9	1.0	1.1	1.7
Methyl 2-hydroxyacetate	0.09	1.1	1.2	6.0	0.5	0.0	0.0	1.0	1.9	1.7
1,3-Dioxol-2-one	0.09	2.4	0.6	1.9	0.9	2.2	0.0	1.4	0.0	0.0

3-Hydroxy-2-butanone	0.13	0.6	0.7	0.5	0.0	0.6	0.7	1.1	1.7	1.3
Propanoic acid	0.12	1.7	1.8	1.1	1.6	1.8	2.5	2,4	3.5	3.6
2-Propenoic acid	0.11	0.9	0.6	0.7	3.5	0.9	0.6	0.3	0.3	1.9
(E)-2-Penten-2-one	0.18	1.2	0.5	0.3	0.2	1.4	0.5	0.4	0.0	1.7
Ethyl 3-hydroxypropanoate	0.15	0.0	0.0	0.0	0.0	0.0	0.0	0.0	0.0	9.5
Propylene oxide	0.15	2.5	0.9	2.7	0.0	1.2	2.6	0.0	0.0	0.0
Acetic anhydride	0.13	61.0	3.3	4.5	0.0	0.0	0.0	0.0	5.2	13.2
Ethyl 2-oxopropanoate	0.16	4.2	0.0	0.0	0.0	0.0	0.0	3.1	3.7	0.0

1-Hydroxy-2-butanone	0.15	5.7	7.4	6.3	3.2	6.1	3.7	6.1	7.9	12.4
Methyl 2-oxopropanoate	0.16	0.0	3.9	5.8	2.2	4.3	2.7	0.6	2.0	0.0
Toluene	0.16	0.9	0.5	0.7	0.2	1.0	0.2	0.0	0.0	2.0
Cyclopentanone	0.25	0.9	0.8	0.4	0.7	1.0	0.4	0.6	7.3	2.0
2-Cyclopenten-1-one	0.22	1.9	2.8	2.4	2.6	2.1	1.8	1.9	3.8	2.5
Furfural	0.13	9.1	6.9	5.4	3.9	9.7	2.6	7.0	15.7	3.7
2-Ethylbutanal	0.29	1.7	1.3	1.3	0.7	1.8	0.0	0.0	0.0	0.0
2-Oxopropyl acetate	0.19	3.0	2.5	1.2	0.0	1.0	1.8	2.2	2.3	2.6

Furanyl-2-methanol	0.18	4.2	5.1	4.1	3.2	4.5	3.0	4.1	7.2	9.2
2(5H)-Furanone	0.18	7.6	5.4	5.0	3.7	8.1	3.8	4.8	0.0	0.0
Cyclohexanone	0.31	0.3	0.5	3.3	1.5	0.3	0.0	0.2	3.0	0.5
2-Methyl-2-cyclopenten-1-one	0.30	0.0	1.6	0.0	1.2	0.4	0.0	0.9	1.1	0.0
1-(Furan-2-yl)ethanone	0.24	0.7	1.3	0.0	0.5	0.8	0.6	0.4	0.8	1.6
4-Methylfuran-2-carbaldehyde	0.22	0.0	0.0	0.0	0.0	0.0	0.0	0.0	2.7	8.3
3-Methylcyclopentanone	0.33	4.5	2.5	0.0	0.0	0.0	0.0	0.0	0.0	0.0
5-Methylfuran-2-carbaldehyde	0.24	0.0	3.6	0.0	0.6	0.0	0.0	0.0	2.7	7.7

3-Methyl-2-cyclopenten-1-one	0.32	0.0	0.0	1.1	0.0	0.0	0.0	0.0	2.6	1.9
Phenol	0.34	16.4	17.4	9.4	8.5	17.5	6.1	8.5	13.9	35.8
Butanoic acid	0.08	1.4	1.3	2.3	0.0	0.0	0.0	0.0	0.0	0.7
2-Methoxy-3,4-dihydro-2H-pyran	0.30	1.8	0.0	0.0	0.7	0.0	0.6	0.0	0.0	4.0
2-Hydroxy-3-methyl-2-cyclopenten-1-one	0.29	0.0	0.0	0.0	0.0	0.1	0.2	3.4	7.1	9.1
3-Hydroxy-2-methyl-2-cyclopenten-1-one	0.30	4.1	3.6	3.0	1.7	0.0	0.0	0.0	0.0	0.0
o-Cresol	0.38	3.5	4.2	1.8	1.6	11.0	1.3	1.4	1.2	22.5
3-Methyl-cyclohexanone	0.46	0.4	0.0	0.0	0.0	4.8	2.4	0.0	0.0	0.0

Pentanal	0.35	0.0	0.0	6.3	0.0	1.7	5.3	0.0	0.0	0.0
m-Cresol	0.38	10.1	10.0	0.0	3.2	10.7	0.0	0.9	0.0	0.0
p-Cresol	0.38	0.0	0.0	0.0	0.0	0.0	0.0	0.0	0.0	22.0
Guaiacol	0.43	4.8	3.9	2.8	0.2	5.1	2.4	0.0	3.3	10.4
5-Oxotetrahydrofuran-2-carboxylic acid	0.24	0.2	0.0	0.0	0.0	0.0	2.0	0.5	0.9	1.9
Pyrocatechol	0.32	7.6	6.0	4.0	2.1	8.1	3.8	3.8	5.5	16.4
2-Methoxy-5-methylphenol	0.44	2.2	1.8	1.3	0.6	2.3	0.8	0.0	1.2	0.0
Naphthalene	0.71	1.1	1.3	0.6	0.5	1.2	0.0	0.0	0.0	2.4

4-Methyl-pyrocatechol	0.41	2.3	1.7	1.1	0.4	0.1	0.3	0.7	1.3	4.9
3-Methoxybenzene-1,2-diol	0.35	2.1	1.4	1.5	0.5	1.0	0.8	1.1	0.0	4.5
2-Methylbenzene-1,4-diol	1.45	0.0	0.0	0.0	0.0	0.5	0.3	0.0	0.1	4.8
4-Hydroxy-2-methylacetophenone	0.55	2.2	1.8	1.0	0.6	0.0	0.5	0.0	0.1	0.0
Syringol	0.45	4.7	3.9	2.5	1.1	0.0	0.0	2.5	0.1	0.8
m-Eugenol	0.67	2.5	2.3	1.8	0.7	2.5	0.1	0.1	0.0	0.0
1,2,4-Trimethoxybenzene	0.55	2.2	1.8	1.1	0.4	2.3	0.5	0.7	0.0	4.7
Levoglucosan	0.40	4.4	3.0	1.5	0.0	0.0	0.8	0.0	0.0	9.6

1,2,3-Trimethoxy-5-methylbenzene	0.67	1.7	1.6	0.8	0.0	1.8	0.5	0.4	0.0	0.0
1-(3,4-Dimethoxyphenyl)ethanone	0.66	1.3	0.9	0.8	0.3	1.4	0.7	0.0	0.1	0.2
Total assignment [wt%]		52.0	39.0	40.0	27.0	42.0	35.0	21.0	30.0	69.0

a) Total assignment was calculated with formula : 100*(summa of weight of assigned compounds)/(1 mL bio-oil)

Phenol, guiacol and its derivatives, pyrocatechol and its derivatives from pyrolysis of lignin together with levoglucosan, and furan derivatives from pyrolysis of cellulose were detected in all bio-oils. Also aromatic single ring and polycyclic compounds were detected in a concentration up to 156.3 mg/mL in **ID42**, **Figure 47**.

Figure 47: Aromatic compounds concetrations in bio-ils
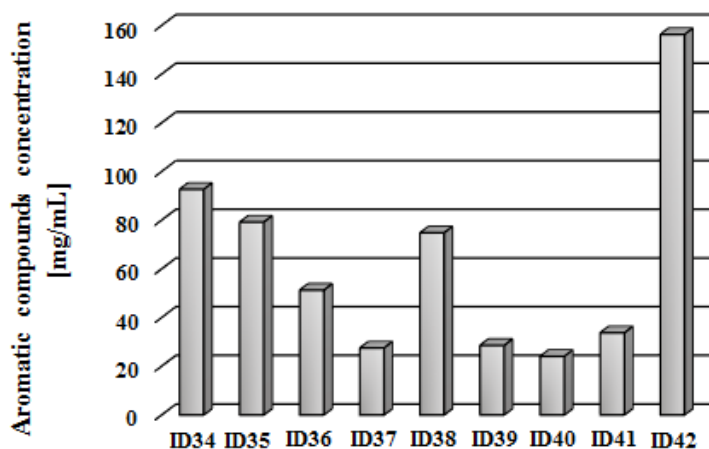
The use of setup B, that is increasing the permanence of products in the pyrolysis oven leaded to a decrease of aromatic compounds into bio-oils (**ID36** and **ID37**) caused by their rearrangement for formation of GC undetectable high molecular weight compounds and carbon. Moreover bio-oil from clone I (**ID38**) showed a high percentage of aromatic compounds than clone II (**ID39**). Use of iron as MW absorber (**ID40**), instead of carbon (**ID38**) caused a lower formation of aromatic compounds when the same type of clone (clone I) was employed while an opposite behaviour was shown for clone II (**ID41** and **ID42**), indicating that the type of clone plays an important role on the amount of aromatic products present in bio-oils. The amount of levoglucosan in the bio-oil was influenced by use of a MW absorber employed in the course of the pyrolysis [182] and the operative conditions adopted [183]. Iron and setup B caused a strongly decrease of levoglucosan amount in bio-oils. Side reactions on iron surface might take place in

agreement with the hypothesis reported by Undri et al. [89] as well as an increased of the residence time into MW oven, due to setup B, might cause further reactions of levoglucosan decreasing its concentration (**ID36** and **ID37**). Secondary reactions of levoglucosan produced a wide variety of furanosidic compounds like furfural, detected through GC-MS, in agreement with results reported by Kawamoto et *al*.[184]. Use of leaves of clone III as starting material and carbon as a MW absorber allowed to produce a bio-oil rich in levoglucosan (9.6 mg/mL). Acetic acid was always present in very large amount with concentration close to 250 mg/mL in **ID34**-**ID39**. A lower concentration of acetic acid was detected in **ID40** and **ID41** probably due to the presence of iron as MW absorber because it may catalysed its decomposition. Bio-oil from experiment **ID42** (leaves of clone III) showed the surprisingly highest concentration of acetic acid (534.3 mg/mL) among all bio-oil formed. This high concentration of acetic acid may be attributed to a different composition of leaves with respect to stump-roots [176, 185] and to different temperatures of processes as suggest by Demirbas [186]. Indeed experiments **ID34**-**ID39** showed different temperatures of pyrolysis but close range of acetic acid concentration while opposite results were obtained in experiment **ID40**-**ID42**.

4.6.3.3 Gas

Gas from MAP of poplar was analysed through FT-IR spectroscopy. Spectra collected are shown in **Figure 48**.

Figure 48: FT-IR spectra of gas from MAP of SRC of poplar
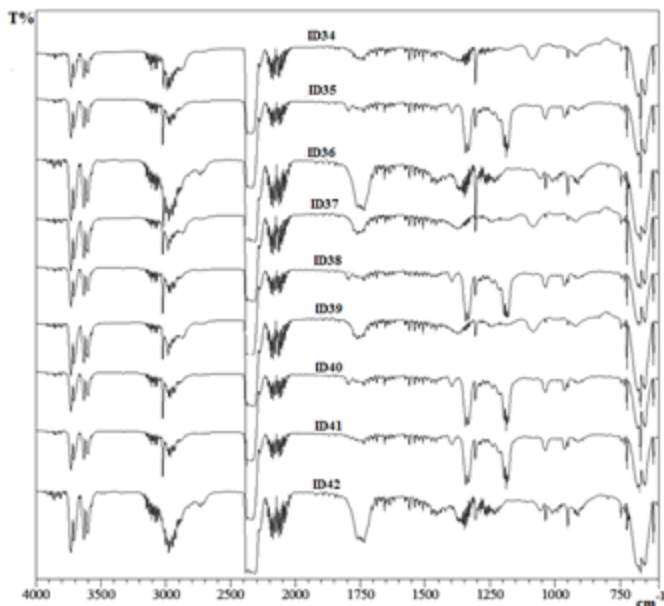
Bands in the range of 3750-3500 cm^{-1} showed the presence of water (v_{OH}) while the presence of CO and CO_2 were proved by bands at 2150-2000 cm^{-1}(v_{CO}) and band at 2300 cm^{-1} (v_{OCO}), respectively. The presence of light hydrocarbons such as methane, ethane, ethylene were confirmed by bands in the range of 3250-3000 (stretching of CH of methylenic groups) cm^{-1} and 2950-2750 cm^{-1} (stretching of CH of methyl groups). Presence of light carbonyl compounds (such as

formaldehyde or acetaldehyde) was evidenced by bands in the range of 1875-1750 cm^{-1} ($\nu_{C=O}$) and these bands were particularly appreciable in **ID37** and **ID42**.

5. CONCLUSIONS

This research has clarified some key points about Microwave Assisted Pyrolysis (MAP) of lignocellulosic biomass.

Pyrolysis of waste biomasses using an alternative energy source, such as microwave, has been realized obtaining three relevant classes of materials: a solid, a liquid and a gas.

The relevance of different apparatus on MAP yield were tested. Generally the use of different set-ups allow to exploit sample differences, avoiding hard pyrolysis conditions as shown in the **ID34**-**ID42** for different poplar clones. Also the reduced pressure used in the study of MAP of lignin had a very appreciable effect on the MAP yields as reported for **ID9-ID14**. Using the data collected a mechanism was proposed to explain these results.

Various MW absorbers, very different among them, were tested. MW absorber type affected MAP yields and bio-oils composition. Carbonaceous types promote bio-oils formation around 30-40 wt% but it is very interesting the different behaviour shown by metal traces containing carbon with respect to graphite in MAP of cellulose. The use of graphite allowed to recovery a high concentration levoglucosan up 138 mg/mL in **ID8** because it was avoided its further cracking reactions. On the contrary metal trace present in carbon recovered by MAP of tire cause a catalytic decomposition of levoglucosan. The use of pure metal as Fe power allow to run stronger pyrolysis conditions during MAP experiments with higher values of maximum temperature reached. Metal oxides like SiO_2 and Al_2O_3 were tested and according with data reported by several authors they induce a very

efficient cracking degradation of biomass. Particularly interesting was the use of Al_2O_3 (**ID25)** because it was used to monitor the temperature reached through a characterization of the bio-char with XRPD analysis. Results obtained are an indication of the absence of hot-spots during pyrolysis on the contrary of results reported by Undri et al.[115] for MAP of tire. Using NaOH as MW absorber (**ID26**) acetic acid was detected in the bio-oil and this result indicate that acetic acid is mainly formed in gas phase. In fact acetic acid concentration was comparable to those reached in other experiments where a strong base as MW absorber was absent. Using SiC promote a large formation of bio-char due to a strong cracking process even if a high temperature was not reached, in agreement with previous results reported by Bartoli et al.[81] for MAP of waste polystyrene.

The relevance of different biomass organs on yields of MAP were tested on different clones of poplar or *A.donax*. Results showed a strong correlation of yield and bio-oil composition with the organ processed for both species. At same time MAP of different poplar clones showed how it possible magnified or reduce the differences in yields and bio-oils compositions using different set-up (A or B), different dimension of the biomass (powder or chips) and different MW absorber (carbon or Fe).

Various methodology for bio-oils characterization were developed and applied. Particularly the NMR analysis was employed for the estimation of water content while and quantitative GC-MS method very developed and employed for identification and quantification of the various components present in bio-oil samples in order to realize as an ordinary laboratory activity the analysis of these very complex mixtures.

The method for quantitative GC-MS analysis, was originally developed for GC/FID, it was modified and standardized for GC-MS systems, then it was successfully employed to identify and quantify up to three hundred compounds present in bio-oils. The identification and quantification of the compounds present allowed to suggest some consideration on mechanisms of degradation of biomasses during MAP. Particularly it was described for the first time the pathway of aromatic formation during cellulose pyrolysis and the amount of some key intermediates was reported.

Bio-oil usually contained a high acetic acid concentrations, in the range among 75.8 mg/ml in **ID28** to 543.3 mg/mL in **ID42**. Also a large amount of aromatic compounds, and furans as advanced pyrolysis products were identified in some bio-oils.

Bio-chars showed interesting properties like low ash content and high combustion value but they were mixed with MW absorber, so, depending on the use of this material, a separation processes through elutriation, washing, magnetic separation Is required. To avoid the separation MAP may be carried out using the bio-char of a previous process as a MW absorber.

Gas fractions were mainly composed by water and CO_2 with trace of small organic molecule such as formaldehyde, acetaldehyde and organic acids.

The data collected from MAP of biomass showed this methodology as a sound and promising way to process biomass wastes. Solids recovered from MAP processes can be employed as solid fuels, eventually after a separation of MW absorber and gas fraction can be treated and then disposed as non-pollutant gas. Bio-oils can be find a lot of application as a source of some

chemicals such as pesticides [187] or mixtures for chemical treatments [141] or employed to separate through an extraction or a fractionating process [179] the more interesting compounds present, such as acetic acid, aromatics and furans. The residue after separation may be employed as a fuel to produce part of the energy required to carry out the MAP process.

ACKNOWLEDGEMENTS

"All fled-all done, so lift me on the pyre;
The feast is over and the lamps expire"
Robert Erwin Howard

First of all I wish to thank Dr. Marco Frediani and Dr.Luca Rosi for the chance to test my attitude for research with a PhD. It was hard but I tried and I liked it, not everytimes but oftenly. I loved to work with both of you and I am remembering from now to the end all the laughs, the jokes and all the conversations, the bad and good ones. Thanks for all, seriously.

A special thanks to prof.Piero Frediani and Dr. Alessio Giovannelli for the help and the kindness everytimes that I was need them.

I should to thank prof. Franco Berruti, prof. Cedric Briens, Dr.Charlels Greenhalf and all of the guys from ICFAR. It was a long and hard journey but it was very important for me.

At the end I cannot miss to thanks my family who have always believed, always helped and encouraged without asked anything back. Many thanks to all, for all

Mattia

150

BIBLIOGRAPHY

[1] E. Pepke, Global Wood Markets: Consumption, Production and Trade, in: International Forestry and Global Issues, Nancy (FR), 2010.

[2] S. Thelandersson, H.J. Larsen, Timber engineering, John Wiley & Sons, 2003.

[3] M. Parikka, Global biomass fuel resources, Biomass and Bioenergy, 27 (2004) 613-620.

[4] R. Kaplinsky, O. Memedovic, M. Morris, J. Readman, The global wood furniture value chain: What prospects for upgrading by developing countries, UNIDO Sectoral Studies Series Working Paper, (2003).

[5] G.A. Smook, Handbook for pulp & paper technologists, Tappi, 1992.

[6] M. Peksa-Blanchard, P. Dolzan, A. Grassi, J. Heinimö, M. Junginger, T. Ranta, A. Walter, Global wood pellets markets and industry: policy drivers, market status and raw material potential, IEA Bioenergy Task 40, (2007).

[7] A. Demeyer, J.V. Nkana, M. Verloo, Characteristics of wood ash and influence on soil properties and nutrient uptake: an overview, Bioresource technology, 77 (2001) 287-295.

[8] J. Chave, H.C. Muller-Landau, T.R. Baker, T.A. Easdale, H.t. Steege, C.O. Webb, Regional and phylogenetic variation of wood density across 2456 neotropical tree species, Ecological applications, 16 (2006) 2356-2367.

[9] H. Pereira, Variability in the chemical composition of plantation eucalypts (Eucalyptus globulus Labill.), Wood and Fiber Science, 20 (2007) 82-90.

[10] S. Lamlom, R. Savidge, A reassessment of carbon content in wood: variation within and between 41 North American species, Biomass and Bioenergy, 25 (2003) 381-388.

[11] A.C. O'SULLIVAN, Cellulose: the structure slowly unravels, Cellulose, 4 (1997) 173-207.

[12] E. Sjostrom, Wood chemistry: fundamentals and applications, Elsevier, 2013.

[13] E.O. Kraemer, Molecular weights of celluloses and cellulose derivates, Industrial & Engineering Chemistry, 30 (1938) 1200-1203.

[14] D. Myers, S. Stolton, Organic cotton: from field to final product, Intermediate Technology, 1999.

[15] K. Goetze, Viscose Rayon Production (Russian translation), Khimiya, Moscow, (1972) 234.

[16] A. Carroll, C. Somerville, Cellulosic biofuels, Annual review of plant biology, 60 (2009) 165-182.

[17] J.E. Kline, Paper And Paperboard: Manufacturing And Converting Fundamentals, Miller Freeman Publications, 1982.

[18] M. Kunioka, Y. Inuzuka, F. Ninomiya, M. Funabashi, Biobased Contents of Biodegradable Poly (ε-caprolactone) Composites Polymerized and Directly Molded Using Aluminium Triflate from Caprolactone with Cellulose and Inorganic Filler, Macromolecular bioscience, 6 (2006) 517-523.

[19] A. Dufresne, M.R. Vignon, Improvement of starch film performances using cellulose microfibrils, Macromolecules, 31 (1998) 2693-2696.

[20] W. Zhang, X. Zhang, M. Liang, C. Lu, Mechanochemical preparation of surface-acetylated cellulose powder to enhance mechanical properties of cellulose-filler-reinforced NR vulcanizates, Composites Science and Technology, 68 (2008) 2479-2484.

[21] A. Ishikawa, T. Shffiata, Cellulosic chiral stationary phase under reversed-phase condition, Journal of Liquid Chromatography & Related Technologies, 16 (1993) 859-878.

[22] N. Breum, T. Schneider, O. Jørgensen, T.V. Rasmussen, S.S. Eriksen, Cellulosic building insulation versus mineral wool, fiberglass or perlite: installer's

exposure by inhalation of fibers, dust, endotoxin and fire-retardant additives, Annals of Occupational Hygiene, 47 (2003) 653-669.

[23] G. Camino, L. Costa, G. Martinasso, Intumescent fire-retardant systems, Polymer Degradation and Stability, 23 (1989) 359-376.

[24] E.F. Kurtz, Gunpowder substituted composition and method, in, Google Patents, 1985.

[25] H. Hatakeyama, T. Hatakeyama, Lignin structure, properties, and applications, in: Biopolymers, Springer, 2009, pp. 1-63.

[26] C. Felby, B. Nielsen, P. Olesen, L. Skibsted, Identification and quantification of radical reaction intermediates by electron spin resonance spectrometry of laccase-catalyzed oxidation of wood fibers from beech (Fagus sylvatica), Applied Microbiology and Biotechnology, 48 (1997) 459-464.

[27] F.S. Chakar, A.J. Ragauskas, Review of current and future softwood kraft lignin process chemistry, Industrial Crops and Products, 20 (2004) 131-141.

[28] E.K. Pye, Industrial lignin production and applications, Biorefineries-industrial processes and products: status quo and future directions, (2008) 165-200.

[29] S.E. Lebo, J.D. Gargulak, T.J. McNally, Lignin, in: Kirk-Othmer Encyclopedia of Chemical Technology, John Wiley & Sons, Inc., 2000.

[30] A. Berlin, M. Balakshin, Chapter 18 - Industrial Lignins: Analysis, Properties, and Applications, in: V.K. Gupta, M.G.T.P. Kubicek, J.S. Xu (Eds.) Bioenergy Research: Advances and Applications, Elsevier, Amsterdam, 2014, pp. 315-336.

[31] Y. Li, H. Zhu, C. Yang, Y. Zhang, J. Xu, M. Lu, Synthesis and super retarding performance in cement production of diethanolamine modified lignin surfactant, Construction and Building Materials, 52 (2014) 116-121.

[32] Z. Li, Y. Kong, Y. Ge, Synthesis of porous lignin xanthate resin for Pb2+ removal from aqueous solution, Chemical Engineering Journal, 270 (2015) 229-234.

[33] Q. Bu, H. Lei, A.H. Zacher, L. Wang, S. Ren, J. Liang, Y. Wei, Y. Liu, J. Tang, Q. Zhang, R. Ruan, A review of catalytic hydrodeoxygenation of lignin-derived phenols from biomass pyrolysis, Bioresource Technology, 124 (2012) 470-477.

[34] H.V. Scheller, P. Ulvskov, Hemicelluloses, Plant Biology, 61 (2010) 263.

[35] S.V. Vassilev, D. Baxter, L.K. Andersen, C.G. Vassileva, T.J. Morgan, An overview of the organic and inorganic phase composition of biomass, Fuel, 94 (2012) 1-33.

[36] S.V. Vassilev, D. Baxter, L.K. Andersen, C.G. Vassileva, An overview of the chemical composition of biomass, Fuel, 89 (2010) 913-933.

[37] R.C. Pettersen, The chemical composition of wood, The chemistry of solid wood, 207 (1984) 57-126.

[38] T. Kozlowski, Responses of woody plants to flooding and salinity, Tree physiology, (1997).

[39] E.A.E. Elsheikh, M. Wood, Effect of salinity on growth, nodulation and nitrogen yield of chickpea (Cicer arietinum L.), Journal of Experimental Botany, 41 (1990) 1263-1269.

[40] C.W. Huie, A review of modern sample-preparation techniques for the extraction and analysis of medicinal plants, Analytical and bioanalytical chemistry, 373 (2002) 23-30.

[41] B. Qi, T. Fraser, S. Mugford, G. Dobson, O. Sayanova, J. Butler, J.A. Napier, A.K. Stobart, C.M. Lazarus, Production of very long chain polyunsaturated omega-3 and omega-6 fatty acids in plants, Nature biotechnology, 22 (2004) 739-745.

[42] J. Dunkerley, International comparisons of energy consumption, Routledge, 2016.

[43] A. Malik, J. Lan, M. Lenzen, Trends in global greenhouse gas emissions from 1990 to 2010, Environmental science & technology, 50 (2016) 4722-4730.

[44] P.E. Brockway, J.K. Steinberger, J.R. Barrett, T.J. Foxon, Understanding China's past and future energy demand: An exergy efficiency and decomposition analysis, Applied Energy, 155 (2015) 892-903.

[45] I. Jouette, B. Le Ngoc, A. Chenu, J.-J. Nieuviaert, The key role of nuclear energy to strengthen economic safety for France and the European Union, (2015).

[46] D.F. Dominković, I. Bačeković, B. Ćosić, G. Krajačić, T. Pukšec, N. Duić, N. Markovska, Zero carbon energy system of South East Europe in 2050, Applied Energy, (2016).

[47] Y. Yang, J.P. Poon, Y. Liu, S. Bagchi-Sen, Small and flat worlds: A complex network analysis of international trade in crude oil, Energy, 93 (2015) 534-543.

[48] J. Ferrier, Is European gas about to confirm its entry into the golden age?, Revue de l', (2015) 93-102.

[49] T. Dietrich, M.V. Velasco, P. Echeverría, B. Pop, A. Rusu, Crop and Plant Biomass as Valuable Material for BBB. Alternatives for Valorization of Green Wastes, Biotransformation of Agricultural Waste and By-Products: The Food, Feed, Fibre, Fuel (4F) Economy, 2014 (2016) 1.

[50] J. Pang, M. Zheng, R. Sun, A. Wang, X. Wang, T. Zhang, Synthesis of ethylene glycol and terephthalic acid from biomass for producing PET, Green Chemistry, 18 (2016) 342-359.

[51] K.C. Badgujar, B.M. Bhanage, The green metric evaluation and synthesis of diesel-blend compounds from biomass derived levulinic acid in supercritical

carbon dioxide, Biomass and Bioenergy, 84 (2016) 12-21.

[52] J. Gupta, B.W. Wilson, P.V. Vadlani, Evaluation of green solvents for a sustainable zein extraction from ethanol industry DDGS, Biomass and Bioenergy, 85 (2016) 313-319.

[53] C. Guizani, F.E. Sanz, S. Salvador, Influence of temperature and particle size on the single and mixed atmosphere gasification of biomass char with H_2O and CO_2, Fuel Processing Technology, 134 (2015) 175-188.

[54] D. Barisano, G. Canneto, F. Nanna, E. Alvino, G. Pinto, A. Villone, M. Carnevale, V. Valerio, A. Battafarano, G. Braccio, Steam/oxygen biomass gasification at pilot scale in an internally circulating bubbling fluidized bed reactor, Fuel Processing Technology, 141 (2016) 74-81.

[55] S. Cheah, W.S. Jablonski, J.L. Olstad, D.L. Carpenter, K.D. Barthelemy, D.J. Robichaud, J.C. Andrews, S.K. Black, M.D. Oddo, T.L. Westover, Effects of thermal pretreatment and catalyst on biomass gasification efficiency and syngas composition, Green Chemistry, (2016).

[56] A. Molino, S. Chianese, D. Musmarra, Biomass gasification technology: The state of the art overview, Journal of Energy Chemistry, 25 (2016) 10-25.

[57] F. Behrendt, Y. Neubauer, M. Oevermann, B. Wilmes, N. Zobel, Direct Liquefaction of Biomass, Chemical Engineering & Technology, 31 (2008) 667-677.

[58] J. Akhtar, N.A.S. Amin, A review on process conditions for optimum bio-oil yield in hydrothermal liquefaction of biomass, Renewable and Sustainable Energy Reviews, 15 (2011) 1615-1624.

[59] Z. Liu, F.-S. Zhang, Effects of various solvents on the liquefaction of biomass to produce fuels and

chemical feedstocks, Energy conversion and management, 49 (2008) 3498-3504.

[60] S. Zou, Y. Wu, M. Yang, C. Li, J. Tong, Thermochemical catalytic liquefaction of the marine microalgae Dunaliella tertiolecta and characterization of bio-oils, Energy & Fuels, 23 (2009) 3753-3758.

[61] A.A. Peterson, F. Vogel, R.P. Lachance, M. Fröling, M.J. Antal Jr, J.W. Tester, Thermochemical biofuel production in hydrothermal media: a review of sub-and supercritical water technologies, Energy & Environmental Science, 1 (2008) 32-65.

[62] W.S.L. Mok, M.J. Antal Jr, Uncatalyzed solvolysis of whole biomass hemicellulose by hot compressed liquid water, Industrial & Engineering Chemistry Research, 31 (1992) 1157-1161.

[63] C. Zhong, X. Wei, A comparative experimental study on the liquefaction of wood, Energy, 29 (2004) 1731-1741.

[64] M. Grilc, B. Likozar, J. Levec, Biofuel from Lignocellulosic Biomass Liquefaction in Waste Glycerol and Its Catalytic Upgrade, in: World Sustainable Energy Days Next 2014, Springer, 2015, pp. 137-144.

[65] E.C. Tan, L.J. Snowden-Swan, M. Talmadge, A. Dutta, S. Jones, K.K. Ramasamy, M. Gray, R. Dagle, A. Padmaperuma, M. Gerber, Comparative techno-economic analysis and process design for indirect liquefaction pathways to distillate-range fuels via biomass-derived oxygenated intermediates upgrading, Biofuels, Bioproducts and Biorefining, (2016).

[66] T.P. Wampler, Applied pyrolysis handbook, CRC Press, 2006.

[67] A. Bridgwater, G. Peacocke, Fast pyrolysis processes for biomass, Renewable and sustainable energy reviews, 4 (2000) 1-73.

[68] R. Ragucci, P. Giudicianni, A. Cavaliere, Cellulose slow pyrolysis products in a pressurized steam flow reactor, Fuel, 107 (2013) 122-130.

[69] W. Tsai, M. Lee, Y. Chang, Fast pyrolysis of rice straw, sugarcane bagasse and coconut shell in an induction-heating reactor, Journal of analytical and applied pyrolysis, 76 (2006) 230-237.

[70] A. Karaduman, E.H. Şimşek, B. Çiçek, A.Y. Bilgesü, Flash pyrolysis of polystyrene wastes in a free-fall reactor under vacuum, Journal of Analytical and Applied Pyrolysis, 60 (2001) 179-186.

[71] D. Li, C. Briens, F. Berruti, Improved lignin pyrolysis for phenolics production in a bubbling bed reactor – Effect of bed materials, Bioresource Technology, 189 (2015) 7-14.

[72] Y. Shen, K. Yoshikawa, Recent progresses in catalytic tar elimination during biomass gasification or pyrolysis—A review, Renewable and Sustainable Energy Reviews, 21 (2013) 371-392.

[73] A.V. Bridgwater, Review of fast pyrolysis of biomass and product upgrading, Biomass and Bioenergy, 38 (2012) 68-94.

[74] S.A. Galema, Microwave chemistry, Chem. Soc. Rev., 26 (1997) 233-238.

[75] A. Undri, L. Rosi, M. Frediani, P. Frediani, Microwave heating, Microwave pyrolysis of polymeric materials, (2011).

[76] N.E. Leadbeater, Microwave heating as a tool for sustainable chemistry, CRC Press, 2010.

[77] D.K. Ghodgaonkar, V.V. Varadan, V.K. Varadan, A free-space method for measurement of dielectric constants and loss tangents at microwave frequencies, IEEE Transactions on Instrumentation and measurement, 38 (1989) 789-793.

[78] E. Grant, B.J. Halstead, Dielectric parameters relevant to microwave dielectric heating, Chemical Society Reviews, 27 (1998) 213-224.

[79] J. Menéndez, A. Arenillas, B. Fidalgo, Y. Fernández, L. Zubizarreta, E.G. Calvo, J.M. Bermúdez,

Microwave heating processes involving carbon materials, Fuel Processing Technology, 91 (2010) 1-8.

[80] A. Undri, L. Rosi, M. Frediani, P. Frediani, Conversion of poly (lactic acid) to lactide via microwave assisted pyrolysis, Journal of Analytical and Applied Pyrolysis, 110 (2014) 55-65.

[81] M. Bartoli, L. Rosi, M. Frediani, A. Undri, P. Frediani, Depolymerization of polystyrene at reduced pressure through a microwave assisted pyrolysis, Journal of Analytical and Applied Pyrolysis, 113 (2015) 281-287.

[82] A. Undri, L. Rosi, M. Frediani, P. Frediani, Efficient disposal of waste polyolefins through microwave assisted pyrolysis, Fuel, 116 (2014) 662-671.

[83] A. Undri, L. Rosi, M. Frediani, P. Frediani, Fuel from microwave assisted pyrolysis of waste multilayer packaging beverage, Fuel, 133 (2014) 7-16.

[84] A. Undri, L. Rosi, M. Frediani, P. Frediani, Microwave assisted pyrolysis of corn derived plastic bags, Journal of Analytical and Applied Pyrolysis, 108 (2014) 86-97.

[85] A. Undri, S. Meini, L. Rosi, M. Frediani, P. Frediani, Microwave pyrolysis of polymeric materials: Waste tires treatment and characterization of the value-added products, Journal of Analytical and Applied Pyrolysis, 103 (2013) 149-158.

[86] P. Frediani, L. Rosi, M. Frediani, A. Undri, S. Occhialini, Production of hydrocarbons from copyrolysis of plastic and tyre material with microwave heating Eur. Pat., in, PCT/IB2012/050747, 2012.

[87] P. Frediani, L. Rosi, M. Frediani, A. Undri, S. Occhialini, S. Meini, Production of hydrocarbons from pyrolysis of tyres Eur. Pat, in, PCT/IB2012/050748, 2012.

[88] A. Undri, L. Rosi, M. Frediani, P. Frediani, Upgraded fuel from microwave assisted pyrolysis of waste tire, Fuel, 115 (2014) 600-608.

[89] A. Undri, M. Zaid, C. Briens, F. Berruti, L. Rosi, M. Bartoli, M. Frediani, P. Frediani, Bio-oil from pyrolysis of wood pellets using a microwave multimode oven and different microwave absorbers, Fuel, 153 (2015) 464-482.

[90] M. Bartoli, L. Rosi, A. Giovannelli, P. Frediani, M. Frediani, Bio-oil from residues of short rotation coppice of poplar using a microwave assisted pyrolysis, Journal of Analytical and Applied Pyrolysis, 119 (2016) 224-232.

[91] M. Bartoli, L. Rosi, A. Giovannelli, P. Frediani, M. Frediani, Pyrolysis of α-cellulose in a microwave multimode batch reactor, Journal of Analytical and Applied Pyrolysis, 120 (2016) 284-296.

[92] A.a. Metaxas, R.J. Meredith, Industrial microwave heating, IET, 1983.

[93] D.J. Macquarrie, J.H. Clark, E. Fitzpatrick, The microwave pyrolysis of biomass, Biofuels, Bioproducts and Biorefining, 6 (2012) 549-560.

[94] X. Zhang, W. Yang, C. Dong, Levoglucosan formation mechanisms during cellulose pyrolysis, Journal of Analytical and Applied Pyrolysis, 104 (2013) 19-27.

[95] T. Kotake, H. Kawamoto, S. Saka, Mechanisms for the formation of monomers and oligomers during the pyrolysis of a softwood lignin, Journal of Analytical and Applied Pyrolysis, 105 (2014) 309-316.

[96] X. Miao, Q. Wu, C. Yang, Fast pyrolysis of microalgae to produce renewable fuels, Journal of Analytical and Applied Pyrolysis, 71 (2004) 855-863.

[97] W.T. Tsai, M.K. Lee, Y.M. Chang, Fast pyrolysis of rice straw, sugarcane bagasse and coconut shell in an induction-heating reactor, Journal of Analytical and Applied Pyrolysis, 76 (2006) 230-237.

[98] Z. Du, Y. Li, X. Wang, Y. Wan, Q. Chen, C. Wang, X. Lin, Y. Liu, P. Chen, R. Ruan, Microwave-assisted

pyrolysis of microalgae for biofuel production, Bioresource Technology, 102 (2011) 4890-4896.

[99] A.A. Salema, F.N. Ani, Microwave induced pyrolysis of oil palm biomass, Bioresource Technology, 102 (2011) 3388-3395.

[100] K. El harfi, A. Mokhlisse, M.B. Chanâa, A. Outzourhit, Pyrolysis of the Moroccan (Tarfaya) oil shales under microwave irradiation, Fuel, 79 (2000) 733-742.

[101] H. Zhang, R. Xiao, D. Wang, Z. Zhong, M. Song, Q. Pan, G. He, Catalytic fast pyrolysis of biomass in a fluidized bed with fresh and spent fluidized catalytic cracking (FCC) catalysts, Energy & Fuels, 23 (2009) 6199-6206.

[102] M. Asadullah, M.A. Rahman, M.M. Ali, M.A. Motin, M.B. Sultan, M.R. Alam, M.S. Rahman, Jute stick pyrolysis for bio-oil production in fluidized bed reactor, Bioresource Technology, 99 (2008) 44-50.

[103] L. Ingram, D. Mohan, M. Bricka, P. Steele, D. Strobel, D. Crocker, B. Mitchell, J. Mohammad, K. Cantrell, C.U. Pittman Jr, Pyrolysis of wood and bark in an auger reactor: physical properties and chemical analysis of the produced bio-oils, Energy & Fuels, 22 (2007) 614-625.

[104] N. Özbay, E. Apaydın-Varol, B.B. Uzun, A.E. Pütün, Characterization of bio-oil obtained from fruit pulp pyrolysis, Energy, 33 (2008) 1233-1240.

[105] C.A. Mullen, A.A. Boateng, N.M. Goldberg, I.M. Lima, D.A. Laird, K.B. Hicks, Bio-oil and bio-char production from corn cobs and stover by fast pyrolysis, Biomass and bioenergy, 34 (2010) 67-74.

[106] S.A. Galema, Microwave chemistry, Chemical Society Reviews, 26 (1997) 233-238.

[107] S.-J. Kim, S.-H. Jung, J.-S. Kim, Fast pyrolysis of palm kernel shells: influence of operation parameters on the bio-oil yield and the yield of phenol

and phenolic compounds, Bioresource technology, 101 (2010) 9294-9300.

[108] D. Radlein, J. Piskorz, D. Scott, Fast pyrolysis of natural polysaccharides as a potential industrial process, Journal of Analytical and Applied Pyrolysis, 19 (1991) 41-63.

[109] A.M. Sarotti, R.A. Spanevello, A.G. Suárez, An efficient microwave-assisted green transformation of cellulose into levoglucosenone. Advantages of the use of an experimental design approach, Green Chemistry, 9 (2007) 1137-1140.

[110] http://www.huayinenergy.com/, in.

[111] https://www.alibaba.com/product-detail/waste-plastic-recycling-pyrolysis-machine_1775784961.html, in.

[112] https://www.alibaba.com/product-detail/high-yield-efficiency-microwave-pyrolysis-with_1951075553.html, in.

[113] M. Haworth, M. Centritto, A. Giovannelli, G. Marino, N. Proietti, D. Capitani, A. De Carlo, F. Loreto, Xylem morphology determines the drought response of two Arundo donax ecotypes from contrasting habitats, GCB Bioenergy, (2015).

[114] R. Spinelli, N. Magagnotti, C. Nati, C. Cantini, G. Sani, G. Picchi, M. Biocca, Integrating olive grove maintenance and energy biomass recovery with a single-pass pruning and harvesting machine, Biomass and Bioenergy, 35 (2011) 808-813.

[115] A. Undri, B. Sacchi, E. Cantisani, N. Toccafondi, L. Rosi, M. Frediani, P. Frediani, Carbon from microwave assisted pyrolysis of waste tires, Journal of Analytical and Applied Pyrolysis, 104 (2013) 396-404.

[116] W.M. Haynes, SECTION 6: Fluid properties, CRC Press, 2014.

[117] G. Dorez, L. Ferry, R. Sonnier, A. Taguet, J.M. Lopez-Cuesta, Effect of cellulose, hemicellulose and lignin contents on pyrolysis and combustion of natural

fibers, Journal of Analytical and Applied Pyrolysis, 107 (2014) 323-331.

[118] N. Ozbay, A.E. Pütün, E. Pütün, Bio-oil production from rapid pyrolysis of cottonseed cake: product yields and compositions, International journal of energy research, 30 (2006) 501-510.

[119] R.M. Silverstein, G.C. Bassler, Spectrometric identification of organic compounds, 2nd ed., 1963.

[120] A. Undri, M. Abou-Zahid, C. Briens, F. Berruti, L. Rosi, M. Bartoli, M. Frediani, P. Frediani, A simple procedure for chromatographic analysis of pyrolysis bio-oils, Journal of Analytical and Applied Pyrolysis, 114 (2015) 208-221.

[121] M. Bartoli, L. Rosi, M. Frediani, P. Frediani, A simple protocol for quantitative analysis of bio-oils through gas-chromatography/mass spectrometry, European Journal of Mass Spectroscopy, 22 (2016) 1-14.

[122] F. Mushtaq, R. Mat, F.N. Ani, A review on microwave assisted pyrolysis of coal and biomass for fuel production, Renewable and Sustainable Energy Reviews, 39 (2014) 555-574.

[123] G.Y. Yurkov, A.S. Fionov, Y.A. Koksharov, V.V. Koleso, S.P. Gubin, Electrical and magnetic properties of nanomaterials containing iron or cobalt nanoparticles, Inorg Mater, 43 (2007) 834-844.

[124] K. Young, H. Frederikse, Compilation of the static dielectric constant of inorganic solids, Journal of Physical and Chemical Reference Data, 2 (1973) 313-410.

[125] J. Devi, J. Akhtar, Multiphysics modeling of metal ceramic compact for microwave processing, Proceedings of the 7th European Microwave Integrated Circuits Conference, (2012) 920-923.

[126] A. Undri, S. Meini, L. Rosi, M. Frediani, P. Frediani, Microwave pyrolysis of polymeric materials: waste tires treatment and characterization of the

value-added products, Journal of Analytical and Applied Pyrolysis, 103 (2013) 149-158.

[127] F.-X. Collard, J. Blin, A review on pyrolysis of biomass constituents: Mechanisms and composition of the products obtained from the conversion of cellulose, hemicelluloses and lignin, Renewable and Sustainable Energy Reviews, 38 (2014) 594-608.

[128] S. Eser, R.G. Jenkins, F.J. Derbyshire, M. Malladi, Carbonization of coker feedstocks and their fractions, Carbon, 24 (1986) 77-82.

[129] A.-M. Domenach, A. Moiroud, L. Jocteur-Monrozier, Leaf carbon and nitrogen constituents of some actinorhizal tree species, Soil Biology and Biochemistry, 26 (1994) 649-653.

[130] K.A. Spokas, Review of the stability of biochar in soils: predictability of O:C molar ratios, Carbon Managment, 1 (2010) 289-303.

[131] H. Yang, R. Yan, H. Chen, D.H. Lee, C. Zheng, Characteristics of hemicellulose, cellulose and lignin pyrolysis, Fuel, 86 (2007) 1781-1788.

[132] M.W. Nolte, M.W. Liberatore, Viscosity of biomass pyrolysis oils from various feedstocks, Energy & Fuels, 24 (2010) 6601-6608.

[133] F. Shafizadeh, R.H. Furneaux, T.G. Cochran, J.P. Scholl, Y. Sakai, Production of levoglucosan and glucose from pyrolysis of cellulosic materials, Journal of Applied Polymer Science, 23 (1979) 3525-3539.

[134] X. Bai, P. Johnston, S. Sadula, R.C. Brown, Role of levoglucosan physiochemistry in cellulose pyrolysis, Journal of Analytical and Applied Pyrolysis, 99 (2013) 58-65.

[135] X. Bai, P. Johnston, R.C. Brown, An experimental study of the competing processes of evaporation and polymerization of levoglucosan in cellulose pyrolysis, Journal of Analytical and Applied Pyrolysis, 99 (2013) 130-136.

[136] P.K. Kanaujia, D. Tripathi, R. Singh, Review of analytical strategies in the production and upgrading of bio-oils derived from lignocellulosic biomass, Journal of Analytical and Applied Pyrolysis, 105 (2014) 55-74.

[137] C. Lai, Y. Liu, J. Ma, Q. Ma, H. He, Degradation kinetics of levoglucosan initiated by hydroxyl radical under different environmental conditions, Atmospheric Environment, 91 (2014) 32-39.

[138] X. Zhang, J. Li, W. Yang, W. Blasiak, Formation Mechanism of Levoglucosan and Formaldehyde during Cellulose Pyrolysis, Energy & Fuels, 25 (2011) 3739-3746.

[139] G.N. Richards, G. Zheng, Influence of metal ions and of salts on products from pyrolysis of wood: applications to thermochemical processing of newsprint and biomass, Journal of Analytical and Applied Pyrolysis, 21 (1991) 133-146.

[140] P.T. Williams, P.A. Horne, The role of metal salts in the pyrolysis of biomass, Renewable Energy, 4 (1994) 1-13.

[141] G. Yildiz, F. Ronsse, R. Venderbosch, R.v. Duren, S.R.A. Kersten, W. Prins, Effect of biomass ash in catalytic fast pyrolysis of pine wood, Applied Catalysis B: Environmental, 168–169 (2015) 203-211.

[142] D.K. Shen, S. Gu, The mechanism for thermal decomposition of cellulose and its main products, Bioresource Technology, 100 (2009) 6496-6504.

[143] A. Al Shra'ah, R. Helleur, Microwave pyrolysis of cellulose at low temperature, Journal of Analytical and Applied Pyrolysis, 105 (2014) 91-99.

[144] J. Huang, C. Liu, D. Wu, H. Tong, L. Ren, Density functional theory studies on pyrolysis mechanism of β-O-4 type lignin dimer model compound, Journal of Analytical and Applied Pyrolysis, 109 (2014) 98-108.

[145] C. Yin, Microwave-assisted pyrolysis of biomass for liquid biofuels production, Bioresource Technology, 120 (2012) 273-284.

[146] A. Tumbalam Gooty, D. Li, F. Berruti, C. Briens, Kraft-lignin pyrolysis and fractional condensation of its bio-oil vapors, Journal of Analytical and Applied Pyrolysis, 106 (2014) 33-40.

[147] C. Peng, G. Zhang, J. Yue, G. Xu, Pyrolysis of lignin for phenols with alkaline additive, Fuel Processing Technology, 124 (2014) 212-221.

[148] A.V. Bridgwater, D. Meier, D. Radlein, An overview of fast pyrolysis of biomass, Organic Geochemistry, 30 (1999) 1479-1493.

[149] A. Forte, A. Zucaro, M. Fagnano, S. Bastianoni, R. Basosi, A. Fierro, LCA of Arundo donax L. lignocellulosic feedstock production under Mediterranean conditions, Biomass and Bioenergy, 73 (2015) 32-47.

[150] B.M. Jenkins, Global Agriculture: Industrial Feedstocks for Energy and Materials, in: N.K.V. Alfen (Ed.) Encyclopedia of Agriculture and Food Systems, Academic Press, Oxford, 2014, pp. 461-498.

[151] D. Pirozzi, N. Fiorentino, A. Impagliazzo, F. Sannino, A. Yousuf, G. Zuccaro, M. Fagnano, Lipid production from Arundo donax grown under different agronomical conditions, Renewable Energy, 77 (2015) 456-462.

[152] L. Corno, R. Pilu, F. Adani, Arundo donax L.: A non-food crop for bioenergy and bio-compound production, Biotechnology Advances, 32 (2014) 1535-1549.

[153] A. Boose, J. Holt, Environmental effects on asexual reproduction, Weed Research, 39 (1999) 117-127.

[154] A.M. Lambert, T.L. Dudley, K. Saltonstall, Ecology and impacts of the large-statured invasive grasses Arundo donax and Phragmites australis in

North America, Invasive Plant Science and Management, 3 (2010) 489-494.

[155] D. Scordia, S.L. Cosentino, J.-W. Lee, T.W. Jeffries, Bioconversion of giant reed (Arundo donax L.) hemicellulose hydrolysate to ethanol by Scheffersomyces stipitis CBS6054, Biomass and Bioenergy, 39 (2012) 296-305.

[156] I. De Bari, F. Liuzzi, A. Villone, G. Braccio, Hydrolysis of concentrated suspensions of steam pretreated Arundo donax, Applied Energy, 102 (2013) 179-189.

[157] A. Graziani, S.J. Steinmaus, Hydrothermal and thermal time models for the invasive grass, Arundo donax, Aquatic Botany, 90 (2009) 78-84.

[158] R. Saikia, R.S. Chutia, R. Kataki, K.K. Pant, Perennial grass (Arundo donax L.) as a feedstock for thermo-chemical conversion to energy and materials, Bioresource Technology, 188 265-272.

[159] M. Jeguirim, G. Trouvé, Pyrolysis characteristics and kinetics of Arundo donax using thermogravimetric analysis, Bioresource Technology, 100 (2009) 4026-4031.

[160] O. Faix, D. Meier, O. Beinhoff, Analysis of lignocelluloses and lignins from Arundo donax L. and Miscanthus sinensis Anderss., and hydroliquefaction of Miscanthus, Biomass, 18 (1989) 109-126.

[161] C.H. Chia, B. Gong, S.D. Joseph, C.E. Marjo, P. Munroe, A.M. Rich, Imaging of mineral-enriched biochar by FTIR, Raman and SEM–EDX, Vibrational Spectroscopy, 62 (2012) 248-257.

[162] W.N.R.W. Isahak, M.W.M. Hisham, M.A. Yarmo, T.-y. Yun Hin, A review on bio-oil production from biomass by using pyrolysis method, Renewable and Sustainable Energy Reviews, 16 (2012) 5910-5923.

[163] J. Cai, W. Wu, R. Liu, An overview of distributed activation energy model and its application in the

pyrolysis of lignocellulosic biomass, Renewable and Sustainable Energy Reviews, 36 (2014) 236-246.

[164] A. Roig, M. Cayuela, M. Sánchez-Monedero, An overview on olive mill wastes and their valorisation methods, Waste Management, 26 (2006) 960-969.

[165] V. Kavvadias, M. Doula, K. Komnitsas, N. Liakopoulou, Disposal of olive oil mill wastes in evaporation ponds: Effects on soil properties, Journal of Hazardous Materials, 182 (2010) 144-155.

[166] M. Rinaldi, G. Rana, M. Introna, Olive-mill wastewater spreading in southern Italy: effects on a durum wheat crop, Field Crops Research, 84 (2003) 319-326.

[167] M. Niaounakis, C.P. Halvadakis, Olive Processing Waste Management: Literature Review and Patent Survey 2nd Edition, Elsevier, 2006.

[168] D.-l. Guo, S.-b. Wu, B. Liu, X.-l. Yin, Q. Yang, Catalytic effects of NaOH and Na 2 CO 3 additives on alkali lignin pyrolysis and gasification, Applied Energy, 95 (2012) 22-30.

[169] A. Boumaza, L. Favaro, J. Lédion, G. Sattonnay, J. Brubach, P. Berthet, A. Huntz, P. Roy, R. Tétot, Transition alumina phases induced by heat treatment of boehmite: an X-ray diffraction and infrared spectroscopy study, Journal of solid state chemistry, 182 (2009) 1171-1176.

[170] R. Howitt, J. Medellín-Azuara, D. MacEwan, J. Lund, D. Sumner, Economic analysis of the 2014 drought for California agriculture, Center for Watershed Sciences, University of California, Davis, (2014).

[171] B. Jenkins, H. Sumner, Harvesting and handling agricultural residues for energy, Transactions of the ASAE, 29 (1986) 824-0836.

[172] O. El Kasmioui, R. Ceulemans, Financial analysis of the cultivation of poplar and willow for bioenergy, Biomass and Bioenergy, 43 (2012) 52-64.

[173] T. Johansson, B. Hjelm, Stump and root biomass of poplar stands, Forests, 3 (2012) 166-178.

[174] Nurmi, J., Heating values of mature trees, Acta Forestalia Finnica, 256 (1997) 1-28.

[175] R. Spinelli, C. Nati, N. Magagnotti, Harvesting and transport of root biomass from fast-growing poplar plantations, Silva Fennica, 39 (2005) 539.

[176] B. Coldwell, W. DeLong, Studies of the composition of deciduous forest tree leaves before and after partial decomposition, Scientific Agriculture, 30 (1950) 456-466.

[177] M. Berta, A. Giovannelli, E. Potenza, M.L. Traversi, M.L. Racchi, Type 3 metallothioneins respond to water deficit in leaf and in the cambial zone of white poplar (Populus alba), Journal of Plant Physiology, 166 (2009) 521-530.

[178] J. Akhtar, N. Saidina Amin, A review on operating parameters for optimum liquid oil yield in biomass pyrolysis, Renewable and Sustainable Energy Reviews, 16 (2012) 5101-5109.

[179] R. Westerhof, D.W. Brilman, M. Garcia-Perez, Z. Wang, S. Oudenhoven, W. van Swaaij, S. Kersten, Fractional condensation of biomass pyrolysis vapors, Energy & Fuels, 25 (2011) 1817-1829.

[180] X. Wang, H. Chen, K. Luo, J. Shao, H. Yang, The Influence of Microwave Drying on Biomass Pyrolysis, Energy & Fuels, 22 (2007) 67-74.

[181] D. Mohan, C.U. Pittman, P.H. Steele, Pyrolysis of wood/biomass for bio-oil: a critical review, Energy & Fuels, 20 (2006) 848-889.

[182] S.M. Shaik, P.N. Sharratt, R.B.H. Tan, Influence of selected mineral acids and alkalis on cellulose pyrolysis pathways and anhydrosaccharide formation, Journal of Analytical and Applied Pyrolysis, 104 (2013) 234-242.

[183] X. Zhang, W. Yang, C. Dong, Levoglucosan formation mechanisms during cellulose pyrolysis,

Journal of Analytical and Applied Pyrolysis, 104 (2013) 19-27.

[184] H. Kawamoto, H. Morisaki, S. Saka, Secondary decomposition of levoglucosan in pyrolytic production from cellulosic biomass, Journal of Analytical and Applied Pyrolysis, 85 (2009) 247-251.

[185] W. Guidi, C. Tozzini, E. Bonari, Estimation of chemical traits in poplar short-rotation coppice at stand level, Biomass and Bioenergy, 33 (2009) 1703-1709.

[186] A. Demirbas, The influence of temperature on the yields of compounds existing in bio-oils obtained from biomass samples via pyrolysis, Fuel Processing Technology, 88 (2007) 591-597.

[187] R. Bedmutha, C.J. Booker, L. Ferrante, C. Briens, F. Berruti, K.K.-C. Yeung, I. Scott, K. Conn, Insecticidal and bactericidal characteristics of the bio-oil from the fast pyrolysis of coffee grounds, Journal of Analytical and Applied Pyrolysis, 90 (2011) 224-231.